

PLASMA RESPONSE TO TRANSIENT HIGH VOLTAGE PULSES

By

SATYANANDA KAR

Institute for Plasma Research, Gandhinagar

A thesis submitted to the

Board of Studies in Physical Sciences

In partial fulfillment of requirements

For the Degree of

DOCTOR OF PHILOSOPHY

Of

HOMI BHABHA NATIONAL INSTITUTE



August, 2011

“The scientist is not a person who gives the right answers; he’s one who asks the right questions.”

- **Claude Lévi-Strauss**

“Back off, man. I am a scientist.”

- **Peter Venkman**

“Don’t worry about people stealing your ideas. If your ideas are any good, you’ll have to ram them down people’s throats.”

- **Howard Aiken**

“There are sadistic scientists who hurry to hunt down errors instead of establishing the truth.”

- **Marie Curie**

“I am acutely aware of the fact that the marriage between mathematics and physics, which was so enormously fruitful in past centuries, has recently ended in divorce.”

- **Freeman John Dyson**



Homi Bhabha National Institute

Programme: Ph.D.

Board of Studies in Physical Sciences

1. Name of the Constituent Institution:

Institute for Plasma Research, Bhat, Gandhinagar - 382 428, India

2. Name of the Student: Mr. Satyananda Kar

3. Enrolment Number: PHYS06200704001

4. Date of Enrolment in HBNI: September 3, 2007

5. Date of Submission of Thesis: August 16, 2011

6. Title of the Thesis: Plasma Response to Transient High Voltage Pulses

7. Composition of the Doctoral Committee:

Sr No	Composition	Designation in HBNI	Name
a.	Chairman	Prof	P I John
b.	Convener (Guide)	Asst Prof	S Mukherjee
c.	Co-Guide, if any	—	—
d.	Member	Asst Prof	S Sengupta
e.	Member	Asst Prof	P Chattopadhyay
f.	The Technology Adviser, if any	Invitee	—

8. Number of Doctoral Committee Meetings held with respective dates:

- (i) 29/10/2007 (iv) 02/11/2010
(ii) 30/09/2008 (v) 28/06/2011
(iii) 20/10/2009

9. Name and Organization of the Examiner 1: Prof. A. N. Sekar Iyengar

Head, Plasma Physics Division, SINP, Kolkata, India ✓

Recommendations of the Examiner 1 (Thesis Evaluation) (i) accepted, (ii) ~~accepted after revisions~~, or (iii) ~~rejected~~:

10. Name and Organization of the Examiner 2: Prof. P. K. Barhai

Head, Dept. of Applied Physics, BIT-Meshra, Ranchi, India ✓

Recommendations of the Examiner 2 (Thesis Evaluation) (i) ~~accepted~~, (ii) ~~accepted after revisions~~, or (iii) ~~rejected~~:

Name & Signature of Dean-Academic, CI:

Dr. Subroto Mukherjee, Dean-Academic Affairs, IPR

Recommendations of the Viva Voce Board

1. Date of Viva Voce Examination: 09/12/2011

2. Recommendations for the award of the Ph.D. degree: Recommended / Not Recommended

(If Recommended, give summary of main findings and overall quality of thesis)

(If Not Recommended, give reasons for not recommending and guidelines to be communicated by Convener of the Doctoral committee to the student for further work)

The quality of the thesis is excellent and has relevance in plasma applications. The candidate has explored and investigated the plasma effects of high voltages (of both polarities -ve and +ve) which is sometimes ignored by industrial application. The finding of the electron hole is an original and novel contribution to these systems. These results have been published in reputed, refereed journals with highest impact factor in "Plasma Physics" - "Physics of Plasmas".

The future plan is also exciting since they will complete the work that has been carried out so far.

A. N. Sekar Iyengar
09/12/11

In case Not Recommended, another date will be fixed by the Dean-Academic, CI, which shall not be earlier than a month after and not later than six months from the date of first viva.

Date: December 9, 2011

Name and Signature of the Viva Voce Board (Doctoral Committee and External Examiner):

Prof. A. N. Sekar Iyengar (External Examiner)

A. N. Sekar Iyengar

Prof. P. I. John (Chairman)

P. I. John

Dr. Subroto Mukherjee (Guide)

Subroto Mukherjee

Dr. Sudip Sengupta (Member)

Sudip Sengupta

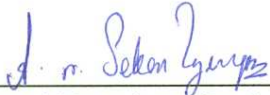
Dr. Prabal Chattopadhyay (Member)

Prabal Chattopadhyay

Homi Bhabha National Institute

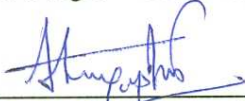
Recommendations of the Viva Voice Board

As members of the Viva Voice Board, we certify that we have read the dissertation prepared by **Satyananda Kar** entitled "**Plasma Response to Transient High Voltage Pulses**" and recommend that it may be accepted as fulfilling the dissertation requirement for the Degree of Doctor of Philosophy.


Date: 09/12/11
External Examiner: **Prof. A. N. Sekar Iyengar**
Saha Institute of Nuclear Physics
Bidhannagar, Kolkata - 700064, India


Date: 09/12/11
Chairman: **Prof. P. I. John**
Institute for Plasma Research
Bhat, Gandhinagar – 382428, India


Date: 09/12/11
Guide: **Dr. Subroto Mukherjee**
Institute for Plasma Research
Bhat, Gandhinagar – 382428, India


Date: 09/12/11
Member: **Dr. Sudip Sengupta**
Institute for Plasma Research
Bhat, Gandhinagar – 382428, India


Date: 09/12/11
Member: **Dr. Prabal Chattopadhyay**
Institute for Plasma Research
Bhat, Gandhinagar – 382428, India

CERTIFICATION FROM GUIDE

This is to certify that viva voice of **Mr. Satyananda Kar** took place on 9th December 2011 in the Institute for Plasma Research, Bhat, Gandhinagar, India in the presence of all the following Doctoral Committee members and the external referee **Prof. A. N. Sekar Iyengar**.

Prof. A. N. Sekar Iyengar (External Referee): 

Prof. P. I. John (Chairman): 

Dr. Subroto Mukherjee (Guide): 

Dr. Sudip Sengupta (Member): 

Dr. Prabal Chattopadhyay (Member): 

There are no corrections indicated by the referees in the thesis.

Date: 09/12/2011


(Dr. Subroto Mukherjee)
Guide



Homi Bhabha National Institute

Ph.D. Thesis Evaluation Report

1. **Name of the Constituent Institution:** Institute for Plasma Research
2. **Name of the Student:** Satyananda Kar
3. **Enrolment No. :** PHYS06200704001
4. **Title of the Thesis:** Plasma Response to Transient High Voltage Pulses
5. **Board of Studies:** Physical Sciences

Recommendations

Tick one of the following:

1. The thesis in its present form is commended for the award of the Ph.D. Degree.
2. The thesis is commended for the award of the Ph.D. degree. However, my suggestions for improving the thesis may be considered at the time of the viva voce examination and if the viva voce board deems it appropriate, the same may be incorporated in the thesis based on the discussions during the viva voce examination. The revised thesis need not be sent to me.
3. The thesis should be revised as per the suggestions enclosed. I would like to see the revised thesis incorporating my suggestions before I give further recommendations.
4. The thesis is not acceptable for the award of the Ph.D. degree.

(Signature): *A. N. Sekar Iyengar*

Name of Examiner: A.N.Sekar Iyengar

Date: 03/11/11

Please give your detailed report in the attached sheet. You may use additional sheets, if required.

1. **Name of the Student:** Satyananda Kar
2. **Enrolment No.:** PHYS06200704001
3. **Title of the Thesis:** Plasma Response to Transient High Voltage Pulses
4. **Board of Studies:** Physical Sciences

DETAILED REPORT

I have gone through the above thesis. This topic will be very useful for both plasma physicists and those working on applications of plasma physics in the area of plasma processing etc. The sheath plays a very significant role in determining the dynamics of the charged particles in the bulk of the plasma and it responds differently to both amplitude and time of application of a perturbation. These effects have been investigated elaborately in the form of propagation of coherent structures in the plasma-namely the holes and rarefactive waves. Most of the results have been published in reputed, high impact journals in plasma physics and I strongly recommend the award of the Ph.D degree.

Name of Examiner: A. N. Sekar. Iyengar


Signature and Date: 03/11/11



Homi Bhabha National Institute

Ph.D. Thesis Evaluation Report

1. Name of the Constituent Institution: *HOMI BHABHA NATIONAL INSTITUTE*
2. Name of the Student: *SATY NANDA KAR*
3. Enrolment No. :
4. Title of the Thesis: *Plasma Response to Transient High Voltage Pulses*
5. Board of Studies: *Physical Sciences*

Recommendations

Tick one of the following:

1. The thesis in its present form is commended for the award of the Ph.D. Degree.
2. The thesis is commended for the award of the Ph.D. degree. However, my suggestions for improving the thesis may be considered at the time of the viva voce examination and if the viva voce board deems it appropriate, the same may be incorporated in the thesis based on the discussions during the viva voce examination. The revised thesis need not be sent to me.
3. The thesis should be revised as per the suggestions enclosed. I would like to see the revised thesis incorporating my suggestions before I give further recommendations.
4. The thesis is not acceptable for the award of the Ph.D. degree.

P.K. Barha
(Signature):

Name of Examiner: *Prof P.K. BARHA*

Date: *12.11.2011*

Please give your detailed report in the attached sheet. You may use additional sheets, if required.

1. **Name of the student: Satyananda Kar**
2. **Enrolment No.:**
3. **Title of the Thesis: Plasma Response To Transient High Voltage Pulses**
4. **Board of Studies: Board of Studies in Physical Sciences**

Detailed Report

The thesis is well organized and well written except a few minor grammatical mistakes. It contains some very novel results on ion acoustic waves. The findings of the investigations will help in the understanding of the physics of surface modifications using plasma based ion implantation. To put it succinctly the thesis reports on experimental investigation of plasma response to transient high negative and positive voltage pulses in a low pressure unmagnetized argon plasma. Its aim was to study the excitation and propagation characteristics of electrostatic waves, particle balance in plasmas during pulse biasing, wave excitation after pulse withdrawal, and wave excitation using capacitive coupling. The contents may be summarized as below.

The first chapter provides an introduction to a brief genesis of plasma physics, plasma sheath and plasma waves.

The second chapter describes the experimental setup, instrumentation, different diagnostics, plasma production and plasma characterization. The diagnostic tools like Langmuir probe, emissive probe and their circuitry for biasing has also been explained. The plasma production from thoriated tungsten filaments and the determination of the plasma parameters like electron temperature, plasma density, etc. using a disc Langmuir probe has been detailed. Also the pulse forming circuit has been explained.

Chapter three contains the experimental investigation to estimate the number of electrons lost to the walls and the origin of these electrons during the bias period (for $\tau_i > \tau_p > \tau_e$) for different applied voltages, densities and pulse durations in collisionless plasma. The experimental results have been shown to closely agree with PDP1 simulation results.

Chapter four contains study of the excitation of ion rarefaction waves even when the applied pulse duration is kept intermediate of electron and ion plasma response times. It has been shown that the excitation of a wave may also depend on the pulse width as well as the pulse magnitude. The mechanism of the excitation of ion

rarefaction waves has been correlated with nonambipolar diffusion.

Chapter five describes the excitation of solitary electron holes using a metal disc electrode in homogeneous electron-ion plasma. The speed of the EHs has been shown to increase with increase in plasma density and to be independent of the applied pulse magnitude. The existence and identification of solitary electron holes are also explained.

Chapter six is devoted to the study of plasma response during both high positive and negative pulse bias to a metallic electrode covered by a dielectric film. Experiments have been carried out with different plasma parameters. The excitation of electrostatic waves has been found to depend on the dielectric thickness and polarity of the applied pulse. It has been observed that when the electrode of dielectric thickness 0.1-0.5 mm is biased pulsed positive, solitary electron holes are excited and up to this dielectric thickness, the electrode covered by the dielectric film has been found to behave as a conducting electrode.

Chapter seven summarizes the results of all the four sets of experiments. It also discusses the future scope of the work embodied in this thesis.

The thesis fulfils all the requirements for award of the Ph.D. degree and I recommend that the candidate be awarded the Ph.D. degree.

**Name of Examiner: Prof. P. K. Barhai,
(Formerly Vice-Chancellor, BIT, Mesra,
Ranchi)
Dean Faculty & Sponsored Research,
BIT, Mesra, Ranchi-835215
Ph: 0651227522(O), 06512275911(R),
9431707060(M)
E-mail: pkbarhai@bitmesra.ac.in**



**November 12, 2011
Signature & Date:**

DECLARATION

I, hereby declare that the investigation presented in the thesis has been carried out by me. The work is original and has not been submitted earlier as a whole or in part for a degree/diploma at this or any other Institution/University.



Satyananda Kar

I hereby certify that I have read this dissertation prepared under my direction and recommend that it may be accepted as fulfilling the dissertation requirement.



Guide: Dr. Subroto Mukherjee

STATEMENT BY AUTHOR

This dissertation has been submitted in partial fulfillment of requirements for an advanced degree at Homi Bhabha National Institute (HBNI) and is deposited in the Library to be made available to borrowers under rules of the HBNI.

Brief quotations from this dissertation are allowable without special permission, provided that accurate acknowledgement of source is made. Requests for permission for extended quotation from or reproduction of this manuscript in whole or in part may be granted by the Competent Authority of HBNI when in his or her judgment the proposed use of the material is in the interests of scholarship. In all other instances, however, permission must be obtained from the author.

Satyananda Kar

Satyananda Kar

Dedicated to

My Parents

ACKNOWLEDGEMENTS

I wish to express my deep sense of respect and gratitude to my thesis supervisor, Dr. Subroto Mukherjee who has been a constant source of inspiration during this thesis work. During the early of my PhD, he taught me the experimental techniques. He has given me the freedom to do the experiments of my own, has rebuilt my self-beliefs and has inspired to think about the experimental plasma physics. His motivating ideas and fruitful discussions are very meaningful to this thesis. He has helped me in many ways and it's very hard to count those. As a guide he can know the potential of a student and guide him/her accordingly. As a human being, he is very good in nature and has a patience to hear from others. Special thanks to Doctoral Committee chairman Prof. P. I. John and Doctoral Committee members Dr. Sudip Sengupta and Dr. Prabal Chattopadhyay for their support, encouragement and critical discussions during the annual reviews.

I also owe a debt of gratitude to Prof. Y. C. Saxena who was always ready for discuss the experimental results and share his ideas with me. I have also learnt the experimental techniques from him. I like his 'always' pleasant personality much. Also, I would like to thank Dr. G. Ravi for his many suggestions. I would like to thank Rane and Kishor for their helps during the start of my experiments and thanks to Pintu da, who was like a mentor for me during the start of my PhD. I have learnt a lot (experimental and computer techniques) from him. Whenever you want him, he is ready to help you.

I would also like to thank the faculty members who taught me experimental, theoretical and computational aspects of plasma physics during the course work. Especially thanks to Dr P. Vasu, Dr. R. Ganesh, Dr, P. Chattopadhyay, Dr. R. Srinivasan, Dr. S. Sengupta, Dr. D. Raju, Prof. R. Jha, Dr. S. Chaturvedi, Prof. Amita Das, Dr. Manoj Warior, Dr. S. K. Pathak, Dr. S. Deshpande, Dr. S. Pradhan and Prof. D. Bora. I am also thankful to Dr. Ramshubramanian (Mani), Dr. Raole and Dr. Nema for their help in different aspects regarding my work.

I also intend to thank all my colleagues and friends working at FCIPT for their help during my PhD. Special thanks to Kaila (Mama), Adam, Satyaprasad, Ghanshyam bhai, Vaghela bhai, Mukesh bhai, Alphonsa, Keena, Guptaaji, Purvi, Bhoomi, Chetan bhai, Prajapati, Chawada, Raju, Vijay, Chirayu, Anil, Nisha, Sadhu, Tyagi, Ravi, Viren, Sagar,

Vishal, Deelip, Pratik, Sachin, Arun, Murugan, Akshay, Anand, Bhupendra bhai, Mayur, Santosh for their kind help for carrying out my experiments.

I am also thankful to my seniors, friends and juniors Shyama da, Pintu da, Jain shab, Suraj, Santosh, Anand, Manas, Rajneesh, Bhaskar, Vikrant, Kishor, Maya, Subhash, Sirji, Mishraji, Shekar, Sharad, Jugal, Sunita, Puraram, Vikram Sr., Ujjwal, Deepak, Kshitish, Prabal, Tayab, Gurudatt, Sita, Ashwin, Rameshwar, Sanat, Sushil, Pravesh, Partha, Nishant, Sayak, Manjit, Soumen, Aditya, Iliyas, Vikram Jr. and Shoubhik for providing me a friendly atmosphere. Specially, the week end cricket and volleyball with these guys will memorable.

I would also like to thank my summer school students Neepa, Manisha, Suchismita and Rosyla. I am also thankful to computer centre staffs, library staffs, stores staffs and administration staffs for their co-operation during my PhD. It's very difficult to name all; those have useful contributions in the completion of this thesis. I apologize for any omission.

Finally, I would like to convey my heartiest regards to my parents whose blessings and moral support helped me in achieving my goal.

Satyananda Kar

Satyananda Kar

LIST OF PUBLICATIONS

1. **“Study of Electron Behavior in a Pulsed Ion Sheath”,**
S. Kar and S. Mukherjee
Physics of Plasmas **15**, 063504 (2008).
2. **“Possible Excitation of Solitary Electron Holes in a Laboratory Plasma”,**
S. Kar, S. Mukherjee, G. Ravi and Y. C. Saxena
Physics of Plasmas **17**, 102113 (2010).
3. **“Excitation of Ion Rarefaction Waves in a Low Pressure Plasma by Applying a Short High Negative Voltage Pulse”,**
S. Kar, S. Mukherjee and Y. C. Saxena
Physics of Plasmas **18**, 053506 (2011).
4. **“Excitation of Electrostatic Plasma Waves using a Dielectric Covered Metallic Electrode ”,**
S. Kar and S. Mukherjee
Physics of Plasmas **18**, 112303 (2011).

Synopsis

The present thesis reports on experimental investigation of plasma response to transient high negative and positive voltage pulses in a low pressure unmagnetized argon plasma. The main aim is to study the excitation and propagation characteristics of electrostatic waves, particle balance in plasmas during pulse biasing, wave excitation after pulse withdrawal, and wave excitation using capacitive coupling. The experiments are performed using single pulse excitation.

When a metallic electrode is immersed in a low pressure plasma and biased pulsed negative, with very fast rising high negative pulse; in the time scale of the inverse electron plasma frequency (or electron plasma period) electrons are repelled from the vicinity of the electrode, leaving behind a uniform density ion matrix sheath or transient sheath. Subsequently, on the time scale of inverse ion plasma frequency (or ion plasma period) ions within the sheath are accelerated towards the electrode and impinge into the electrode and surface modification occurs. Normally, the applied pulse magnitude is much greater than the electron temperature. So pulsed ion sheath plays a very important role in material surface modification. One of the major applications that have been developed using pulsed bias on the electrode is plasma immersion ion implantation [1-15]. Switching on a high negative voltage pulse, three phases on different time scales may be distinguished: the matrix extraction phase, the sheath expansion phase and the pre-sheath relaxation initiated by a rarefaction wave. Correspondingly, switching off a high negative voltage pulse results in a fill-up process followed by a sheath constriction and by a compression wave rearranging the pre-sheath. All these phenomena are mixed if voltage pulses of finite duration are applied [16]. In all the theoretical models and the experiments for surface modification and sheath dynamics [16-22], the applied pulse width to the electrode is much greater than the ion plasma period.

In the first part of the thesis, similar experiments (plasma response to negative voltage pulse) have studied *for the applied pulse width less than the ion plasma period*. The used electrode was a metallic stainless steel (SS) disc, which was immersed in a low pressure argon plasma. Plasma was generated by impact ionization of argon gas neutrals by primary electrons coming out from dc biased hot thoriated tungsten filaments of diameter 0.25 mm. It

is presumed that electrons will be repelled; but are the electrons near the vicinity of the electrode only repelled leaving electrons in the bulk plasma unaffected or both are affected. The experiments have done for to estimate the number of electrons leaving the system and to trace the origin of these repelled electrons (near the electrode or bulk plasma). The applied pulse duration was varied in between electron and ion plasma periods, assuming ions are stationary. The experiments were performed in a grounded cylindrical chamber of SS 304 with an inner diameter of 29 cm and a length of 50 cm. To estimate the number of electrons lost to the chamber wall during the negative pulse bias, another grounded extended chamber (inner diameter 14 cm and length 30 cm) was attached to the main chamber, which was isolated from the main chamber by a metallic mesh whose grid size was less than Debye length. In the extended chamber, an axially movable disc probe (collector) was kept, which was grounded. The collector was for the collection of the energetic displaced electrons (in terms of current, measured by a current transformer) from the main chamber through the metallic mesh during the application of pulse and was placed at 0.5 cm behind the mesh for the optimal signal. The integral of the collector current signal gives the total area under the curve. This area under the curve is a measure of the total number of electrons ejected from the main chamber and the number of electrons lost the chamber wall during the bias. The results indicate that the electrons that are lost to the chamber wall come from the ion matrix sheath and bulk plasma as well. For higher plasma density and applied pulse magnitude, the number of electrons lost to the wall increases. Another thing is, the energetic electrons (high speed) repelled from the vicinity of the electrode during the negative pulse bias, can be a cause of extra ionization due to occurrence of ordinary collision ionization between these energetic electrons and gas neutrals. In our experiments, the extra ionization can be neglected, because the mean free path of the energetic electrons is much larger than the mean free path of unperturbed background electrons. So few such ionizing interactions occur, and the energetic electrons leave the main chamber with almost the same (initial) energy and with no significant additional ionization. This part is published in

S. Kar and S. Mukherjee, "Study of electron behavior in a pulsed ion sheath", Phys. Plasmas 15, 063504 (2008).

In the last part, we measured the properties of the repelled electrons to the chamber walls, when a metal electrode was negatively pulsed biased for pulse duration in between the ion and electron plasma periods. In that case no attention was given to the wave propagation in plasma. In this work, the propagation of ion rarefaction waves is observed experimentally

though the applied pulse width is less than the ion plasma period. According to general understanding, for the applied pulse width less than the ion plasma period, ions are collectively undisturbed and no energy is given. Hence no ion rarefaction waves should be excited. But contrary, excitation of rarefaction wave is observed. In our experiments, the rarefaction waves are excited by applying a negative high voltage pulse to a metallic electrode. Three types of measurements have done to detect the ion rarefaction waves: floating potential measurements, ion saturation current and electron saturation current measurements. The rarefaction waves are excited after the pulse goes off. These rarefaction waves are accompanied by a non-propagating electrostatic coupling signal. For all three types of measurements, i.e., floating potential measurement, ion and electron saturation current measurements, the ion rarefaction waves propagate with comparable to sonic speed. When the applied pulse magnitude is much greater than (100-1500 times) the electron temperature, the shielding effect is not perfect and some negative potential penetrates into the quasi-neutral plasma region (pre-sheath) where the ions are accelerated. After the pulse goes to zero, ion rarefaction waves are excited in the pre-sheath region, though the applied pulse width is less than the ion plasma period. This rarefaction can also be because of ballistic response of the ions which are in the vicinity of the biased electrode. After the pulse goes off, plasma relaxes to its quasi-neutrality after some time, which is close to rarefaction wave sustaining time. Another observation is, after a distance of $\frac{3}{4}$ th of exciter diameter from the exciter, the rarefaction waves turned to ion acoustic waves due to the ion-neutral collision effects. Both the above experiments are matched with PDP1 simulation to identify trends with respect incidences happening in the initial phases of application of pulse. In the first set of experiments, we saw that there is no significant additional ionization during the negative pulse bias to the electrode. So we can't say these ion waves are ionization wave, because the ionization wave propagates by changing of ionization rate in the plasma, causing the stratification. In addition, ionization waves differ from all other types of waves primarily in the abundance of dispersion relation. This part is published in

S. Kar, S. Mukherjee and Y. C. Saxena, "Excitation of ion rarefaction waves in a low pressure plasma by applying a short high negative voltage pulse", Phys. Plasmas 18, 053506 (2011).

Many experiments have been done for the excitation of electrostatic waves, such that ion acoustic waves or solitons [16-34] or electron acoustic waves or solitons [35-52]. Mainly all these waves are excited using mesh grids mostly. The obtained results are same for both

negative and positive bias to the grid or the exciter [53-54]. In our experiment we observed ion rarefaction waves for the negative bias to a metallic disc electrode. When the disc electrode is positive biased, totally different results are obtained, i.e., solitary electron holes (SEHs) [55-63]. The electron holes are the positive potential structures and propagate with comparable to electron thermal speed. The experiments were performed in a cylindrical chamber and a positive high voltage pulse was applied to a metallic disc electrode. To detect the SEHs, one axially movable disc probe was kept floating to measure the floating potential. Here the applied pulse width was varied from less than to greater than ion plasma period. For the applied pulse width less than the thrice of ion plasma period, the SEHs propagate in two opposite directions from a location from the exciter, indicating the presence of a virtual source, which is first time observed in our experiment in the field of solitary electron hole. For the applied pulse width equal or greater than the thrice of ion plasma period, the SEHs propagate away from the exciter in one direction only. These SEHs propagates with 1.36 times of electron thermal speed. When these SEHs interact with an ion rich region, then a sudden slow down of speed occurs, i.e., 0.4 times of electron thermal speed. This part is published in

S. Kar, S. Mukherjee, G. Ravi and Y. C. Saxena, "Possible excitation of solitary electron holes in a laboratory plasma", Phys. Plasmas 17, 102113 (2010).

A less number of experiments and theoretical models have been done for surface modification of dielectric materials [64-69]. Only dielectric charging effect and surface modification is described in all the models and experiments. There is no study on excitation of some kind of plasma waves from the dielectric material. In our experiment we have used Kapton as the dielectric material and some electrostatic waves are excited in a capacitive process. The experiments were performed in a cylindrical chamber and positive and negative high voltage pulses were applied to a metallic electrode covered by a dielectric film. The applied full potential to the metallic electrode will not appear same on the dielectric surface. The calculations have done for the reduced dielectric surface potential for both positive and negative pulse bias. To detect the plasma waves, one axially movable disc probe was kept floating to measure the floating potential. Here the applied pulse widths were varied from less than to greater than ion plasma period. First the experiments were done for positive pulse bias to the metallic electrode covered by the dielectric. From the dielectric thickness of 0.1-0.5 mm, solitary electron holes and from 0.6-0.9 mm thickness, solitary ion holes [59-61, 70-72] are excited. Solitary ion holes are the negative potential structures, propagate with less than

or comparable to ion thermal speed. For the dielectric thickness 0.1-0.5 mm, charging effect is less and behaves as a metal exciter as discussed in the last set of experiments. On increasing dielectric thickness (0.6 – 0.9 mm), the dielectric surface potential will drop more and solitary ion holes are observed in this case. Initially ion holes are propagated towards the electrode covered by the dielectric with the speed of comparable to ion thermal speed and after some distance there is a sudden transition to ion acoustic speed. These waves are dependent on the combined effect of applied pulse magnitude, pulse duration and dielectric film characteristics (thickness and dielectric constant) for positive bias. First time we observed the excitation of solitary electron and ion holes using a pulsed capacitive process. For the negative bias to the dielectric exciter, ion rarefaction waves are excited for the dielectric thickness of 0.1-0.9 mm. After 0.9 mm dielectric (Kapton) thickness no structures are excited for both positive and negative bias. This part is published in

S. Kar and S. Mukherjee, “Excitation of electrostatic plasma waves using a dielectric covered metallic electrode”, *Physics of Plasmas* **18**, 112303 (2011).

Possible extension of this work can be in the areas of fundamental studies. All the experiments described above are for the un-magnetized plasma. These experiments can be repeated for the magnetized plasma to show the magnetic field effects on the un-magnetized results, like for positive plate bias electron or ion acoustic shocks may be excited instead of solitary electron holes. To understand more the solitary electron and ion holes in laboratory and space plasma, computer simulations of Chapters 5 and 6 can be done. Another experiment can be done that is; scattered dust charging with positive biased plate.

In summary, we have carried out experimental investigations of excitation and propagation characteristics of electrostatic plasma waves. The thesis is organized as follows. In the first chapter, we provide an introduction to plasma sheath and plasma waves. In the second chapter, the experimental set-up, the vacuum system, plasma production, diagnostics, plasma characterization (density, temperature etc.), pulse forming circuit are given. Chapter 3 describes the electron behavior in a pulsed ion sheath. In this chapter we have estimated the number of electrons lost to the chamber wall during the pulse bias, where the pulse width is less than the ion plasma period. In Chapter 4, excitation and propagation of ion rarefaction waves are described, though the applied pulse width is less than the ion plasma period. Chapter 5 is devoted for the excitation and propagation of solitary electron holes, when the exciter is positively biased. In Chapter 6, excitation of electrostatic plasma waves using

pulsed capacitive process is described. The final Chapter, Chapter 7, provides some concluding remarks and a discussion about possible future extensions of the work is reported in this thesis.

-
- [1] J. R. Conrad, J. L. Radtke, R. A. Dodd, F. J. Worzala, and N. C. Tran, *J. Appl. Phys.* **62**, 4591 (1987).
 - [2] M. A. Lieberman, *J. Appl. Phys.* **66**, 2926 (1989).
 - [3] K. G. Kostov, J. J. Barroso, and M. Ueda, *Braz. J. Phys.* **34**, 1689 (2004).
 - [4] M. Shamim, J. T. Scheuer, and J. R. Conrad., *J. Appl. Phys.* **69**, 2904 (1991).
 - [5] R. A. Stewart and M. Lieberman, *J. Appl. Phys.* **70**, 3481 (1991).
 - [6] B. P. Wood, *J. Appl. Phys.* **73**, 4770 (1993).
 - [7] B. Briehl and H. M. Urbassek, *Surf. Coat. Technol.* **156**, 131 (2002).
 - [8] D. Israel, K. –U. Riemann, and L. Tsendin, *J. Appl. Phys.* **95**, 4565 (2004).
 - [9] K. Yukimura, X. Ma, and T. Ikehata, *Surf. Coat. Technol.* **186**, 73 (2004).
 - [10] J. R. Conrad, *J. Appl. Phys.* **62**, 777 (1987).
 - [11] J. T. Scheuer, M. Shamim, and J. R. Conrad, *J. Appl. Phys.* **67**, 1241 (1990).
 - [12] S. Radovanov, L. Godet, R. Dorai, Z. Fang, B. W. Koo, C. Cardinaud, G. Cartry, D. Lenoble, and A. Grouillet, *J. Appl. Phys.* **98**, 113307 (2005).
 - [13] S. Mukherjee, M. Ranjan, R. Rane, N. Vaghela, A. Phukan, and K. S. Suraj, *Surf. Coat. Technol.* **201**, 6502 (2007).
 - [14] J. Brutscher, R. Gunzel, and W. Moller, *Surf. Coat. Technol.* **93**, 197 (1997).
 - [15] Y. X. Huang, X. B. Tian, S. Q. Yang, R. K. Y. Fu, and P. K. Chu, *Surf. Coat. Technol.* **201**, 5458 (2007).
 - [16] Th. Daube, P. Meyer, K. –U. Riemann and H. Schmitz, *J. Appl. Phys.* **91**, 1787 (2002).
 - [17] H. Ikezi, Y. Kiwamoto and K. E. Lonngren, *Plasma Phys.* **15**, 1141 (1973).
 - [18] R. C. Cross, *Plasma Phys.* **25**, 1377 (1983).
 - [19] I. Alexeff and R. V. Neidigh, *Phys. Rev. Lett.* **7**, 223 (1961).

- [20] K. E. Longren, M. Khazei, E. F. Gable and J. M. Bulson, *Plasma Phys.* **24**, 1483 (1982).
- [21] Y. F. Li, J. X. Ma, Y. R. Li, D. L. Xiao and K. E. Lonngren, *Phys. Lett.* **358A**, 297 (2006).
- [22] M. Widner, I. Alexeff, W. D. Jones and K. E. Lonngren, *Phys. Fluids* **13**, 2532 (1970).
- [23] H. Tanaca, M. Koganei and A. Hirose, *Phys. Rev. Lett.* **16**, 1079 (1966).
- [24] S. Watanabe and H. Tanaca, *J. Phys. Soc. Japan* **27**, 517 (1969).
- [25] Y. C. Saxena, S. K. Mattoo, A. N. Sekar and V. Chandna, *Phys. Lett.* **84A**, 71 (1981).
- [26] L. Oksuz, D. Lee and N. Hershkowitz, *Plasma Sources Sci. Technol.* **17**, 015012 (2008).
- [27] E. Okutsu and Y. Nakamura, *Plasma Phys.* **21**, 1053 (1979).
- [28] T. Honzawa, *Plasma Phys. Controlled Fusion* **26**, 1251 (1984).
- [29] B. Sahu and R. Roychoudhury, *Phys. Plasmas* **14**, 012304 (2007).
- [30] L. Wei and Y. N. Wang, *Phys. Rev.* **B 75**, 193407 (2007).
- [31] S. Ali, W. M. Moslem, P. K. Shukla and R. Schlickeiser, *Phys. Plasmas* **14**, 082307 (2007).
- [32] S. A. Khan and W. Masood, *Phys. Plasmas* **15**, 062301 (2008).
- [33] A. Barkan, R. L. Merlino and N. D'Angelo, *Phys. Plasmas* **2**, 3563 (1995).
- [34] S. Ghosh, S. Sarkar, M. Khan and M. R. Gupta, *Phys. Plasmas* **9**, 1150 (2002).
- [35] M. Berthomier et al, *Phys Plasmas* **7**, 2987 (2000).
- [36] F. Verheest et al, *Space Sci. Rev.* **121**, 299 (2005).
- [37] A. P. Kakad et al, *Adv. Space Res.* **43**, 1945 (2009).
- [38] L. D. Landau, *J. Phys. (Moscow)* **10**, 25 (1946).
- [39] R. L. Mace et al, *Phys. Plasmas* **6**, 44 (1999).
- [40] F. Valentini et al, *Phys. Plasmas* **13**, 052303 (2006).
- [41] S. P. Gary et al, *Phys. Fluids* **28**, 2439 (1985).
- [42] A. A. Mamun et al, *Phys. Plasmas* **9**, 1474 (2002).
- [43] T. H. Stix, *The Theory of Plasma Waves*, McGraw-Hill, New York, 1962), p218.
- [44] J. P. Holloway and J. J. Dorning, *Phys. Rev. A* **44**, 3856 (1991).
- [45] H. Schamel, *Phys. Plasmas* **7**, 4831 (2000).
- [46] I. B. Bernstein, J. M. Greene and M. D. Kruskal, *Phys. Rev.* **108**, 546 (1957).
- [47] F. Anderegge et al, *Phys. Plasmas* **16**, 055705 (2009).
- [48] K. Watanabe et al, *J. Phys. Soc. Japan* **43**, 1819 (1977).
- [49] Y. Kawai et al, *Phys Lett.* **36A**, 149 (1971).
- [50] Y. Kawai et al, *J Phys. Soc. Japan* **30**, 857 (1971).
- [51] T. Kawabe et al, *Phys Rev. Lett.* **28**, 889 (1972).
- [52] S. Ikezawa et al, *J. Phys. Soc. Japan* **50**, 962 (1981).
- [53] H. Ikezi et al, *Phys. Fluids* **14**, 1997 (1971).

- [54] K. Saeki et al, Phys. Rev. Lett. **42**, 501 (1979).
- [55] H. Schamel, Plasma Phys. **14**, 905 (1972).
- [56] H. Schamel, J. Plasma Phys. **13**, 139 (1975).
- [57] H. Schamel, Physica Scripta **20**, 336 (1979).
- [58] H. Schamel, Phys. Reports **140**, 161 (1986).
- [58] J. Korn and H. Schamel, J. Plasma Phys. **56**, 307 (1996); *ibid* **56**, 339 (1996).
- [59] A. Luque and H. Schamel, Phys. Reports **415**, 261 (2005).
- [60] H. Schamel and S. Bujarbarua, Phys. Fluids **23**, 2498 (1980).
- [61] S. Bujarbarua and H. Schamel, J. Plasma Phys. **25**, 515 (1981).
- [62] H. Schamel, Phys. Plasmas **7**, 4831 (2000).
- [63] H. Schamel and A. Luque, New J. Phys. **7**, 69 (2005).
- [64] Xue-Chun Li and You-Nian Wang, Surf. Coat. Technol. **201**, 6569 (2007).
- [65] G. A. Emmert, J. Vac. Sci. Technol. **B 12**, 880 (1994).
- [66] X. Tian, R. K. Y. Fu, J. Chen, P. K. Chu and I. G. Brown, Nuclear Inst. Methods in Phys. **B 187**, 485 (2002).
- [67] A. Lacoste, F. L. Coeur, Y. Arnel, J. Pelletier and C. Grattepain, Surf. Coat. Technol. **135**, 268 (2001).
- [68] X. B. Tian, K. Y. Fu, P. K. Chu and S. Q. Yang, Surf. Coat. Technol. **196**, 162 (2005).
- [69] B. P. Linder and N. W. Cheung, IEEE Trans. Plasma Sci. **24**, 1383 (1996).
- [70] H. Schamel, Phys. Lett. **89A**, 280 (1982).
- [71] H. L. Pecseli, R. J. Armstrong and J. Trulsen, Phys. Lett. **81A**, 386 (1981).
- [72] C. Franck, T. Klinger, A. Piel and H. Schamel, Phys. Plasmas **8**, 4271 (2001).

Contents

Acknowledgement.....	i
List of Publications.....	iii
Synopsis of Thesis.....	iv
Contents.....	xii
List of Figures.....	xv
List of Tables.....	xx
1 Introduction	1
1.1 Introduction and Motivation.....	1
1.2 Basics of Plasma Sheath	4
1.2.1 Sheath	4
1.2.2 Presheath.....	5
1.2.3 High-Voltage Sheaths.....	6
1.3 An Overview of Electrostatic Waves	8
1.4 Outline of the Thesis	12
1.5 References.....	14
2 Experimental Set-up and Diagnostics	17
2.1 Introduction	17
2.2 Experimental Set-up.....	17
2.2.1 Chamber and Pumping System	18
2.2.2 Cathode and Anode	20
2.2.3 Power Supply	20
2.3 Plasma Production	20
2.4 Diagnostics	21
2.4.1 Langmuir Probe	22
2.4.2 Emissive Probe	25
2.5 Characterization of Plasma	26
2.5.1 Discharge Parameters	26
2.5.2 Plasma Parameters	28

2.6 Pulse Forming Circuit	36
2.7 References.....	38
3 Study of Electron Behavior in a Pulsed Ion Sheath	40
3.1 Motivation.....	40
3.2 An Overview of Previous Works.....	41
3.3 Experimental Set-up.....	42
3.4 Results and Discussions.....	44
3.5 PDP1 Computer Simulation.....	55
3.5.1 Simulation Results.....	57
3.6 Conclusions	61
3.7 References.....	63
4 Excitation of Ion Rarefaction Waves in a Low Pressure Plasma by Applying a Short High Negative Voltage Pulse	65
4.1 Motivation.....	65
4.2 An overview of Previous Works	66
4.3 Experimental Setup.....	68
4.4 Experimental Results.....	71
4.5 Discussions	78
4.6 Summary	84
4.7 References.....	86
5 Excitation of Solitary Electron Holes in a Laboratory Plasma	89
5.1 Motivation.....	89
5.2 An Overview of Previous Works.....	90
5.3 Experimental Setup.....	92
5.4 Experimental Results.....	94
5.5 Discussions	101
5.5 Conclusions	104
5.6 References.....	105
6 Excitation of Electrostatic Waves Using Pulsed Capacitive Process.....	107
6.1 Motivation.....	107
6.2 An Overview of Previous Works.....	107
6.3 Experimental Set-up.....	109
6.4 Experimental Results and Discussions	110

6.4.1 Charging Effect	110
6.4.2 Positive Bias	115
6.4.3 Negative Bias.....	123
6.5 Conclusions	126
6.6 References.....	128
7 Summary and Future Scope.....	130
7.1 Summary	130
7.2 Future Scope	132

List of Figures

Figure 1.1 Formation of ion sheath. **(a)** initial ion and electron density and **(b)** densities, electric field and potential after the formation of sheath [6]. Here l is the plasma length, n_e and n_i are the electron and ion densities respectively, s is the sheath thickness, ϕ is the wall potential, V_p is the plasma potential and E is the electric field. 5

Figure 1.2 Qualitative behavior of sheath and pre-sheath in contact with the wall [6]. 6

Figure 1.3 Qualitative behavior of the transient sheath [6]. Here ω_{pe} and ω_{pi} are the electron and ion plasma frequency respectively. 7

Figure 2.1 Photograph of the experimental set-up. (a) Vacuum chamber. (b) Rotary pump. (c) & (d) are bellows. (e) Diffusion pump. (f) Oscilloscope. (g) Penning gauge head. (h) Penning and Pirani gauge. (i) Langmuir probe shaft. (j) Langmuir probe power supply. (k) Filament heating power supply. (l) Filament bias power supply. (m) High voltage dc power supply. (n) Pulse forming circuit. (o) Argon gas cylinder. 18

Figure 2.2 Schematic of the experimental set-up. (1) Vacuum chamber. (2), (3), (5) and (6) are the filaments. (4) Pumping system. (7) and (8) are the SS rings. (9) is the Langmuir probe. (10) Filament heating voltage. (11) Discharge voltage. 19

Figure 2.3 Schematic of the Langmuir probe.....23

Figure 2.4 Schematic diagram of the Langmuir probe circuit.....24

Figure 2.5 Schematic of emissive probe.....26

Figure 2.6 Typical filament temperature versus emission current density for the filament diameter of 0.25 mm.....27

Figure 2.7 Discharge voltage versus discharge current for various filament heating current (I_{fil}) for a constant pressure.....28

Figure 2.8 Ideal I-V characteristic for a Langmuir probe.....29

Figure 2.9 The upper trace shows the voltage wave front applied to the probe and the lower trace shows the current drawn by the probe.....31

Figure 2.10 Experimentally obtained I-V characteristics of single Langmuir probe.....32

Figure 2.11 Natural logarithmic of electron current versus probe voltage.....33

Figure 2.12 Axial variation of electron temperature and plasma density.....33

Figure 2.13 Radial variation of electron temperature and plasma density.....34

Figure 2.14 Emissive probe heating current versus floating potential.....35

Figure 2.15 The pulse forming circuit. [HV dc Supply = high voltage dc supply (1.5 kV, 500 mA), R_1 = resistor (3k Ω), C = capacitor, R_2 = load resistor, L = inductor (320 nH), P_1 = electrode or the exciter].....37

Figure 2.16 A typical voltage pulse obtained from the pulse forming circuit.....37

Figure 3.1 Schematic of the experimental set-up. (1) Applied negative voltage pulse. (2) and (18) are the SS rods. (3) high-voltage probe; to measure the voltage signal. (4) and (19) are Current transformers, CT₁ and CT₂ respectively; to measure the current signal. (5) and (14) are SS rings. (6) Main chamber or vacuum chamber. (7) Ceramic tube. (8),(9), (12) and (13) are the filaments. (10) Pumping system. (11) Stainless steel disc (substrate); on which bias is applied. (15) Metallic mesh. (16) Stainless steel disc (collector); to measure the electron current in the extended chamber during the bias period. (17) Extended chamber. (20) Discharge voltage. (21) Filament heating voltage. 43

Figure 3.2(a) The applied negative voltage pulse (solid line) and current (dotted line) on the electrode. The arrows indicate the axis side. (b) The response of the collector without plasma (dotted line) and with plasma (solid line). The dashed line indicates the collector signal goes to zero before voltage. Here $U_0 = -650$ V, $n_0 = 8.49 \times 10^9$ cm ⁻³ and $\tau_p = 140$ ns.	44
Figure 3.3 This plot is for a longer pulse duration, i.e., for 250 ns. Here $U_0 = -650$ V and $n_0 = 8.49 \times 10^9$ cm ⁻³	45
Figure 3.4 This plot is for pulse duration of 300 ns. Here $U_0 = -650$ V and $n_0 = 8.49 \times 10^9$ cm ⁻³	45
Figure 3.5 Collector signals for the pulse duration of 300 ns. (a) Shows for different densities and (b) shows for different applied voltages.	46
Figure 3.6 Number of electrons (expelled from the main chamber) collected by the collector are increased for various pulse durations. (a) Shows the number of electrons collected by the collector vs plasma density for a constant applied voltage of -650 V. (b) Shows the number of electrons collected by the collector vs applied voltage for a constant plasma density of 8.49×10^9 cm ⁻³	47
Figure 3.7 Number of electrons lost to the walls is plotted against the number of electrons displaced from the ion matrix sheath for different pulse durations. Number of electrons lost to the walls is increased linearly with the number of displaced electrons. Points are fitted by a straight line for better viewing.	49
Figure 3.8 Percentage of electrons lost to the walls during the bias period for a pulse duration of 300 ns.	51
Figure 3.9 This shows for number of electrons lost to the wall versus plasma density for $U_0 = -550$ V and $\tau_p = 250$ ns.	52
Figure 3.10 Collector current signals for various electrodes tilt angles to the collector. Here $U_0 = -550$ V, $n_p = 6.09 \times 10^9$ cm ⁻³ and $\tau_p = 250$ ns. The electrode diameter is 5 cm. The electrostatic pick-ups are more for smaller electrode diameter.	53
Figure 3.11 Schematic of disc electrode angle, which angle is between collectors and electrodes normal direction.	53
Figure 3.12 Simulation plasma system including the external R-L-C circuit for the planar geometry.	56
Figure 3.13 Results from PDP1 regarding the phase space (y-axis corresponds to the velocity and x-axis is the distance between left electrode and right electrode). All units are in SI. The thick centre line is the ion distribution and dots are electron distribution. This is for at $t = 0$ and at density of 3.63×10^{15} m ⁻³	57
Figure 3.14 (a) The left electrode is biased by a ramp such that its bias reaches -300 V in 50 ns. It is seen that the entire electron distribution is given a uniform velocity much similar to Fig. 3.13, but forming an ion matrix sheath. (b) Zoom of Fig. (a).	58
Figure 3.15 Potential profile which shows the sheath thickness at the left electrode.	58
Figure 3.16 The number of electrons lost to the right electrode after 50 ns when the bias reaches its maximum value. Initially the code was run up to 4.61 μ s for better accuracy of electron and ion distributions. During this time 10 numbers of particles have lost.	59
Figure 3.17 This profile shows for number of particles during fall time of the applied voltage pulse. The fall time was 250 ns. This graph shows that, when voltage pulse goes to zero (after 250 ns) the number of electrons and ions are approximately same.	60
Figure 3.18 Density profile for ions and electrons for $U_0 = -300$ V and $n_0 = 3.63 \times 10^9$ cm ⁻³ after 50 ns. This graph is zoomed for better view.	60
Figure 4.1 Schematic of the experimental setup. (1) Applied negative voltage pulse. (2) and (14) are the SS rods. (3) High-voltage probe; to measure the voltage signal. (4) Current transformer CT; to	

measure the current signal. (5) Main chamber. (6) Ceramic tube which covers the SS rod. (7) and (13) are SS rings. (8), (9), (11) and (12) are the filaments. (10) Pumping system. (15) Exciter (SS disc plate); on which pulse is applied. (16) Detecting probe (SS disc plate); to detect rarefaction disturbances, this can move axially. (17) Filament heating voltage. (18) Discharge voltage..... 68

Figure 4.2 Simultaneous measurement of ion and electron saturation currents using two Langmuir probes. 70

Figure 4.3 The applied voltage pulse (solid line) and current (dotted line) on the metal plate. The arrows indicate the axis side. Here $n_0 = 1.55 \times 10^9 \text{ cm}^{-3}$ 71

Figure 4.4 Oscilloscope traces (floating potential measurements) of the rarefaction disturbances for two detector positions from the exciter, when a single negative pulse is applied. Here $U_0 = -600 \text{ V}$, $n_0 = 1.55 \times 10^9 \text{ cm}^{-3}$ and $\tau_p = 300 \text{ ns}$. ϕ is the amplitude of the perturbed potential. 72

Figure 4.5 (a) The first large negative pulse is zoomed for various distances from the exciter, consisting an electrostatic coupled signal (rectangular box marked) and a fast propagating wave (marked by a long blue color arrow). **(b)** The time-of-flight plot for the fast moving waves..... 73

Figure 4.6 Oscilloscope traces (floating potential measurements) of the rarefaction disturbances observed at various distances from the exciter, when a single negative pulse is applied. Here $U_0 = -600 \text{ V}$, $n_0 = 1.55 \times 10^9 \text{ cm}^{-3}$ and $\tau_p = 300 \text{ ns}$. The arrows show the rarefactive and compressive parts. Scale of Y-axis is taken different to show the low amplitude rarefaction waves. The bracketed values are the time delay and amplitude of the rarefaction waves. ϕ is the amplitude of the perturbed potential..... 74

Figure 4.7 Spatial developments of the rarefaction waves. Here $U_0 = -600 \text{ V}$, $n_0 = 1.55 \times 10^9 \text{ cm}^{-3}$ and $\tau_p = 300 \text{ ns}$ 75

Figure 4.8 Probe separation versus time delay showing the rarefaction wave speed dependence on plasma density. Here $U_0 = -800 \text{ V}$ and $\tau_p = 300 \text{ ns}$ 75

Figure 4.9 Probe separation versus time delay showing the rarefaction wave speed dependence on pulse amplitude. Here $n_0 = 1.9 \times 10^9 \text{ cm}^{-3}$ and $\tau_p = 300 \text{ ns}$ 76

Figure 4.10 Probe separation versus time delay showing the rarefaction wave speed dependence on pulse duration. Here $U_0 = -800 \text{ V}$ and $n_0 = 1.9 \times 10^9 \text{ cm}^{-3}$ 76

Figure 4.11 Ion and electron density perturbations for various probe positions from the exciter. Y-axes scales are taken different. Here $U_0 = -800 \text{ V}$, $n_0 = 8.9 \times 10^8 \text{ cm}^{-3}$ and $\tau_p = 300 \text{ ns}$ 77

Figure 4.12(a) Phase space plot for electron and ion distributions at $t = 0$ for the plasma density of $1.55 \times 10^9 \text{ cm}^{-3}$. X-axis is the distance between left electrode and right electrode, i.e., 0.5 m and the area of electrode is 0.008 m^2 . **(b)** The left electrode is biased by a ramp such that its bias reaches -600 V in 50 ns. It is seen that the entire electron distribution is given a uniform velocity much similar to Fig. (a), but forming an ion matrix sheath. **(c)** The number of electrons and ions lost after 50 ns when the bias reaches its maximum value. The number 5000 is the computer super particles. It shows that even if at 50 ns, a small number of ions are lost to the negative biased electrode. **(d)** Zoom of Fig. (b). 80

Figure 4.13 The sketching of the phase of the plasma relaxation (for different times like at $t = \tau_e$ and $t = \tau_i$) for switching on and off a high negative electrode voltage. 82

Figure 4.14 Variation of amplitude of the rarefaction waves with distance from the exciter for the floating potential measurement. Here $U_0 = -600 \text{ V}$, $n_0 = 1.55 \times 10^9 \text{ cm}^{-3}$ and $\tau_p = 300 \text{ ns}$ 83

Figure 5.1(a) Schematic of the experimental setup. (1) Applied positive pulse. (2) and (15) are the SS rods. (3) High-voltage probe; to measure the voltage signal. (4) Current transformer CT; to measure

the current signal. (5) and (14) are SS rings. (6) Main chamber. (7) Ceramic tube. (8), (9), (12) and (13) are the filaments. (10) Pumping system. (11) Stainless steel disc (metal plate or the exciter); on which pulse is applied. (16) Stainless steel disc (detecting probe); to detect potential disturbances. (17) Filament supply voltage. (18) Discharge voltage. **(b)** The pulse forming circuit. [HV dc Supply = high voltage dc supply (1.5 kV, 500 mA), R_1 = resistor (3 k Ω), C = capacitor, R_2 = load resistor, L = inductor (320 nH), P_1 = metal plate or the exciter]. 93

Figure 5.2 The applied voltage (solid line) and current (dotted line) pulse to the exciter. Here the pulse width $\tau_p=350$ ns ($\tau_p < 3f_i^{-1}$), $U_0=625$ V and $n_0=4 \times 10^9$ cm $^{-3}$ 94

Figure 5.3 The applied voltage (solid line) and current (dotted line) pulse to the exciter. Here the pulse width $\tau_p=2$ μ s ($\tau_p > 3f_i^{-1}$), $U_0=1000$ V and $n_0=4 \times 10^9$ cm $^{-3}$ 95

Figure 5.4 Oscilloscope traces of the potential disturbances measured by the detector from the positive biased exciter. It shows only the second peak propagates with distance from the exciter. The numbers 1-7 show the distances from the exciter. Here pulse width is 350 ns ($\tau_p < 3f_i^{-1}$), $U_0=625$ V and $n_0=4 \times 10^9$ cm $^{-3}$ 96

Figure 5.5 Oscilloscope traces of the potential disturbances for a longer applied pulse width. The numbers 1-7 show the distances from the exciter. Here the pulse width is 2 μ s ($\tau_p > 3f_i^{-1}$), $U_0=625$ V and $n_0=4 \times 10^9$ cm $^{-3}$ 96

Figure 5.6 A plot of distance of virtual source from the exciter as a function of pulse width. Distance of virtual source decreases with increasing pulse width till $\tau_p f_i \approx 3$ and then goes to zero..... 97

Figure 5.7 Time delay vs the detector position for $\tau_p < 3f_i^{-1}$. This plot is for various plasma densities and shows two slopes. It indicates a virtual source around 3 cm from the exciter. It shows that the phase velocity increases with increase in plasma density..... 98

Figure 5.8 Time delay vs the detector position for $\tau_p > 3f_i^{-1}$. This is for various plasma densities and also shows two slopes. Here is no indication of virtual source. 98

Figure 5.9 Time delay vs detector position for various applied pulse magnitude and the pulse width is greater than the thrice of ion plasma response time. It shows the phase velocity is independent of applied pulse magnitude. 99

Figure 5.10 Time delay vs detector position for various applied pulse magnitude and the pulse width is less than the thrice of ion response time..... 99

Figure 5.11 Spatial variation of the disturbances for 350 ns pulse width, which is less than thrice of the ion plasma period. Here $U_0=625$ V and $n_0=4 \times 10^9$ cm $^{-3}$. Potential well structures are observed for L1 and B time scales..... 100

Figure 5.12 Spatial variation of the disturbances for 2 μ s pulse width, which is greater than the thrice of ion plasma period. Here $U_0=625$ V and $n_0=4 \times 10^9$ cm $^{-3}$ 101

Figure 6.1 Schematic of the dielectric layer over a metallic electrode, on which the pulse bias is given..... 110

Figure 6.2 (a) The applied negative voltage (solid line) and total current (dotted line) pulse on the dielectric electrode in the presence of plasma. Here $d_d = 0.8$ mm and $n_0 = 9 \times 10^8$ cm $^{-3}$. **(b)** The total current, vacuum current (capacitive current at vacuum) and the subtracted current (subtraction of vacuum current from the total current). 111

Figure 6.3 (a) The applied positive voltage (solid line) and current (dotted line) pulse on the dielectric electrode. Here $d_d = 0.8$ mm and $n_0 = 9 \times 10^8$ cm $^{-3}$. **(b)** The total current, vacuum current (capacitive current at vacuum) and the subtracted current (subtraction of vacuum current from the total current). 113

Figure 6.4 Oscilloscope traces of the floating potential disturbances measured by the detector from the positive biased dielectric exciter of 0.5 mm thickness. It shows only the second peak propagates with distance from the exciter. The numbers show the distances from the exciter. ϕ is the perturbation potential amplitude. **(a)** Here pulse width is 300 ns ($\tau_p < 3f_i^{-1}$), $U_0=1000$ V and $n_0 = 1.36 \times 10^9$ cm⁻³. **(b)** Here pulse width is 2 μ s ($\tau_p > 3f_i^{-1}$), $U_0=1000$ V and $n_0 = 1.36 \times 10^9$ cm⁻³. 116

Figure 6.5 (a) Time delay vs the detector position for $\tau_p < 3f_i^{-1}$ for the dielectric thickness of 0.5 mm. This plot is for various plasma densities and shows two slopes. It indicates a virtual source around 3 cm from the exciter. **(b)** Time delay vs the detector position for $\tau_p > 3f_i^{-1}$. This is for various plasma densities and also shows two slopes in one direction. Here is no indication of virtual source. 117

Figure 6.6 Time delay vs detector position for various applied pulse magnitude and the pulse width is greater than the thrice of ion plasma response time for the dielectric thickness of 0.5 mm. It shows the phase velocity is independent of applied pulse magnitude. 118

Figure 6.7 Oscilloscope traces of the floating potential signals measured by the detector from the positive biased dielectric exciter of 0.8 mm thickness. Here pulse width is 1 μ s, $U_0= 450$ V and $n_0 = 1.36 \times 10^9$ cm⁻³ 119

Figure 6.8 Time delay vs detector position for various plasma densities for the dielectric thickness of 0.8 mm. 119

Figure 6.9 Time delay vs detector position for various applied pulse magnitude for the dielectric thickness of 0.8 mm. 120

Figure 6.10 Time delay vs detector position for various applied pulse widths for the dielectric thickness of 0.8 mm. 120

Figure 6.11 The electron current drawn for the metal and various dielectric thicknesses. Here $U_0 = 450$ V, $n_0 = 1.36 \times 10^9$ cm⁻³ and $\tau_p = 1$ μ s. 122

Figure 6.12 Oscilloscope traces (floating potential measurements) of the rarefaction disturbances observed at various distances from the dielectric exciter, when a single negative pulse is applied for the dielectric thickness of 0.5 mm. Here $U_0 = -1000$ V, $n_0 = 1.36 \times 10^9$ cm⁻³ and $\tau_p = 300$ ns. 124

Figure 6.13 Time delay versus detector position showing the rarefaction wave speed for various plasma densities. Here $U_0 = -1000$ V and $\tau_p = 2$ μ s. 124

List of Tables

Table 3.1 The sheath thickness, number of electrons displaced from the sheath, the number of electrons lost to the walls, ion plasma period for different pulse durations, applied bias and densities.....	50
Table 3.2 Comparison of number of electrons lost to the wall for various electrode tilt angles. Here $U_0 = -550$ V, $\tau_p = 250$ ns and the electrode diameter is 5 cm.....	54
Table 3.3 Comparison of the percentage of electron loss to the wall between PDP1 simulation and experimental results for various plasma densities and applied voltages. Here 'S' indicates the simulation values and 'E' the experimental values.....	61
Table 4.1 The plasma parameters are varied with filament heating voltage. Here the filament bias potential was -65 V and pressure was 1×10^{-3} mbar.....	69
Table 6.1 Ion and electron charges for various plasma densities for both negative and positive pulse bias. The charges can be calculated from the integration of the current pulses, i.e., the area under the curve. Here $d_d = 0.8$ mm.....	112
Table 6.2 Summary of the observed results for positive and negative pulse bias to the dielectric electrode for various parameters.....	125

CHAPTER 1

1 Introduction

1.1 Introduction and Motivation

In the late 1920s, Irving Langmuir was studying the un-usual magnetic and electric characteristics of super-heated gases [1]. He coined the term ‘Plasma’ to describe the ionized particles. A plasma is a collection of free charged particles (and neutral particles) moving in random directions that is, on the average, electrically neutral. Much of the matter in the universe (99%) is in the plasma state [2]. This is true because stars, as well as most interstellar matter, are plasmas. Although stars are plasmas in thermal equilibrium and fully ionized, this is different from laboratory plasmas (non-thermal and fractionally ionized). Plasma is more complex than we think, which can be expressed *temporally* as well as *spatially*. It is predominantly characterized by the excitation of an enormous variety of collective dynamical modes.

Langmuir, along with his colleague Lewi Tonks [3] was investigating the physics and chemistry of tungsten-filament light-bulbs, with a view to finding a way to greatly extend the lifetime of the filament (a goal which he eventually achieved). In the process, he developed the theory of *plasma sheaths* – the boundary layers which form between ionized plasmas and solid surfaces. He also discovered that certain regions of a plasma discharge tube exhibit periodic variation of the electron density, which is known as Langmuir waves. This was the genesis of plasma physics. Interestingly enough, Langmuir’s research now-a-days forms the basis of most plasma processing techniques for fabricating integrated circuits. After Langmuir, plasma research gradually spread in other directions, of which six are particularly significant.

Chapter 1: Introduction

- (a) Firstly, the development of radio broadcasting led to the discovery of the Earth's ionosphere, a layer of partially ionized gas in the upper atmosphere which reflects radio waves, and is responsible for the fact that radio signals can be received when the transmitter is over the horizon. Unfortunately, the ionosphere also occasionally absorbs and distorts radio waves. For instance, the Earth's magnetic field causes waves with different polarizations (relative to the orientation of the magnetic field) to propagate at different velocities, an effect which can give rise to "ghost signals" (i.e., signals which arrive a little before, or a little after, the main signal). In order to understand, some of the deficiencies in radio communication, various scientists, such as, K. G. Budden [4], systematically developed the theory of electromagnetic wave propagation through non-uniform magnetized plasmas.
- (b) Secondly, astrophysicists quickly recognized that much of the universe consists of plasma. The pioneer in this field was H. Alfvén, who around 1940 developed the theory of *magnetohydrodynamics* or MHD, in which plasma is treated essentially as a conducting fluid. This theory has been both widely and successfully employed to investigate sunspots, solar flares, the solar wind, star formation, etc. Two topics of particular interest in MHD theory are *magnetic reconnection* and *dynamo theory*. Magnetic reconnection is a process by which magnetic field lines suddenly change their topology: it can give rise to the sudden conversion of a great deal of magnetic energy into thermal energy, as well as the acceleration of some charged particles to extremely high energies, and is generally thought to be the basic mechanism behind solar flares. Dynamo theory studies how the motion of an MHD fluid can give rise to the generation of a macroscopic magnetic field.
- (c) Thirdly, the creation of the hydrogen bomb in 1952 generated a great deal of interest in *controlled thermonuclear fusion* as a possible power source for the future. Not surprisingly, fusion physicists are mostly concerned with understanding how a thermonuclear plasma can be trapped – in most cases by a magnetic field – and investigating the many plasma instabilities which may allow it to escape.
- (d) Fourthly, James A. Van Allen's discovery in 1958 of the Van Allen radiation belts surrounding the Earth, opened up the field of space plasma physics. Space scientists borrowed the theory of plasma trapping by a magnetic field from fusion research and the theory of plasma waves from ionospheric physics.
- (e) Fifthly, the development of high powered lasers in the 1960's opened up the field of *laser plasma physics*. When a high powered laser beam strikes a solid target, material

Chapter 1: Introduction

is immediately ablated and a plasma forms at the boundary between the beam and the target. One interesting application of the laser plasma physics is the use of the extremely strong electric fields generated when a high intensity laser pulse passes through a plasma to accelerate particles. High energy physicists hope to use plasma acceleration techniques to dramatically reduce the size and cost of particle accelerators.

- (f) Finally, the use of plasma processing technology to modify the surface properties of materials. Plasma-based surface processes are critical for manufacturing the very large scale integrated circuits, aerospace, steel, biomedical and toxic waste management industries.

Similar like laser plasma interaction, researches are carried out for the interaction of electron beam, ion beam and transient pulses with plasmas in the field of plasma waves. The present thesis reports on experimental investigation of plasma response to transient high negative and positive voltage pulses in a low pressure unmagnetized argon plasma. The main aim is to study the excitation and propagation characteristics of electrostatic waves, particle balance in plasmas during pulse biasing, wave excitation after pulse withdrawal, and wave excitation using capacitive coupling. The experiments are performed using single pulse excitation.

When a metallic electrode is immersed in a low pressure plasma and biased by a high negative voltage pulse, in the time scale of electron plasma period, the electrons are repelled from the vicinity of the electrode, leaving behind a uniform ion-matrix or transient sheath. Subsequently in the time scale of ion plasma period, the ions start accelerating towards the negative biased electrode and impinge into the electrode. Now the sheath expands due to the uncovered ions from the bulk plasma. For a negative biased electrode, the basic fundamentals as well as application wise studies have been carried out. The fundamental studies are like excitation and propagation of ion and electron waves, while the applications are the surface modification of materials. Plasma immersion ion implantation [5] is a novel technique for the surface medication in processing plasmas. For both fundamentals and applications, the applied pulse width to the electrode is much greater than the ion plasma period. We want to do such type of basic experiments, but for the applied pulse width is less than the ion plasma period. For this case:

Chapter 1: Introduction

- (a) What happens to electrons during the negative pulse bias? (It is presumed that electrons would be repelled; but are the electrons near the vicinity of the electrode only repelled leaving electrons in the bulk plasma unaffected or both are affected.)
- (b) Is there any excitation of electrostatic waves? (Though the applied pulse width is less than the ion plasma period, the propagation of ion rarefaction waves is observed.)

Many experiments have been done for the excitation of electrostatic waves, such that ion acoustic waves (solitons) or electron acoustic waves (solitons). Mainly all these waves are excited using mesh grids and in double plasma (DP) devices. We have observed ion rarefaction waves for the negative bias to a metallic disc electrode. When the disc electrode is positive biased, totally different results are obtained, i.e., solitary electron holes. Here the applied pulse width is varied from less than to greater than ion plasma period. For the applied pulse width less than the thrice of ion plasma period, we observed the presence of a virtual source, which is first time observed in our experiment.

A very few experiments and theoretical models have been reported for when a dielectric material is immersed in a plasma and biased pulsed negative. Only dielectric charging effect and surface modification are described in the models and experiments. There is no study on excitation of some kind of plasma waves from the dielectric material. In our experiments we have used Kapton as dielectric material and some electrostatic waves are excited. These waves are dependent on dielectric thickness and applied pulse polarity. From the dielectric thickness of 0.1-0.5 mm, solitary electron holes are excited and from 0.6-0.9 mm thickness, solitary ion holes are excited for the positive pulse bias. For negative pulse bias, ion rarefaction waves are excited from 0.1-0.9 mm dielectric thickness. First time we observed such type of electrostatic waves from a dielectric material. Above 0.9 mm dielectric thickness no signals are excited for both positive and negative pulse bias.

1.2 Basics of Plasma Sheath

1.2.1 Sheath

Plasma consists of equal numbers of positive ions and electrons and the electrons are far more mobile than the ions. The plasma will therefore charge positively with respect to a

Chapter 1: Introduction

grounded wall. The non-neutral potential region between the plasma and the wall is called a sheath, which is shown in Fig. 1.1.

In a weakly ionized plasma the energy to sustain plasma is generally heating of electrons by the source, while the ions are at equilibrium with the background gas. The electron temperature is typically of few eV. The ions are accelerated through the sheath potential, while the electron density decreases according to a Boltzmann factor [2]. The electron density would then decay on the order of a Debye length (λ_D) to shield the electrons from the wall.

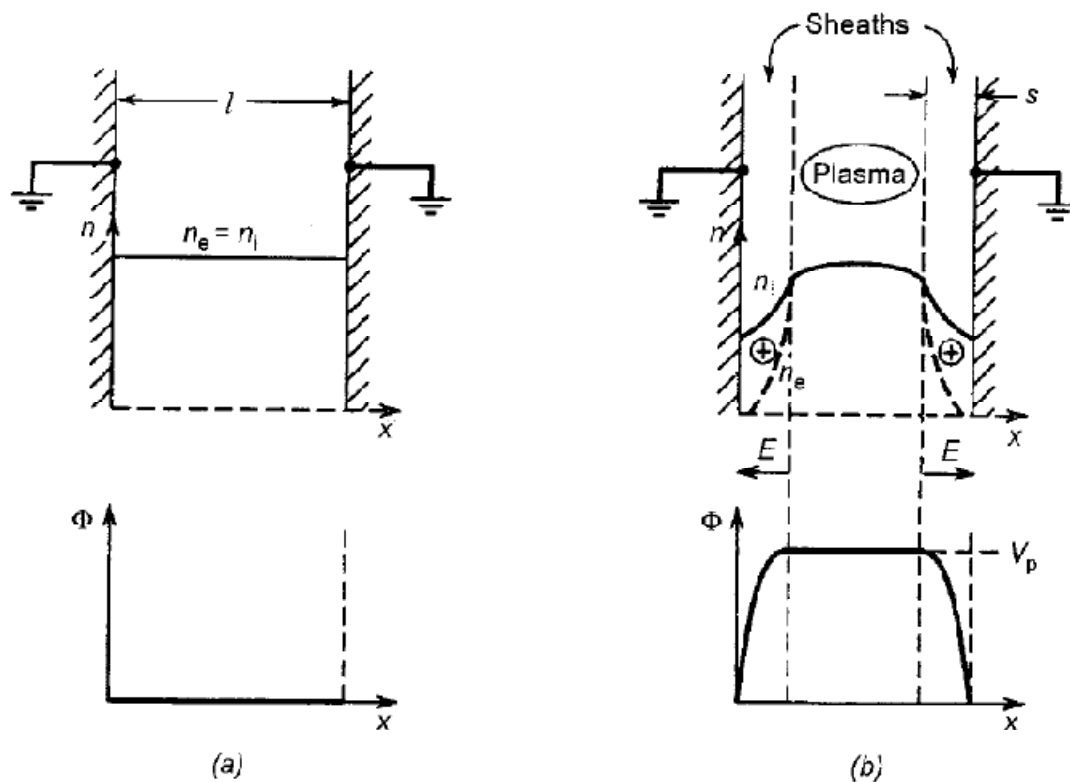


Figure 1.1 Formation of ion sheath. (a) initial ion and electron density and (b) densities, electric field and potential after the formation of sheath [6]. Here l is the plasma length, n_e and n_i are the electron and ion densities respectively, s is the sheath thickness, ϕ is the wall potential, V_p is the plasma potential and E is the electric field.

1.2.2 Presheath

A transition layer or presheath exists between the neutral plasma and the non-neutral sheath in order to maintain the continuity of ion flux, giving rise to an ion velocity at the

Chapter 1: Introduction

plasma-sheath edge known as the Bohm velocity. So, there must exist a finite electric field in this presheath region to give ions the directed velocity. Hence the presheath region is not strictly field free, although \mathbf{E} is very small there. At the sheath-presheath interface there is a transition from subsonic to supersonic ion flow, where the condition of charge neutrality must break down. The schematic of the presheath is given in Fig. 1.2.

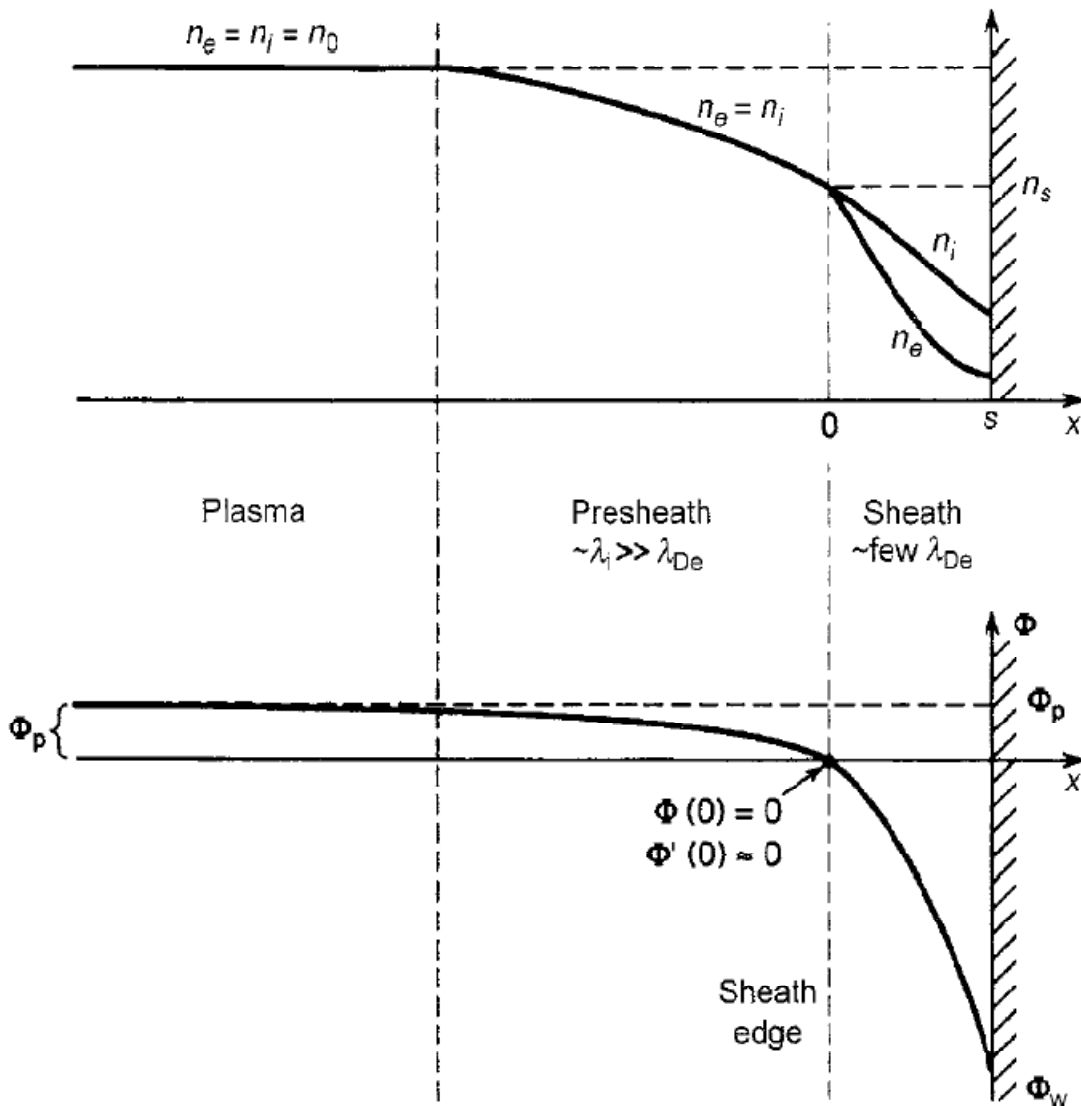


Figure 1.2 Qualitative behavior of sheath and pre-sheath in contact with the wall [6].

1.2.3 High-Voltage Sheaths

When a sudden negative voltage $-U_0$ is applied to a metallic electrode, electrons near the surface are driven away on a time scale of order the inverse electron plasma frequency,

Chapter 1: Introduction

leaving the ions behind to form an *ion matrix sheath* or *transient sheath*, that is, an electron-depleted sheath of not yet accelerated ions. Subsequently, on a time scale of order the inverse ion plasma frequencies, ions within the sheath are accelerated into the electrode. The consequent drop in ion density in the sheath drives the sheath-plasma edge further away, exposing new ions to the accelerating electric field of the sheath and causing these ions to be implanted. The time evolution of the transient sheath determines the implantation current and the energy distribution of implanted ions. On a longer time scale, the system evolves toward a steady-state Child law sheath, with the sheath thickness (s) given by

$$s = \frac{\sqrt{2}}{3} \lambda_D \left(\frac{2U_0}{T_e} \right)^{3/4},$$

where λ_D is Debye length and T_e is the electron temperature and the Child law current (implantation current) density across the sheath is

$$j_C = \frac{4}{9} \epsilon_0 \left(\frac{2e}{M} \right)^{1/2} \frac{U_0^{3/2}}{s^2}.$$

where M is the ion mass, e is the electron charge and ϵ_0 is the permittivity of free space.

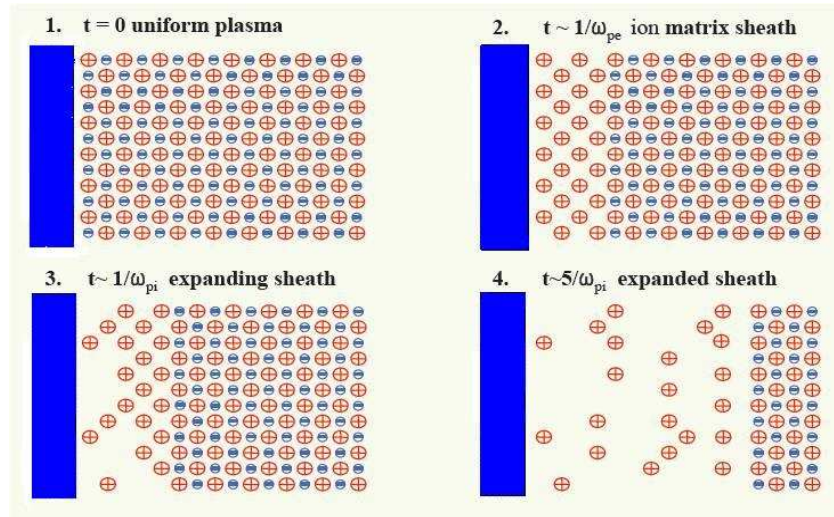


Figure 1.3 Qualitative behavior of the transient sheath [6]. Here ω_{pe} and ω_{pi} are the electron and ion plasma frequency respectively.

Chapter 1: Introduction

The simplest high-voltage sheath, with a uniform ion density, is known as a matrix sheath. Letting $n_i = n_s = \text{const}$ within the sheath of thickness s_0 and choosing $x = 0$ at the plasma-sheath edge ($\Phi = 0$), then from Poisson's equation

$$\frac{dE}{dx} = \frac{en_s}{\epsilon_0}$$

which yields a linear variation of \mathbf{E} with x :

$$E = \frac{en_s}{\epsilon_0} x$$

Integrating $d\Phi/dx = -\mathbf{E}$, we obtain a parabolic profile

$$\Phi = -\frac{en_s}{\epsilon_0} \frac{x^2}{2}$$

Setting $\Phi = -U_0$ at $x = s_0$, we obtain the ion matrix sheath thickness

$$s_0 = \left(\frac{2\epsilon_0 U_0}{en_s} \right)^{1/2}.$$

1.3 An Overview of Electrostatic Waves

Unmagnetized plasmas are generally the first to be studied because they are isotropic, i.e. the properties are the same in all directions. Plasma can support a great variety of wave motion. Both high frequency and low frequency electromagnetic and electrostatic waves may propagate in plasma. Primarily, the thesis emphasizes on the study of electrostatic waves.

Ion acoustic waves (IAWs) are low frequency pressure waves in plasmas. An IAW is like a sound wave in air. IAWs, unlike sound waves, have an oscillating electric field, which arises because of charge separation due to the different masses of ions and electrons. IAW is one of the most well studied electrostatic modes in plasmas experimentally and theoretically. It has been extensively studied in both linear and nonlinear regimes in different plasma environments [7-9]. The low frequency IAWs in unmagnetized plasmas are studied by considering the ions to be dynamic while electrons are Boltzmann distributed. The excitation

Chapter 1: Introduction

of the IAW in collisionless plasma was studied first in late 1970s and early 1980s, by using whistler waves [10-11] and Pottelette [12] also reported the excitation of the IAW by the slow ion beam. The experiments by Honzawa and Nagasawa [13] suggested that the fast ion beam can limit the amplitude of the ion acoustic solitons. It has shown that the ion beam plays an important role in the excitation of the linear as well as nonlinear IAWs [14]. Castro et al. [15] have reported a new technique for creating controlled density perturbations to excite IAWs in an ultra-cold neutral plasma and have measure their dispersion relation.

The ion acoustic solitary wave is one of the fundamental nonlinear wave phenomena appearing in fluid dynamics [16] and plasma physics [17]. The evolution of small but finite amplitude solitary waves is studied by means of Korteweg-de Vries (KdV) equation. Wakil et al. [18] have studied the IAWs for a system of collisionless plasma using the time fractional KdV equation. The density compressions solitary structures are found to exist in the supersonic regime for nonlinear IAW in the usual electron-ion plasma case [17]. However, the density rarefactive ion acoustic solitary structures have been observed by S3-3 and Viking satellites along the auroral magnetic field [19]. Honzawa [20] has reported the excitation of solitary wave by applying a negative potential pulse in double plasma device. Honzawa [21] has also studied the interaction between two ion acoustic solitons using a technique of double-pulse excitation. Different theoretical models have been proposed to explain the formation of ion acoustic rarefactive solitary structures with two-electron population plasmas [22]. Bailung et al. [23] have studied the propagation characteristics of rarefactive solitons excited in a multi-component plasma with negative ions in the presence of a positive ion beam in a double plasma device. The propagation characteristics of rarefactive ion acoustic solitary waves in a dusty plasma containing negative ions has been observed experimentally by Adhikary et al. [24].

Moiseev and Sagdeev [25] have predicted that a laminar ion acoustic shock with an oscillatory structure could be formed in a collisionless plasma with hot electrons and cold ions and with a small dissipation. However, Montgomery and Joyce [26] have indicated theoretically that a laminar monotonic shock solution is possibly constructed in a collisionless plasma by the introduction of a population of trapped electrons, even if no dissipative effects are taken into account. Taylor et al. [27] have reported an observation of laminar ion acoustic shocks with trailing oscillations, which showed a possibility that electrons in such shocks can include the trapped component and hence become non-isothermal, in particular, at large amplitudes. Honzawa [28] has shown that a successful separation of trapped and un-trapped

Chapter 1: Introduction

electron distributions in ion acoustic shocks. The effect of the relativistic ponderomotive force and trapped particles in the presence of ponderomotive force on the rarefaction shock waves are studied by Niknam et al. [29]. Also a review on IAWs is given in chapter 4.

Plasmas support a great variety of coherent nonlinear structures [30]. These include shocks, double layers, bare solitons (or solitary waves), envelop solitons, vortices etc. Coherent nonlinear structures in plasmas involve dispersion and nonlinearities together with collisionless and collisional dissipation. Fluid and kinetic models are frequently used to investigate the formation and dynamics of numerous nonlinear structures which are observed in both laboratory and space plasmas. While in a fluid treatment one considers macroscopic aspects, a kinetic treatment provides the possibility of microscopic plasma behavior including the wave-particle interactions. Coherent nonlinear structures involving the latter are referred to as Bernstein-Greene-Kruskal (BGK) modes [31], which appears in plasma with non-isothermal distribution functions and finite amplitude electrostatic and electromagnetic fluctuations.

The electron and ion holes are BGK modes in which a population of charged particles (electrons and ions) is trapped in a self-created electrostatic potential which is positive for the electron hole and negative for the ion hole. Associated with the electron hole there is a depletion of the electrons at the centre of the hole, while the ion hole is associated with a depletion of both the ion and electron number densities; the latter are due to the negative potential of the ion hole which repels the electrons locally. The existence of ion hole is possible only if the electron temperature is sufficiently large than the ion temperature, so that electrons can form a high pressure background, which doesn't neutralize the ion density depletion of the ion hole. Generally speaking, the electron and ion holes are saturated states of two-stream unstable collisionless (or weakly collisional) plasma in which the fluctuation growth is halted by the particle trapping in the wave potential. The trapping of plasma particles implies that the electron and ion holes are not amenable to macroscopic descriptions like the magnetohydrodynamic or other fluid descriptions. The Vlasov/Boltzmann picture has to be adopted for studying BGK modes in plasma where the distribution functions of charge particles are non-Maxwellian.

The pioneering work of Bernstein, Greene and Krushkal led Dory [32] and Roberts and Berk [33] to carry out computer simulations of the dynamics of linearly unstable electron modes in one-dimensional (1D) electron plasma with a fixed ion background. They followed

Chapter 1: Introduction

the motion of the phase space boundaries of an incompressible and constant-density phase space fluids, and observe the formation and condensation of electron holes, leading to long lived nonlinear structures composed of depleted electron densities and rotating vortices in phase space of trapped particles around the holes. Numerical and theoretical studies of the interaction between the electron and ion holes have been performed by several authors. Newman et al. [34] studied numerically the dynamics and instability of 2D phase-space tubes, whereas Daldorff et al. [35] investigated the formation and dynamics of ion holes in three dimensions. Krasovsky et al. [36] showed theoretically and by computer simulations that the electron holes perform inelastic collisions. Vetoulis and Oppenheim [37] studied the radiation generation due to bounce resonances in electron holes. Guio et al. [38-39] investigated numerically the dynamics of phase space vortices in a collisionless plasma, as well as the generation of phase space structures by an obstacle in a streaming plasma. Saeki and Genma [40] examined the disruption of electron holes in an electron-ion plasma. Dupree [41] found that the BGK mode is the most probable state for turbulent fluctuations which create self-trapping structures in a weakly turbulent plasma. It has also been pointed out that plasma waves can be undamped due to particle trapping effects in waves with arbitrarily small amplitudes [42-43]. Theoretical investigations of trapped particle effects in a magnetized plasma show that trapped ions influence strongly the electromagnetic ion-cyclotron waves [44].

About three decades ago, Schamel presented theories for electron and ion holes [45-49]. The model used by Schamel has been used in theoretical investigations for establishing existence criteria [49], and for determining the stability of the electron and ion holes [43, 48, 50]. Similar to the ion acoustic waves in an electron-ion plasma [51], a modified KdV equation [52-53] can be derived for the dynamics of the electron and ion holes in the small amplitude limit, but with a stronger nonlinearity due to the trapped particles [43].

The existence of electron and ion holes has been demonstrated in both laboratory experiments and by satellites in the Earth's ionosphere and magnetosphere. In laboratory experiments, the formation and dynamics of solitary electron holes [54-55] and ion holes [56-57], as well as accelerated periodic ion holes [58] have been observed. Coherent nonlinear structures, often called electrostatic solitary waves (ESWs), are ubiquitous in the Earth's magnetosphere and in the interplanetary space. The ion holes (or ion solitary waves) were detected first by the S3-3 [59] and Viking [60] spacecrafts, and recently the high resolution measurements by the POLAR [61] and FAST (Fast Auroral SnapshoT) [62] satellites have

Chapter 1: Introduction

provided data about velocity and 3D spatial structures. They have been observed mostly in the low altitude auroral zone, which is strongly magnetized and characterized by strong upward currents carried by ion beams travelling at 100-400 km/s. Also a literature survey on electron and ion holes is given in Chapters 5 and 6.

1.4 Outline of the Thesis

In this thesis, we have addressed the important issues related to plasma sheath and the excitation of new kind of electrostatic waves. In particular, we have investigated the nonlinear ion rarefaction waves, electron and ion holes experimentally.

Chapter 2 is concerned with the experimental setup, instrumentation, different diagnostics, plasma production and plasma characterization. It provides the description of the vacuum chamber, pumping unit and filament configuration. The main diagnostics like Langmuir probe, emissive probe and their circuitry for biasing is explained. The plasma production from thoriated tungsten filaments is described and the plasma parameters like electron temperature, plasma density, etc. are measured by a disc Langmuir probe. Also the pulse forming circuit is explained in this chapter.

Chapter 3 focuses on the plasma response during a high negative pulse bias to a conducting electrode. Here the applied pulse width is less than the ion plasma period (inverse of ion plasma frequency). During the pulse bias, the properties of the ejected electrons from the vicinity of the electrode are studied and the experimental results are compared with computer simulation results. In this chapter, generally, the ejected electrons lost to the chamber wall during the bias are estimated and the origin of these lost electrons is also investigated. In this Chapter, PDP1 code is used for computer simulation and the simulation results have a good agreement with the experimental results.

Chapter 4 investigates the excitation and propagation of ion rarefaction waves after the removal of the pulse bias on the conducting electrode. Though the applied pulse width is less than the ion plasma period, if the pulse magnitude is large enough (much greater than the electron temperature) then a rarefaction wave can be excited. So the excitation of a wave can depend upon the pulse width as well as the pulse magnitude. The mechanism of the excitation of ion rarefaction waves is correlated with nonambipolar diffusion.

Chapter 1: Introduction

Chapter 5 studies on the plasma response during a high positive pulse bias to a conducting electrode. In this Chapter a new kind of electrostatic wave, i.e., solitary electron holes are excited. Here the applied pulse width is varied from less than ion plasma period to greater than ion plasma period. When the pulse width is less than the thrice of ion plasma period, a virtual source is present there. The existence and identification of solitary electron holes are explained in this chapter.

Chapter 6 focuses on the plasma response during the both high positive and negative pulse bias to a metallic electrode covered by a dielectric film. Experiments are carried out for different plasma parameters, to find how the plasma perturbations propagate for various applied pulse widths ion comparison to ion plasma period. For the positive pulse bias, solitary electron and ion holes are excited depending on charging of dielectric. For the negative pulse bias ion rarefaction waves are excited. On or above 1 mm dielectric thickness, there is no excitation of waves.

Chapter 7 provides a summary and conclusion of this thesis. An attempt is made to identify issues that merit future investigations.

1.5 References

- [1] R. Fitzpatrick, “The Physics of Plasmas”, The University of Texas at Austin.
- [2] F. F. Chen, “Introduction to Plasma Physics and Controlled Fusion”, Springer, New York (1983).
- [3] L. Tonks and I. Langmuir, Phys. Rev. **33**, 195 (1929).
- [4] K. G. Budden, “Radio Waves in the Ionosphere”, Cambridge University Press, Cambridge, UK (1961).
- [5] J. R. Conrad, J. L. Radtke, R. A. Dodd, F. J. Worzala, and N. C. Tran, J. Appl. Phys. **62**, 4591 (1987).
- [6] B. P. Wood et al., in Handbook of Plasma Immersion Ion Implantation and Deposition, edited by A. Anders (John Wiley & Sons, INC. 2000), Chap. 2 & 4.
- [7] H. Washimi and T. Tanuiti, Phys. Rev. Lett. **17**, 996 (1966).
- [8] S. Mahmood and H. Saleem, Phys. Plasmas **9**, 724 (2002).
- [9] W. Masood, N. Jehan, A. M. Mirza and P. H. Sakanaka, Phys. Lett. **371A**, 4279 (2008).
- [10] M. S. Sodha, T. Singh, D. P. Singh and R. P. Sharma, **25**, 255 (1981).
- [11] J. E. Willett, Phys. Lett. **90A**, 45 (1982).
- [12] R. Pottelette and J. M. Illiano, Phys. Lett. **91A**, 351 (1982).
- [13] T. Honzawa and T. Nagasawa, Phys. Plasmas **4**, 3954 (1997).
- [14] Y. Li, J. X. Ma, Y. Li, D. Xiao and K. E. Lonngren, Phys. Lett. **358A**, 297 (2006).
- [15] J. Castro, P. McQuillen and T. C. Killian, Phys. Rev. Lett. **105**, 065004 (2010).
- [16] G. Whitham, “Linear and Nonlinear Waves”, New York, Wiley (1974).
- [17] R. Davidson, “Methods in Nonlinear Plasma Theory”, New York, Academic Press (1972).
- [18] S. A. El-Wakil, E. M. Abulwafa, E. K. El-Shewy and A. A. Mahmoud, Chin. Phys. **20B**, 040508 (2011).
- [19] M. Bertomier, R. Pottelette and M. Malingre, J. Geophys. Res. **103**, 4261 (1998).
- [20] T. Honzawa, Plasma Phys. Control. Fusion **26**, 1251 (1984).
- [21] T. Honzawa, Plasma Phys. Control. Fusion **26**, 459 (1984).
- [22] W. Masood, S. Hussain, S. Mahmood and A. M. Mirza, Chin. Phys. Lett. **26**, 122301 (2009).
- [23] H. Bailung, S. K. Sharma and Y. Nakamura, Phys. Plasmas **17**, 062103 (2010).
- [24] N. C. Adhikary, M. K. Deka and H. Bailung, Phys. Plasmas **16**, 063701 (2009).
- [25] S. Moiseev and R. Z. Sagdeev, J. Nucl. Energy, Part **C5**, 43 (1963).

Chapter 1: Introduction

- [26] D. Montgomery and G. Joyce, *J. Plasma Phys.* **3**, 1 (1969).
- [27] R. J. Taylor, D. R. Baker and H. Ikezi, *Phys. Rev. Lett.* **24**, 206 (1970).
- [28] T. Honzawa, *Phys. Fluids* **31**, 1766 (1988).
- [29] A. R. Niknam, M. Hashemzadeh, B. Shokri and M. R. Rouhani, *Phys. Plasmas* **16**, 122109 (2009).
- [30] R. Z. Sagdeev, *Rev. Mod. Phys.* **51**, 11 (1979).
- [31] I. B. Bernstein, J. M. Greene and M. D. Kruskal, *Phys. Rev.* **108**, 546 (1957).
- [32] R. A. Dory, *J. Nucl. Energy, Part C Plasma Phys.* **6**, 511 (1964).
- [33] K. V. Roberts and J. L. Berk, *Phys. Rev. Lett.* **19**, 297 (1967).
- [34] D. L. Newman, M. V. Goldman, M. Spector and F. Perez, *Phys. Rev. Lett.* **86**, 1239 (2001).
- [35] L. K. S. Daldorff, P. Guio, S. Børve, H. L. Pécseli and J. Trulsen, *Europhys. Lett.* **54**, 161 (2001).
- [36] V. L. Krasovsky, H. Matsumoto and Y. Omura, *Nonlinear Proc. Geophys.* **6**, 205 (1999).
- [37] G. Vetoulis and M. Openheim, *Phys. Rev. Lett.* **86**, 1235 (2001).
- [38] P. Guio, S. Børve, L. K. S. Daldorff, J. P. Lynov, P. Michelsen, H. L. Pécseli, J. J. Rasmussen, K. Saiki and J. Trulsen, *Nonlinear Proc. Geophys.* **10**, 75 (2003).
- [39] P. Guio and H. L. Pécseli, *Geophys. Res. Lett.* **31**, L03806/1-4 (2004).
- [40] K. Saeki and H. Genma, *Phys. Rev. Lett.* **80**, 1224 (1998).
- [41] T. H. Dupree, *Phys. Fluids* **25**, 277 (1982).
- [42] J. P. Holloway and J. J. Dorning, *Phys. Rev.* **44A**, 3856 (1991).
- [43] H. Schamel, *Phys. Plasmas* **7**, 4831 (2000).
- [44] H. Abbasi, N. L. Tsintsadze and D. D. Tskhakaya, *Phys. Plasmas* **6**, 2373 (1999).
- [45] H. Schamel, *Plasma Phys.* **13**, 491 (1971).
- [46] H. Schamel, *Plasma Phys.* **14**, 905 (1972).
- [47] H. Schamel, *Physica Scripta* **20**, 336 (1979).
- [48] H. Schamel, *Phys. Rep.* **140**, 161 (1986).
- [49] S. Bujarbarua and H. Schamel, *J. Plasma Phys.* **25**, 515 (1981).
- [50] H. Schamel, *Phys. Rev. Lett.* **48**, 481 (1982).
- [51] L. Stenflow, N. L. Tsintsadze and T. D. Buadze, *Phys. Lett.* **135A**, 37 (1989).
- [52] R. Fedele, *Phys. Scripta* **65**, 502 (2002).
- [53] R. Fedele and H. Schamel, *Euro Phys. J.* **27B**, 313 (2002).
- [54] K. Saiki, P. Michelsen, H. L. Pécseli and J. J. Rasmussen, *Phys. Rev. Lett.* **42**, 501 (1979).

Chapter 1: Introduction

- [55] G. Petraconi and H. S. Maciel, *J. Phys. D: Appl. Phys.* **36**, 2798 (2003).
- [56] H. L. Pécseli, J. Trulsen and R. J. Armstrong, *Phys. Lett.* **81A**, 386 (1981).
- [57] H. L. Pécseli, J. Trulsen and R. J. Armstrong, *Phys. Scripta* **29**, 241 (1984).
- [58] C. Franck, T. Klinger, A. Piel and H. Schamel, *Phys. Plasmas* **8**, 4271 (2001).
- [59] M. Temerin, K. Cherny, W. Lotko and F. S. Mozer, *Phys. Rev. Lett.* **48**, 1175 (1982).
- [60] R. Boström, G. Gustafsson, B. Holback, G. Holmgren, H. Koskinen and P. Kintner, *Phys. Rev. Lett.* **61**, 82 (1988).
- [61] C. Cattell, J. Crumley, J. Dombeck, J. Wygant and F. S. Mozer, *Geophys. Res. Lett.* **29**, 1065 (2002).
- [62] J. P. McFadden, C. W. Carlson, R. E. Ergun, F. S. Mozer, L. Muschietti, I. Roth and E. Moebius, *J. Geophys. Res.* **108**, 8018 (2003).

CHAPTER 2

2 Experimental Set-up and Diagnostics

2.1 Introduction

The experiments presented in this thesis work have been performed in a low pressure argon plasma. Experiments are carried out to study the plasma response to transient high voltage pulses in a uniform and unmagnetized plasma. This chapter provides the detailed description of experimental set up, the diagnostics used for characterizing the plasma, pulse forming circuit, plasma production and plasma characterization.

The chapter is organized as follows. Section **2.2** describes the experimental device and the pumping system. Section **2.3** describes the method of plasma production. In Sec. **2.4** different diagnostics are described for the characterization of plasma, followed by the plasma characterization in Sec. **2.5**. Pulse forming circuit is discussed in Sec. **2.6**. Finally a list of references is given.

2.2 Experimental Set-up

In this Section, the experimental set-up used for the excitation of some collective phenomena in a plasma medium is discussed. The set-up mainly consists of a vacuum vessel, a pumping unit, filaments, power supply etc. and these are described in the following sub-sections.

2.2.1 Chamber and Pumping System

The entire sets of experiments were carried out in a cylindrical vacuum chamber, shown in Figures 2.1 and 2.2. The vacuum chamber is made of stainless steel (SS-304) of 50 cm length and 29 cm in diameter. The chamber has four radial ports of 9 cm in diameter, two axial ports of 13 cm in diameter and eight 10 KF couplers that were used for diagnostics, pumping, connection of gauges, introducing gas into chamber, feeding power to the filaments, viewing, etc..

The chamber was pumped down to a base pressure of 5×10^{-5} mbar using a combination of rotary pump (pumping speed = 250 lit/min) and diffusion pump (pumping speed = 500 lit/sec). The Pirani gauge was used to measure the high pressure inside the chamber and the Penning gauge was used to measure the low pressure. The chamber was filled with argon gas (99.999% pure) by a precision gas dosing valve (Balzers made) at a working pressure (P) of 1×10^{-3} mbar.

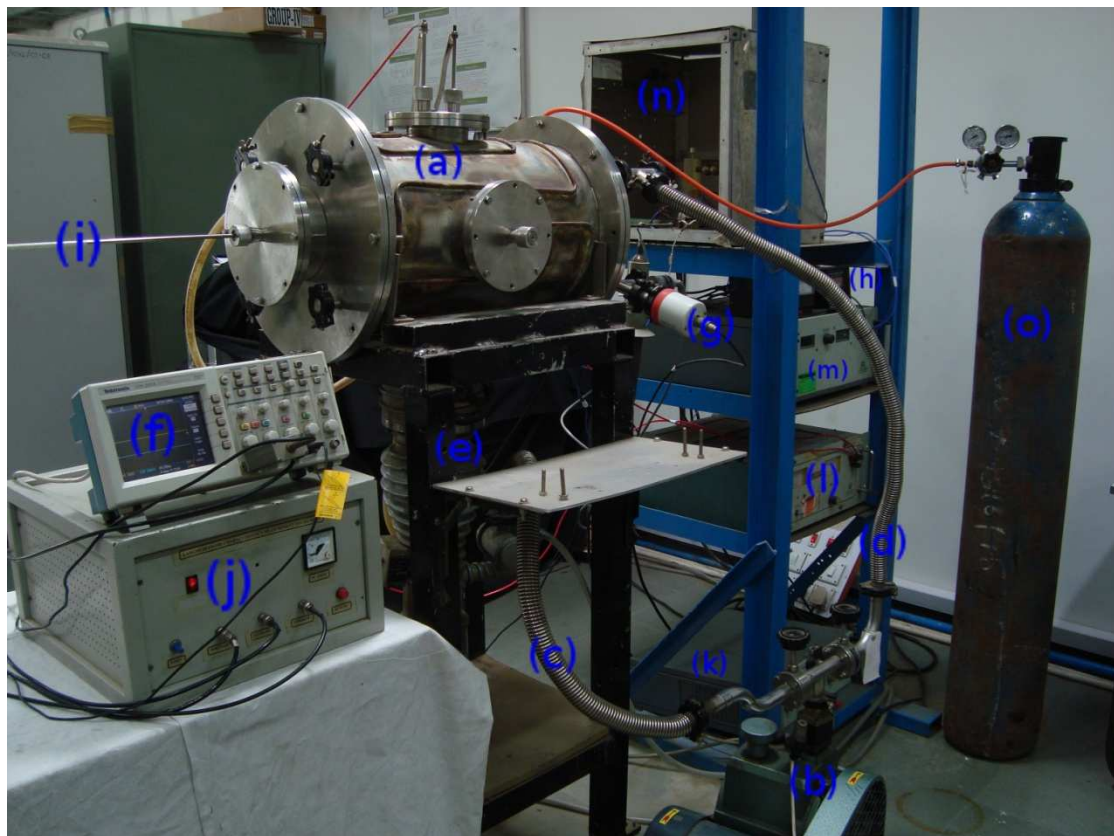


Figure 2.1 Photograph of the experimental set-up. (a) Vacuum chamber. (b) Rotary pump. (c) & (d) are bellows. (e) Diffusion pump. (f) Oscilloscope. (g) Penning gauge head. (h) Penning and Pirani gauge. (i) Langmuir probe shaft. (j) Langmuir probe power supply. (k) Filament heating power supply. (l) Filament bias power supply. (m) High voltage dc power supply. (n) Pulse forming circuit. (o) Argon gas cylinder.

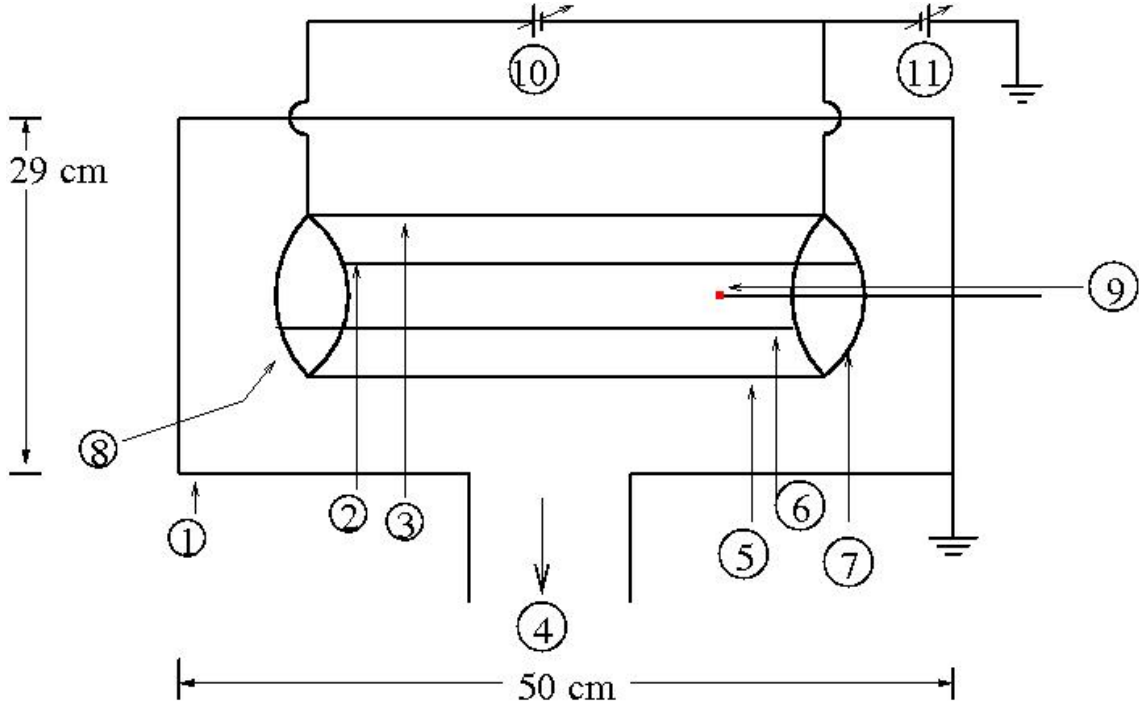


Figure 2.2 Schematic of the experimental set-up. (1) Vacuum chamber. (2), (3), (5) and (6) are the filaments. (4) Pumping system. (7) and (8) are the SS rings. (9) is the Langmuir probe. (10) Filament heating voltage. (11) Discharge voltage.

Such a working pressure is chosen, so that at 1×10^{-3} mbar, the electron-neutral collision mean free path is greater than the vacuum chamber dimension, forming a collisionless plasma. The mean free path can be calculated from the below equation

$$\lambda = \frac{1}{n_n \sigma}$$

where n_n is the gas neutral density and σ is the neutral atom cross-section. For a working pressure of 1×10^{-3} mbar, the base pressure should be significantly lower than the working pressure. The base pressure can be taken as 5×10^{-5} mbar, because at this low pressure the residual gas composition [1] is low and mainly of H_2 originating from the metal walls of the vacuum chamber. Such a high vacuum is required to keep reactive gases out of process and to reduce the number of atom/molecule collisions.

First we should discuss the raise of pumping speed number. Pumping speed is one of the important quantities that govern the behavior of all vacuum systems. The relationship can be written as [1]

Chapter 2: Experimental Set-up and Diagnostics

$$Q = S \times P_b$$

where Q is the gas load or throughput, S is the pumping speed and P_b is the base pressure. Gas load is referred to as mass flow while pumping speed is referred to as volume flow. Mass flow is the total number of molecules that a pump has to deal with and volume flow as the volume of gas, a pump can draw at a given pressure. The gas load can be written as [2]

$$Q = R \times A$$

where R is the out-gassing rate of material and A is the surface area of the vacuum chamber. Out-gassing rate of stainless steel 304 is 8.5×10^{-7} mbar lit s⁻¹ cm⁻² [2] and surface area of the vacuum chamber is 5.87×10^3 cm². Due to surface roughness and the presence of several ports, A can be doubled, i.e., 1.17×10^4 cm². Now at base pressure 5×10^{-5} mbar, the pumping speed would be 200 lit/sec. Keeping margin, the required diffusion pump speed should be greater than the 400 lit/sec.

2.2.2 Cathode and Anode

In our entire experiments the filament was used as cathode. Inside the vacuum chamber, 4 thoriated tungsten (1% thorium and 99% tungsten) filaments of diameter 0.25 mm were mounted on two SS rings (Fig. 2.2). The diameter of the SS rings was 23 cm and the length of each filament was 20 cm. The vacuum chamber was used as anode which was connected with ground.

2.2.3 Power Supply

Power supply is important for production of plasma and excitation of different collective plasma modes. A regulated dc power supply of voltage rating 0 to 32 V and current rating 0 to 30 A was used for filament heating. To produce plasma, another dc power supply of voltage rating 0 to 300 V and current rating 0 to 3 A was used. To excite the electrostatic waves one pulse forming circuit was made. For the pulse forming circuit one high voltage dc power supply of voltage rating 75 V to 1.5 kV and current rating 0 to 0.5 A was used.

2.3 Plasma Production

After filling the vacuum chamber with argon gas at desired working pressure, hot filament discharge plasma was produced. Four thoriated tungsten filaments were connected in

Chapter 2: Experimental Set-up and Diagnostics

parallel to each other through two SS rings. The filaments were heated by feeding a dc current from a floating dc power supply, such that each filament got a current of 6-7 A and were hot enough to emit thermionic electrons. There was no other electric field to capture these thermionic emitted electrons. So the emitted electrons form the filament, again attracted towards the filament and made a space charge cloud around the filament. To emit these electrons from the filament another dc power supply (Fig. 2.2) was connected in between the filament and chamber wall (grounded). So plasma was generated by impact ionization [3-4] of argon gas neutrals by primary electrons coming out from dc biased hot filaments. The filament bias potential was -65 V and the discharge current was about 0.05 – 0.4 A.

Now we can estimate the plasma parameters and their variation with power, pressure and source geometry from this cylindrical discharge system. The effective area of our cylindrical system is 0.18 m^2 , which can be calculated from below equation

$$A_{eff} = 2\pi R(Lh_R + Rh_L)$$

where L is the system length, R is the system radius and h_R and h_L are the ratio of densities reaching at wall compared to bulk plasma and $h_R = h_L \approx 0.3$ for argon plasma [5]. Assuming electrons are Maxwellian in the cylindrical system and the absorbing electrical power is

$$P_{abs} = n_0 e C_s A_{eff} \varepsilon_T$$

where n_0 is the plasma density, $C_s \left(= \sqrt{\frac{kT_e}{m_i}} \right)$ is the ion acoustic speed and $\varepsilon_T (= \varepsilon_{collisional} + 2T_e + \varepsilon_{meanK.E./ion})$ is the total energy lost per ion from the system. ε_T is 72 V for argon [5]. For one example, i.e., for $n_0 = 3.92 \times 10^{15} \text{ m}^{-3}$, $T_e = 6 \text{ eV}$, $P_{abs} = 30 \text{ W}$. This is called as uniform density discharge model [5]. For these plasma parameters, discharge voltage is 65 V and discharge current is 0.4 A. So the power absorbed by the system is 26 W, which is closer to the above calculated theoretical value.

2.4 Diagnostics

During the past few decades, plasma physics has become established as a major research field. As a result, the field includes a very substantial knowledge covering a wide

Chapter 2: Experimental Set-up and Diagnostics

variety of branches, from the theoretical to the most experimental study. As with any other science, progress has been made most effectively when an early quantitative confrontation between theory and experiment has been possible. This confrontation places strong demands upon theory to do calculations in realistic configurations and circumstances, but it is also requires that the properties of plasmas be measured experimentally as completely and accurately as possible. For this reason much of the effort in experimental plasma physics is devoted to devising, developing and providing techniques for diagnosing the plasma properties: plasma diagnostics. The overall objective of plasma diagnostics is to deduce information about the state of the plasma from practical observations of physical processes and their effects. To reach useful and accurate results requires rather complete quantitative mathematical and computational analysis; more so sometimes, than in a general text where a qualitative treatment is sufficient.

In 1924 Langmuir [6] presented the basic techniques for investigating plasma parameters with electric probes. He described two basic types: collecting probes or cold probes (Langmuir probe) and electron emitting probes or hot probes (emissive probe). They are simple to construct and allow localized measurements. In our experiments, plasma properties, like plasma density (n_0), electron temperature (T_e), floating potential (V_f) and plasma potential were measured by using a disc Langmuir probe. In addition, a hot emissive probe was used to measure the plasma and floating potentials. The technical details of the diagnostics are described below.

2.4.1 Langmuir Probe

Langmuir probe [4, 6-11] is a diagnostic device used to determine the plasma parameters like electron temperature, electron density, floating potential and plasma potential. This device was named after Nobel Prize winning chemist Irving Langmuir. Mainly the Langmuir probes are used in low temperature plasma [8]. Basically plasma parameters are obtained from (I - V) characteristic of a Langmuir probe, which is described in detail in Section 2.5.

According to Langmuir probe theory, Langmuir probe is a small conducting electrode and it can be a sphere, cylinder or planar. Generally the Langmuir probe inserts into plasma with a constant or time varying electric potential between the probe and the reference. As the charged plasma particles collide with the probe, then the probe draws electrical current which provides the condition of plasma. The amount of current flowing through the probe depends

Chapter 2: Experimental Set-up and Diagnostics

on the plasma parameters and the probe collecting area. The necessary conditions of Langmuir probe are

- (1) The probe area should be small, in order to minimize the perturbation of the plasma.
- (2) The electrode dimension is larger in comparison to the Debye length (λ_D).
- (3) The electrons should obey the Maxwellian distribution.

2.4.1.1 Construction of Langmuir Probe

Langmuir probe theory is determined by the probe geometry and the sheath dimensions. The relative size of the probe sheath, the probe radius r_p and the collision mean free path λ_m in the plasma determine the probe characteristics. A very general requirement for Langmuir probe construction is [7]

$$\lambda_m \gg r_p \gg \lambda_D. \quad (2.1)$$

The requirement for probe theory is that the probe dimension must be much larger than the Debye length to neglect the edge effect [10]. For disc or planar Langmuir probes the below condition [10] should be satisfied:

$$10 < r_p / \lambda_D < 45. \quad (2.2)$$

The schematic diagram of Langmuir probe is shown in Fig. 2.3. In our experiments, Langmuir probe consists of a disc electrode of radius 4.5 mm was made up of SS 304. The electrical connection to the probe was provided by a Teflon coated wire which was spot welded to the non-plasma facing side of the probe. Teflon coated wire comes out through a vacuum compatible BNC connector mounted on a SS 304 shaft of outer diameter 5 mm. The SS shaft was introduced into the vacuum chamber through a vacuum feedthrough such that the probe could be positioned at the desired locations inside the chamber.

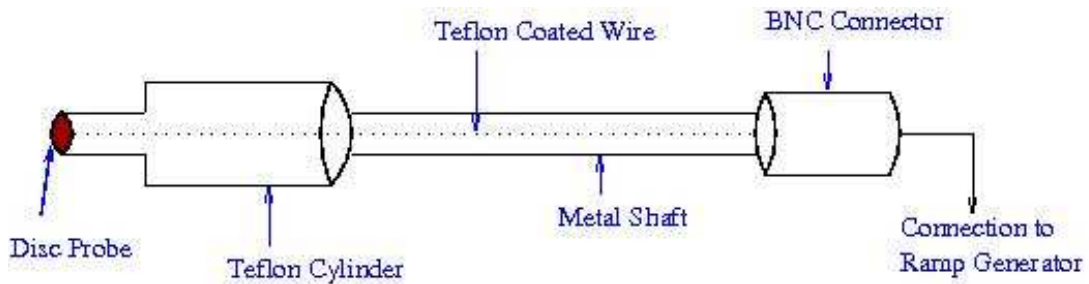


Figure 2.3 Schematic of the Langmuir probe.

2.4.1.2 Langmuir Probe Circuit

The schematic of electrical circuitry of the Langmuir probe is shown in Fig. 2.4. The circuitry works as follows:

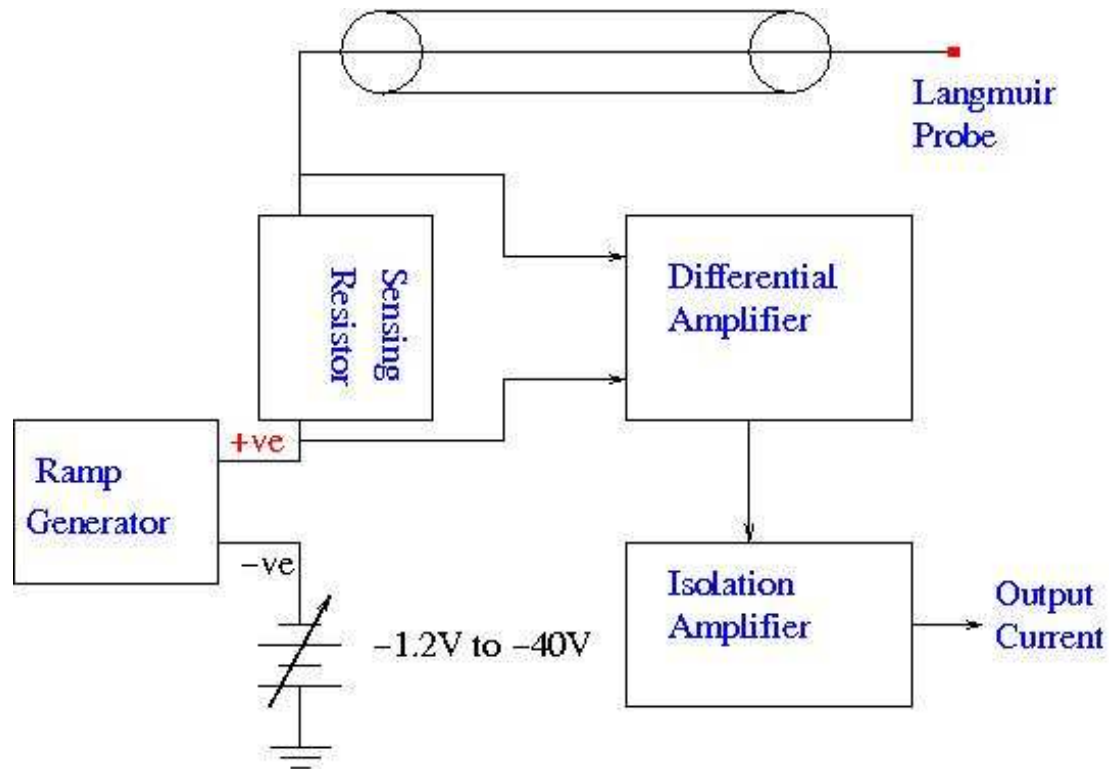


Figure 2.4 Schematic diagram of the Langmuir probe circuit.

(a) Voltage source to bias Langmuir probe

This circuit consists of a ramp generator that generates a ramp voltage of +40 V to -60 V with a frequency of 50 Hz. This ramp voltage was given to probe along with a dc shift of -1.2 V to -40 V. When the probe was exposed to the plasma it acquired a potential known as the floating potential without drawing any net current. It depends on the state of the plasma and the discharge conditions but not on the probe area. Langmuir probe draws electron or ion current according to the positive or negative potential applied with respect to the floating potential. The dc shift was adjusted accordingly to obtain the required electron or ion current.

(b) Sensing resistor

The biasing voltage to the Langmuir probe was applied through a variable sensible resistor (Potentiometer). The resistance could be varied from 1 K Ω to 10 K Ω

Chapter 2: Experimental Set-up and Diagnostics

depending on plasma parameters. The potential drop developed across the resistor was measured using a differential amplifier.

(c) Differential amplifier

The voltage drop across the sensing resistor was fed to the input of the differential amplifier circuit. The circuit was developed by using IC OPA27. It is an ultra low noise and very high precision amplifier. The differential amplifier circuit measures the potential difference across the sensing resistor and gives an output, proportional to the current drawn by the probe corresponding to the applied voltage.

(d) Isolation amplifier

Generally, the probe circuits are designed to measure current in those systems where entire circuit may be floating at a higher voltage, in our case the entire circuit described above was kept floating at a high voltage (+40 V to -60 V ramp with a -1.2 V to -40 V dc shift). To measure such current in an oscilloscope with respect to normal ground, this amplifier was used (using IC ISO106B). It isolates two grounds and gives the same voltage drop across the probe resistance with respect to normal ground at the output side.

The output current obtained at the output of the isolation amplifier and the applied voltage was measured with the help of an oscilloscope (Tektronix TDS 2024, 200 MHz and 2 GS/s). The applied voltage to the probe was attenuated through a 10X probe. These data's could be further stored on a data storage device. This data was used to plot I - V characteristic to determine the plasma parameters.

2.4.2 Emissive Probe

An emissive probe [12-16] was used to measure the plasma potential or the space potential. An emissive probe is essentially a hot wire (commonly tungsten) inserted into the plasma to measure the floating potential and plasma potential. The schematic diagram of the emissive probe is shown in Fig. 2.5. In our experiment, a tungsten wire of 1 cm length and 0.25 mm of diameter was semi circled. The tungsten wire tips were inserted in a two hole cylinder of ceramic. Copper wires inside the cylinder made compression contact with the replaceable tungsten tip. The emissive probe was heated sufficiently by a floating power supply (150 V and 8 A) with respect to plasma potential to allow thermionic emission of

Chapter 2: Experimental Set-up and Diagnostics

electrons. The floating potential measured by the emissive probe increased and begun to saturate when it was sufficiently heated up by passing a high current through it. The plasma potential was estimated from the saturated value of the floating potential. The detailed measurement of emissive probe is given in Sec. 2.5.

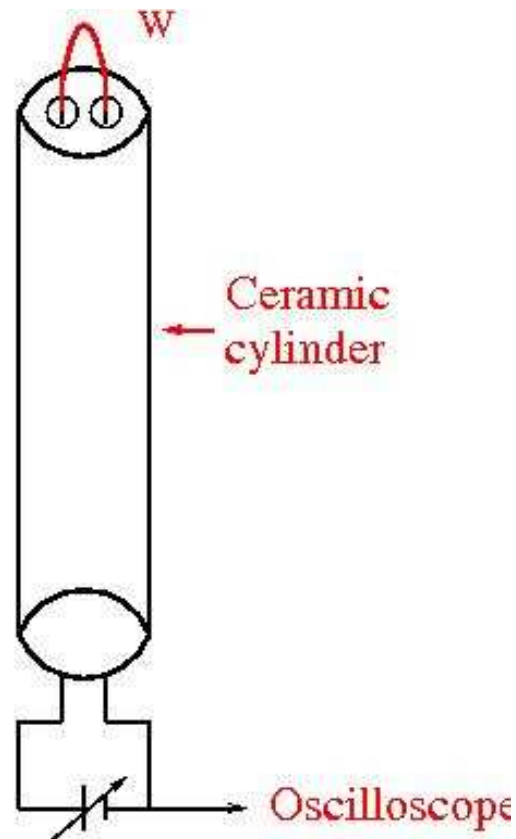


Figure 2.5 Schematic of emissive probe.

2.5 Characterization of Plasma

2.5.1 Discharge Parameters

Tungsten filaments have been widely used in lighting, electronic tubes and as electron emitters for plasma sources. Tungsten is chosen as a thermal electron emitter because of its very high melting point (3683 K). Tungsten is a copious emitter of electrons, when it is heated to a temperature of about 2000 K or more. A tungsten wire is generally directly heated by passing a current through it. The emitted electron current density J_e is limited by space

Chapter 2: Experimental Set-up and Diagnostics

charge [17]. For high extraction electric fields (discharge voltage), a saturation current density J_{\max} is reached, which is approximately given by the Richardson-Dushman equation,

$$J_{\max} = A_0 T^2 \exp\left(-\frac{e\phi}{k_B T}\right) \quad (2.3)$$

where A_0 is Dushman's constant ($1.2 \times 10^6 \text{ A m}^{-2} \text{ K}^{-2}$), T is the tungsten filament temperature in kelvins, e is the electron charge, ϕ is the work function in volts and k_B is the Boltzmann constant. It can be seen that J_{\max} depends very strongly on the filament temperature. Figure 2.6 shows our experimental plot of saturation electron emission current density versus filament temperature when space charges are absent. The filament temperature was found out by Stefan-Boltzmann law through a simple MATLAB program. From the above observation we saw that on increasing of filament voltage and current, filament temperature increases as well as electron emission current density. For a given filament temperature, the electron emission increases linearly with filament diameter [18].

The variation of discharge voltage with discharge current at constant pressure is shown in Fig. 2.7. The filament glow covers the whole chamber and this I - V characteristic is plotted for various filament heating currents. The discharge current increases rapidly with increase in voltage and saturates from near about 40 V. This saturation occurs because of no additional thermionic emission from filament on increase of discharge voltage for a fixed filament current.

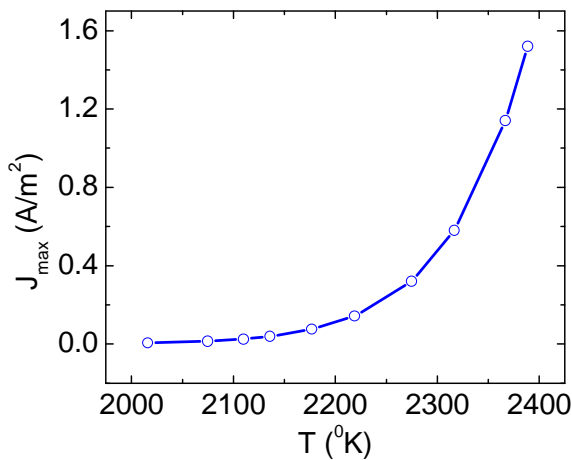


Figure 2.6 Typical filament temperature versus emission current density for the filament diameter of 0.25 mm.

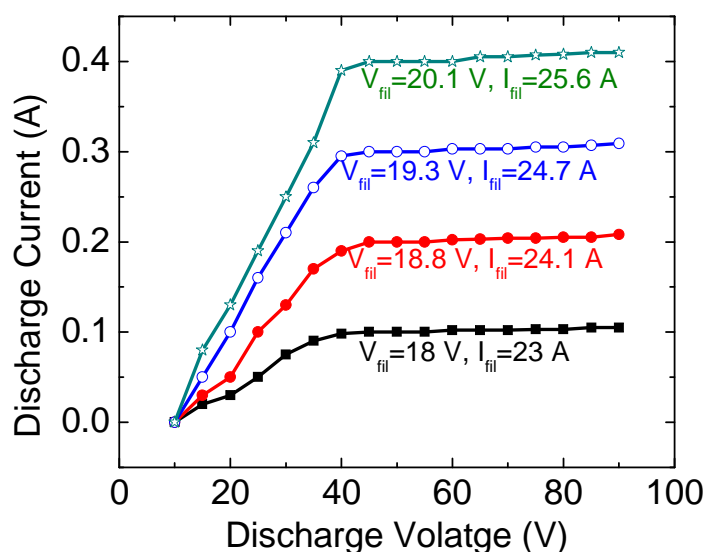


Figure 2.7 Discharge voltage versus discharge current for various filament heating current (I_{fil}) for a constant pressure.

When a tungsten filament is used as a thermal electron emitter, it is important to know the relationships among the filament diameter, heating current, filament temperature, emission current and life time. The life time of a tungsten filament is generally defined as the time required evaporating away 10% of the original diameter [18]. The evaporation rate is a function of filament temperature [19]. So in a filament discharge plasma, the number of electrons that can be extracted from a hot filament is proportional to J_i (ion current density), which is a function of the plasma density, the plasma temperature and the extraction voltage [20-21].

2.5.2 Plasma Parameters

A single Langmuir probe [4, 6-11, 22-29] was used to measure the plasma parameters like, plasma density (n_0), electron temperature (T_e), floating potential (V_f) and plasma potential (V_p). The probe construction and validity of probe theory to our experimental situation have been discussed in Sec. 2.4. The below described Langmuir probe theory is valid for only in the absence of drifting electrons [26]. In addition, an emissive probe was also used to measure plasma potential. The details of measurements are described below.

2.5.2.1 Determination of Plasma Parameters Using Langmuir Probe

Langmuir probe is merely a small metallic electrode inserts into the plasma, with a constant or time varying electric potential between the probe and the surrounding chamber. For a probe inserted in to the plasma, as the voltage on the probe is biased negatively and positively, the I - V characteristics of the probe can be plotted.

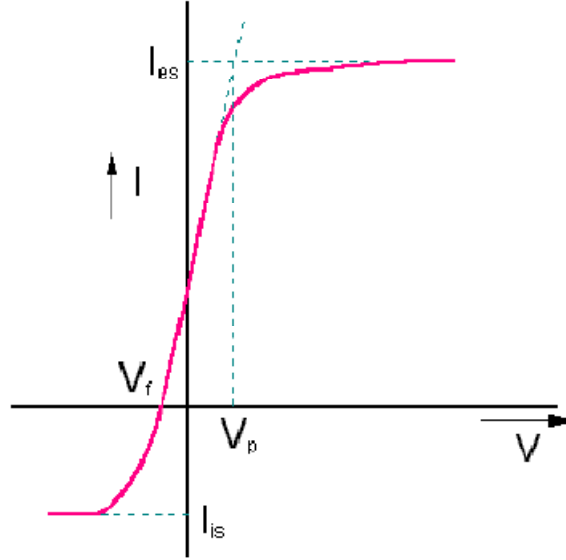


Figure 2.8 Ideal I - V characteristic for a Langmuir probe.

The ideal I - V characteristic for a single probe is shown in Fig. 2.8. When probe bias V is negative with respect to plasma potential V_p , current drawn by the probe from the plasma is positive. The electric field around the probe, confined to the ion sheath will prevent all the energetic electrons from reaching the probe, this causes effectively reducing of the electron current to zero. So, the point at which entire current collected by the probe is due to positive ions. This point is called ion saturation current I_{is} which is given by

$$I_{is} = n_i e A_p C_s \quad (2.4)$$

where n_i is the ion density at the sheath edge, A_p is collecting area of the probe, e is electron charge and C_s is ion acoustic speed or Bohm speed. Bohm speed is the speeds at which ions are enter to the sheath and is given by

$$C_s = \sqrt{\frac{k_B T_e}{m_i}} \quad (2.5)$$

Chapter 2: Experimental Set-up and Diagnostics

where m_i is the ion mass. The ion saturation current density can be calculated from below equation

$$J_{is} = n_i e \sqrt{\frac{k_B T_e}{m_i}}. \quad (2.6)$$

As increase in probe bias (probe bias made more positive), increases the number of electrons which is able to overcome the repulsive electric field. So negative (electron) current increases exponentially and overall current collected by the probe decreases. Eventually the electron current equals to $-I_{is}$. So that the total current is zero. The potential at this point is known as floating potential and is given by [3]

$$V_p - V_f = \frac{1}{2} \left(\frac{k_B T_e}{e} \right) \ln \left(\frac{m_i}{2\pi m_e} \right) \quad (2.7)$$

Further increase of probe bias to V_p allows the electron current to increase. This current is given by

$$I_e = en_e A_p \langle u_e \rangle \quad (2.8)$$

where $\langle u_e \rangle$ is the average electron thermal velocity and is given by

$$\langle u_e \rangle = \sqrt{\frac{k_B T_e}{2\pi m_e}} \exp\left(\frac{eV_{sh}}{k_B T_e}\right) \quad (2.9)$$

where $V_{sh} (=V_p - V)$ is the sheath potential. At V_p electrons are unrestricted from being collected by the probe. Any further increase in bias will simply add energy to electrons, not the current drawn. Current at this point is called electron saturation current I_{es} and is given by

$$I_{es} = en_e A_p \sqrt{\frac{k_B T_e}{2\pi m_e}} \quad (2.10)$$

The inverse of the slope of the steep portion of the graph between logarithm of the electron current and the potential on the probe will give the electron temperature and is given by

Chapter 2: Experimental Set-up and Diagnostics

$$T_e = \frac{dV}{d(\ln I_e)}. \quad (2.11)$$

After obtaining electron temperature from logarithmic graph of current versus potential and ion saturation current from I - V characteristics and putting the values in Equation (2.4), plasma density can be calculated.

In our experiment, first the single disc Langmuir probe was biased with a sweep voltage to draw the probe current at a discharge voltage of -65 V and current $I_{dis} = 0.3$ A at $P = 1 \times 10^{-3}$ mbar. A resistance connected in series to the probe was adjusted in such a way that it can draw sufficient current. The applied probe voltage and the probe current are shown in Fig. 2.9.

Figure 2.10 shows the experimental I - V characteristics of the Langmuir probe. The voltage corresponding to the zero probe current gives the floating potential as -4V. The ion saturation current is about 30 μ A. The electron collection region gives the information about electron temperature and plasma potential.

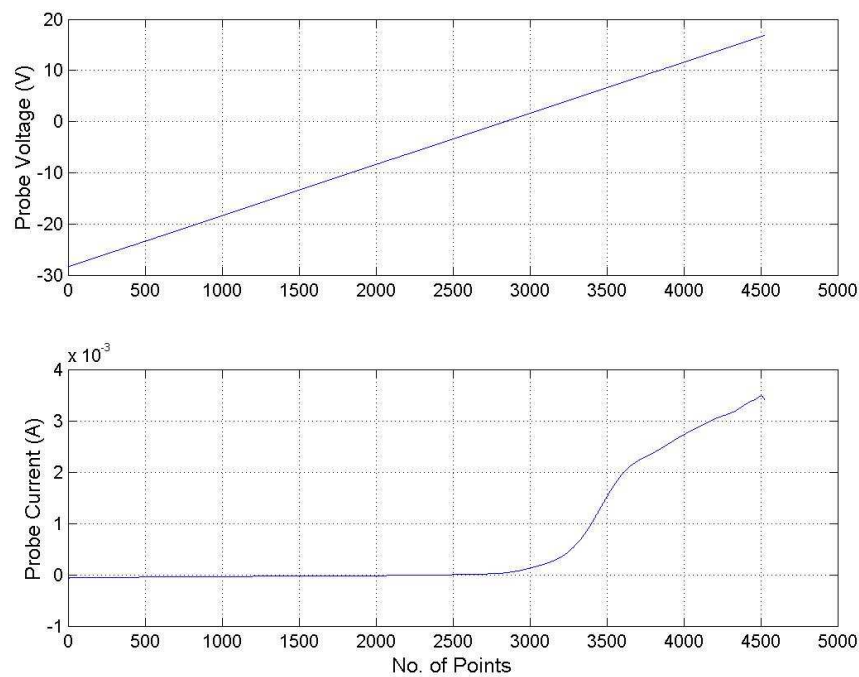


Figure 2.9 The upper trace shows the voltage wave front applied to the probe and the lower trace shows the current drawn by the probe.

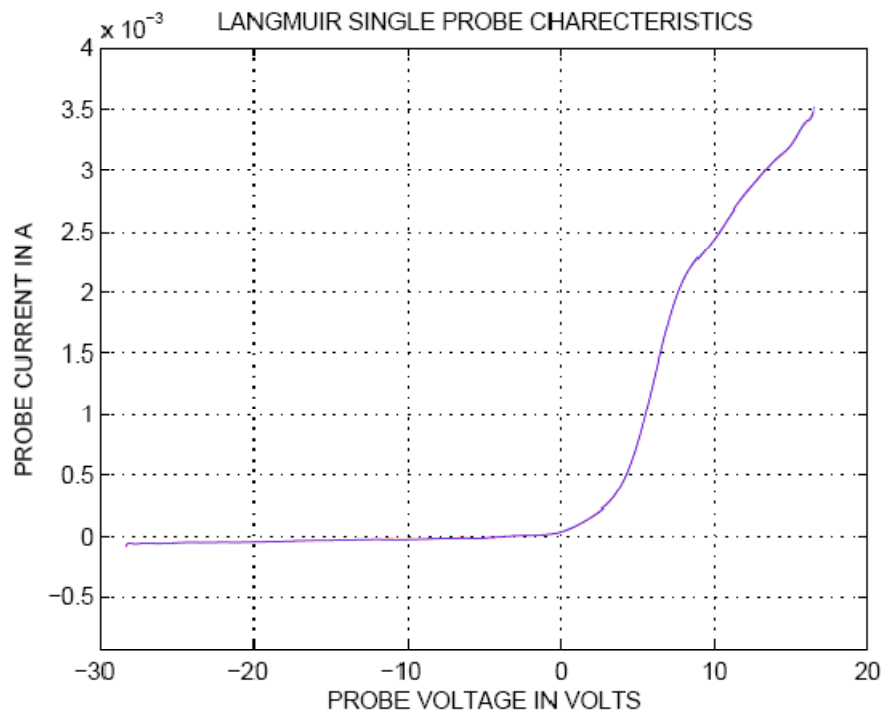


Figure 2.10 Experimentally obtained I - V characteristics of single Langmuir probe.

Before calculating the electron temperature, we have eliminated the contribution of ion current by subtracting a dc voltage equivalent to ion saturation current from the entire probe characteristics. Assuming the electrons are Maxwellian at the transition region or the steep region (the region where the probe current changes significantly with probe voltage) of the Langmuir characteristics. Figure 2.11 is the logarithm of electron current (steep region of Fig. 2.9) versus the probe voltage. The inverse of the slope gives the electron temperature, i.e., 2.04 eV at that particular discharge condition.

Putting the values of ion saturation current and electron temperature in Eq. (2.4), the plasma density is $2.65 \times 10^{15} \text{ m}^{-3}$. Putting the value of electron temperature in Eq. (2.7), the plasma potential for argon gas is +6 V. Again in Fig. 2.10, the electron current saturates at around +7.5 V. Hence the plasma potential is +7.5 V, which is slightly greater than the calculated value. It is to be noted that the plasma parameters vary with the filament heating voltage, current and filament lifetime.

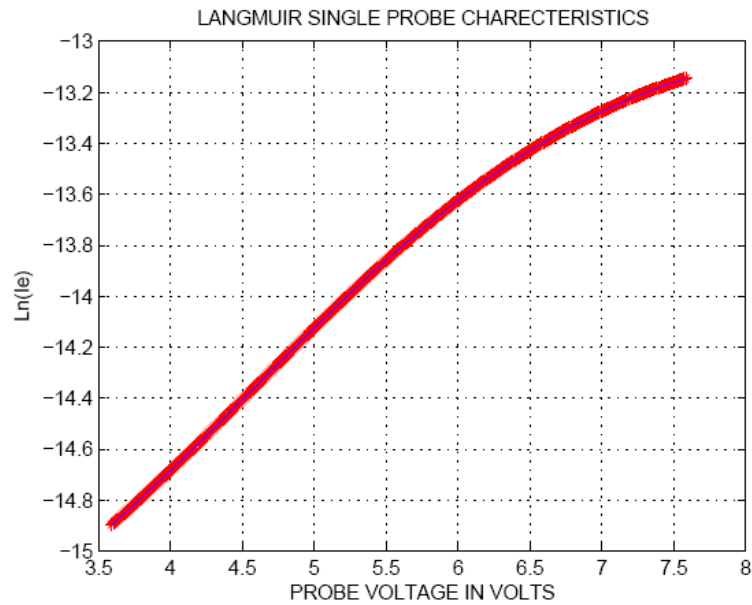


Figure 2.11 Natural logarithmic of electron current versus probe voltage.

Figures 2.12 and 2.13 show the axial and radial variation of electron temperature and plasma density respectively. The plots show that the variation in T_e and n_0 is very low, indicating an almost uniform plasma inside the chamber.

The plasma which is considered in our study, are unmagnetized, uniform and non-equilibrium, with ions and electrons having different temperature ($T_e \gg T_i$).

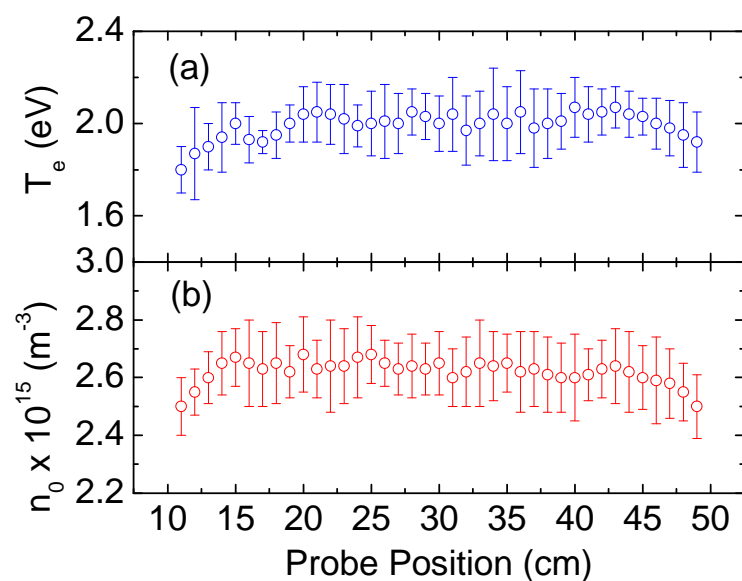


Figure 2.12 Axial variation of electron temperature and plasma density.

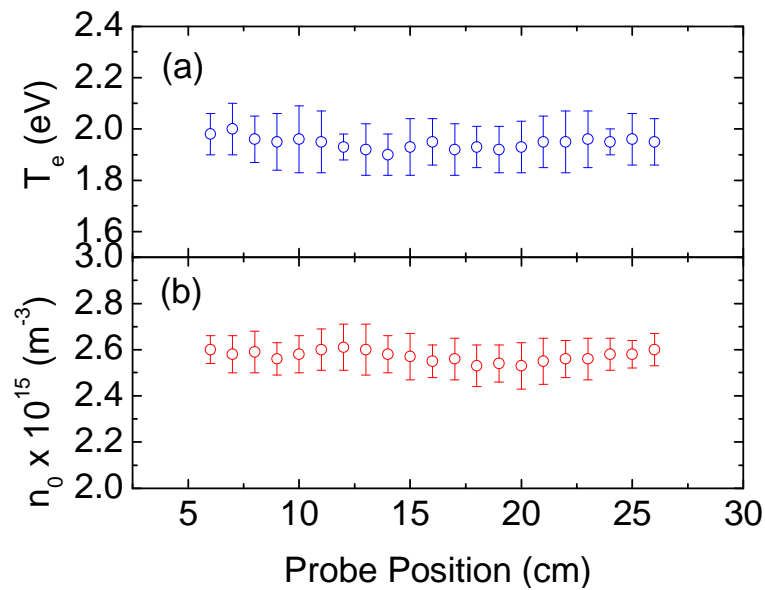


Figure 2.13 Radial variation of electron temperature and plasma density.

2.5.2.2 Plasma Potential Measurements by Using Emissive Probe

The most common method is to determine the plasma potential from the knee of the electron saturation current in the I - V characteristic curve of the Langmuir probe (cold probe). However, this Langmuir probe approach yields incorrect results if the plasma electrons are drifting or if the probe surface is contaminated giving rise to a change in the work function. On the other hand, emissive probe methods can still yield correct results if the plasma electrons are drifting. Unlike collecting probes, emissive probes don't give useful data on plasma density.

In addition to a Langmuir probe, a hot emissive probe was used for measuring floating and plasma potentials [12-16]. Electron temperatures were also estimated from the difference of these two potentials using Eq. (2.7) and compared with the temperature obtained from Langmuir probe data. Several different procedures have been developed to obtain the plasma potential from emissive probe, i.e., (1) Inflection point method [14-15] and (2) Floating potential method [12].

A simple method was used in our experiment to determining the plasma potential from the floating potential using an emissive probe. This method is applicable when the electron temperature is substantially greater than the used tungsten wire temperature. This

Chapter 2: Experimental Set-up and Diagnostics

method was based on the observation that the floating potential of an emissive probe depends on wire temperature. A wire temperature which changed in time caused the floating potential also to vary.

In our experiment, the emissive probe was made of a tungsten wire of 1 cm length and 0.25 mm of diameter and was inserted into plasma. The floating potential obtained without heating the emissive probe is equal to floating potential of cold probe. When the emissive probe was heated by various heating currents (or voltages) in ascending order, then the floating potential was also varied. The floating potential was saturated for large heating currents, as shown in Fig. 2.14. This saturated floating potential is the plasma potential.

When the emissive probe heating voltage is less than the plasma potential ($V_w < V_p$), then there is no potential barrier to obstruct the emitted electrons from the hot tungsten wire. So the emitted electrons can be added to the plasma below V_p and floating potential changes. As one exceeds V_p the flow of electrons from the probe is rapidly reduced by a potential barrier and no variation in floating potential, which is called as plasma potential.

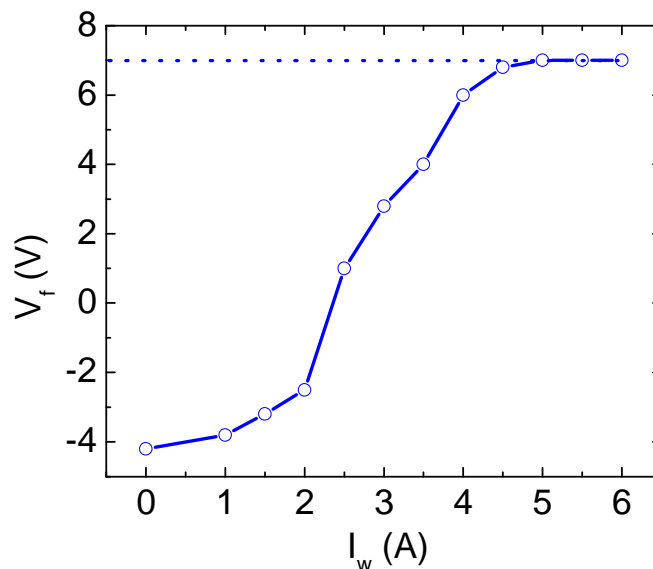


Figure 2.14 Emissive probe heating current versus floating potential.

Chapter 2: Experimental Set-up and Diagnostics

This emissive probe experiment was done for the discharge current of $I_{dis} = 0.3$ A at $P = 1 \times 10^{-3}$ mbar. From the graph the saturated floating potential, i.e., the plasma potential is +7 V, which is approximately equal to Langmuir probe data plasma potential. If we put the emissive probe measured floating potential (-3.8 V) and plasma potential (+7 V) in Eq. 2.7, then electron temperature is 2.16 eV, which is nearly equal to Langmuir probe data.

2.6 Pulse Forming Circuit

The pulse-forming circuit is described in Fig. 2.15. For the experimental requirements the values of the capacitor (C) and the resistor (R_2) were adjusted in such a way that the pulse duration always satisfied for the conditions $\tau_p < f_i^{-1}$ and $\tau_p > f_i^{-1}$ and the pulse height was decided by the voltage to which capacitor was charged. The value of the inductor (L) was fixed. The positive or negative pulse can be obtained by changing the polarity of HV dc supply.

In our case, R_1 was chosen according to HV dc supply current and voltage ratings. In our case, the voltage and current ratings of dc supply was 1.5 kV and 0.5 A respectively and R_1 was 3 k Ω . The value of R_2 was fixed (50 Ω) and it was a thin-film non-inductive resistor. Only the value of C was varied for changing the pulse width. For example, for 140 ns pulse width the capacitance was 0.71 nF. The inductor (320 nH) was used for blocking the high frequency signals (noise) in the voltage signal, which acts as a low pass filter.

A spark gap was used in the pulse forming circuit. A spark gap consists of an arrangement of two conducting electrodes separated by a gap usually filled with a gas such as air. This is designed to allow an electric spark to pass between conductors. When the voltage difference between the conductors exceeds the gap's breakdown voltage, a spark forms, ionizing the gas. An electric current then flows until the ionized gas path is broken or the current reduces below a minimum value called the "holding current". This usually happens when the voltage drops. During the action of ionizing the gas, it leads to sound, light and heat. Spark gaps are generally used to prevent voltage surges from damaging equipments. So spark gaps are used in high voltage switches, i.e., can be used to rapidly switch high voltages and high currents for certain pulsed power applications. In our pulse forming circuit, the spark gap was used instead of electrical switches like thyristor, to keep the circuit floating and easily accessing of a single pulse. But in case of a conventional thyristor, once it has been

Chapter 2: Experimental Set-up and Diagnostics

switched on by the gate terminal, the device remains latched in the on-state (i.e., doesn't need a continuous supply of gate current to conduct or we can say its output may depend not only on its current input, but also its previous inputs). As long as the anode remains positively biased, it can't be switched off, until the anode current falls below the holding current (or a thyristor can be switched off if the external circuit causes the anode to become negatively biased). So in our case the spark gap was used.

One typical voltage pulse is given in Fig. 2.16 using the pulse forming circuit.

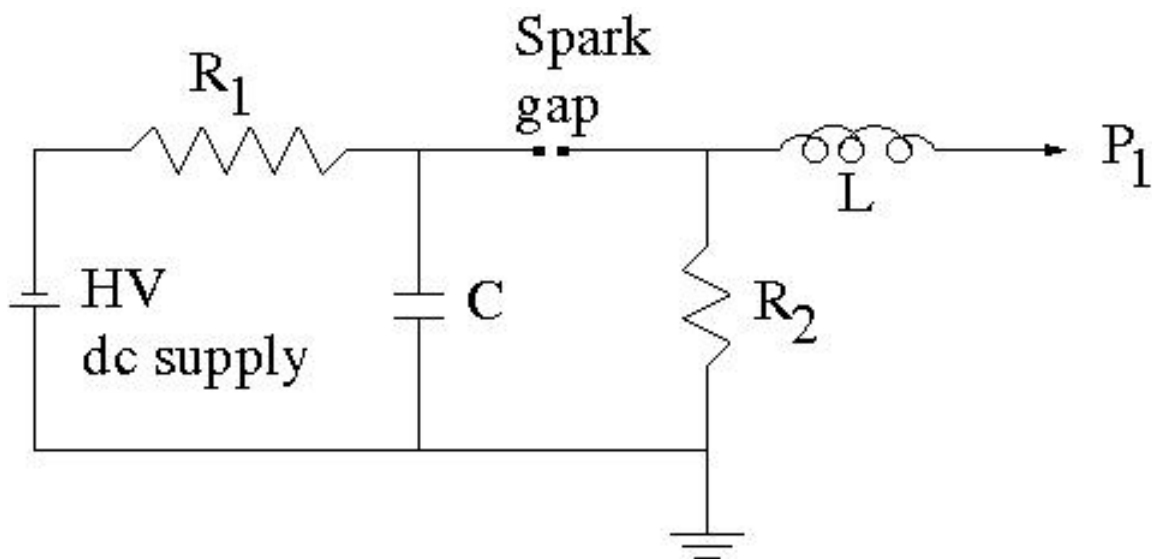


Figure 2.15 The pulse forming circuit. [HV dc Supply = high voltage dc supply (1.5 kV, 500 mA), R_1 = resistor (3 k Ω), C = capacitor, R_2 = load resistor, L = inductor (320 nH), P_1 = electrode or the exciter].

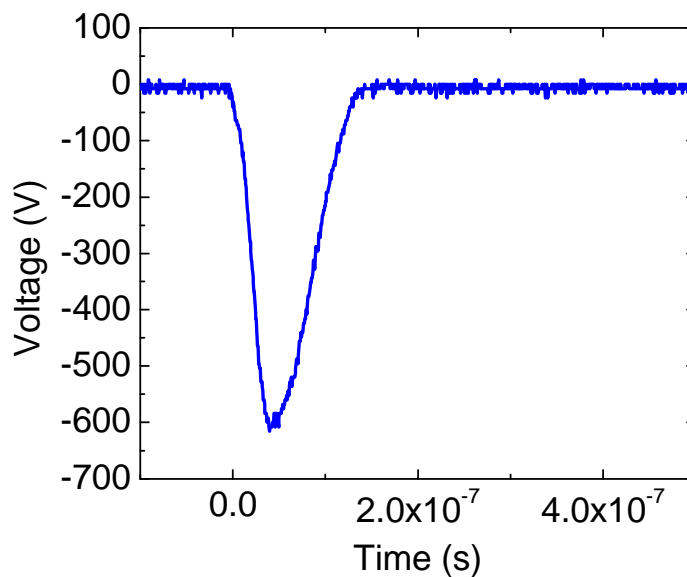


Figure 2.16 A typical voltage pulse obtained from the pulse forming circuit.

2.7 References

- [1] W. Umrath, “Fundamentals of Vacuum Technology”, Cologne (1998).
- [2] W. M. Haynes, “CRC Handbook of Chemistry and Physics”, 91st edition (2011).
- [3] Brian Chapman, “Glow Discharge Processes”, John Wiley & Sons, New York (1980).
- [4] Yuri P. Raizer, “Gas Discharge Physics”, Springer Verlag Heidelberg, New York (1991).
- [5] A. Anders, “Handbook of Plasma Immersion Ion Implantation and Deposition”, John Wiley & Sons, New York (2000).
- [6] I. Langmuir and H. M. Mott-Smith, Gen. Elec. Rev **27**, 449 (1924).
- [7] B. E. Cherrington, Plasma Chem. Plasma Process. **2**, 113 (1982).
- [8] S. Pfau and M. Tichy, Low Temperature Plasma Physics, edited by R. Hippler, S. Pfau, Schmidt and K. H. Schoenbach, Wiley-VCH, Chapter-6 (2001).
- [9] F. F. Chen, Plasma Diagnostics Techniques, edited by R. H. Huddlestone and S. L. Leonard, Chapter-4, New York (1965).
- [10] T. E. Sheridan, Phys. Plasmas **7**, 3084 (2000).
- [11] I. H. Hutchinson, Principles of Plasma Diagnostics, Cambridge University Press, Chapter-3 (1987).
- [12] M. A. Makowski and G. A. Emmart, Rev. Sci. Instrum. **54**, 830, (1983).
- [13] W. E. Yao, T. Intrator and N. Hershkowitz, Rev. Sci. Instrum. **56**, 519, (1985).
- [14] J. R. Smith, N. Hershkowitz and P. Coakley, Rev. Sci. Instrum. **50**, 210 (1979).
- [15] A. Siebenförcher and R. Schrittwieser, Rev. Sci. Instrum. **67**, 849 (1996).
- [16] H. Himura, M. Fukao, H. Wakabayashi and Z. Yoshida, Rev. Sci. Instrum. **74**, 4658 (2003).
- [17] H. Reich, “Theory and Application of Electron Tubes”, McGraw-Hill, New York (1939).
- [18] K. W. Ehlers and K. N. Leung, Rev. Sci. Instrum. **50**, 356 (1979).
- [19] H. A. Jones and I. Langmuir, Gen. Elec. Rev. **30** 310 (1927).
- [20] F. W. Crawford and A. B. Cannara, J. Appl. Phys. **36**, 3135 (1965).
- [21] P. D. Prewett and J. E. Allen, Proc. R. Soc. London A **348**, 435 (1976).
- [22] W. E. Amatucci, M. E. Koepke, T. E. Sheridan, M. J. Alport and J. J. Corroll III, Rev. Sci. Instrum. **64**, 1253 (1993).
- [23] C. Das and D. C. Jana, J. Phys. Sci. **12**, 187 (2008).
- [24] V. A. Godyak, R. B. Piejak and B. M. Alexandrovich, Plasma Sources Sci. Technol. **1**, 36 (1992).

Chapter 2: Experimental Set-up and Diagnostics

- [25] A. Brockhaus, C. Borchardt and J. Engemann, *Plasma Sources Sci. Technol.* **3**, 539 (1994).
- [26] T. E. Sheridan and J. Goree, *Phys. Rev. E* **50**, 2991 (1994).
- [27] R. L. Merlino, *Am. J. Phys.* **75**, 1078 (2007).
- [28] D. Lee and N. Hershkowitz, *Phys. Plasmas* **14**, 033507 (2007).
- [29] T. E. Sheridan, *J. Phys. D: Appl. Phys.* **43**, 105204 (2010).

CHAPTER 3

3 Study of Electron Behavior in a Pulsed Ion Sheath

3.1 Motivation

In many plasma processing applications, like plasma immersion ion implantation (PIII) [1-15], one metallic electrode is immersed in low pressure plasma and is biased with negative voltage pulses. In typical PIII the pulse duration is much larger than the ion response time (f_i^{-1}), and hence the ion matrix sheath expands and ion implantation happens on the negative biased electrode. PIII is a well-developed technique of introducing ions inside a metal surface for enhancement of the surface properties. In most of the cases, the electrode is immersed in a low pressure plasma and biased pulsed negative with finite rise and fall times [4, 5]. In general, the applied negative bias magnitude is much greater than the electron temperature, such that in the time scale of the inverse electron plasma frequency f_e^{-1} , electrons are repelled from the vicinity of the electrode, leaving behind a uniform density of ion matrix sheath in which ions are stationary. Subsequently, on the time scale of inverse ion plasma frequency f_i^{-1} , ions within the ion matrix sheath are accelerated towards the electrode and implanted into the surface of the electrode. This in turn, drives the sheath-plasma edge further away, exposing new ions that are extracted. The detailed about the sheath is described in Chapter 1. If the mean free path for ion momentum transfer $\lambda_i > s$, the sheath width, then the sheath is called as collisionless sheath, otherwise a collisional sheath.

Chapter 3: Study of Electron Behavior in a Pulsed Ion Sheath

In all the earlier experiments and theoretical models, the duration of pulses applied to the electrode in PIII is greater than the ion plasma response time and no attention has been given to that repelled electrons. In the present Chapter, the applied negative pulse duration is varied between ion and electron plasma response times; so as to study the electron behavior assuming ions are stationary. It is assumed that for pulse duration shorter than ion response times, the ions remain stationary and electrons are repelled by the negative bias. The question to be asked, are the electrons near the vicinity of the electrode only repelled leaving electrons in the bulk plasma unaffected or both the repelled and the plasma electrons are affected. This Chapter presents an experimental estimation of the electrons lost to the walls and the origin of these electrons during a high negative electrode pulse bias in an argon dc discharge, when the bias pulse width (τ_p) is in between the electron and ion plasma response times. The experimental results are compared with computer simulation results using PDP1 code. The results indicate that the electrons are lost to the walls come from the ion matrix sheath and probably from the bulk plasma as well. The pulse duration, when it is less than ion response time, plays a crucial role in determining number of electrons lost to the walls. An overview of the previous works is given in Sec. 3.2. The experimental setup is explained in Sec. 3.3 followed by observed results and discussions presented in Sec. 3.4. PDP1 computer simulation is described in Sec. 3.5 and finally conclusions are given in Sec. 3.6.

3.2 An Overview of Previous Works

Plasma sheaths are existing under a variety of conditions; i.e., probes [16], radio frequency (rf) antenna plasma interactions [17], dusty plasmas [18], etc. A detailed understanding of pulsed ion sheath dynamics is important for a number of applications in plasma processing. Examples include material surface modification technique in plasma immersion ion implantation (PIII) [1-15] and semiconductor doping [19]. Fundamental to the understanding of this PIII process is the theoretical description of the plasma-wall interaction, leading to an electrically charged sheath between the wall and the plasma. The Bohm criterion [20], requiring acceleration of the ions to the acoustic sound speed, is necessary for sheath formation.

All of the models published before [2, 4, 5] assume that the charge uncovered by the expanding sheath is equal to the charge implanted in the substrate, that is, conduction current is continuous across the sheath. Wood [6] concluded from his simulation that a significant displacement current, created by the rapidly changing electric field in the sheath, can also

Chapter 3: Study of Electron Behavior in a Pulsed Ion Sheath

contribute to the total current. Lieberman [2] has developed an approximate analytical model to determine the time-varying implantation current, the total dose and the energy distribution of the implanted ions. Speth et al. [21] has investigated that the effect of applied high voltage pulse shape has a minor influence on the ion impact energy. Substrates with irregular geometries [9-11] can be treated in PIII. PIII can also be used in pulsed plasmas [12-14] and non-uniform plasma [15]. An experimental procedure has been developed to measure electron emission [3, 22-25] due to energetic ion bombardment to the metallic surface during PIII. The spatial and temporal growth and collapse of the ion sheath around a spherical electrode during a negative high voltage pulse have been studied by Yatsuzuka et al. [26] in a uniform nitrogen plasma. In recent years, some researchers have addressed about dielectric substrate [27-30]. Recently Schiesko et al. [31] investigated about sheath response in low pressure argon plasma, when the substrate is biased positive. Time evolution of collisionless ion matrix sheath and its dynamics are presented by some models [7-8, 32-35] and experiments [9, 36]. In all the above cases, the duration of pulses applied to the substrate is greater than the ion plasma response time.

3.3 Experimental Set-up

The schematic diagram of the system is shown in Fig. 3.1. The plasma production is explained in Chapter 2. The plasma density (n_0) and electron temperature (T_e) were determined with Langmuir probe for various axial and radial positions. The plasma was uniform throughout the main chamber. For a fixed discharge current (I_{dis}), n_0 and T_e were uniform for relevant locations i.e., for $I_{dis} = 0.4$ A, $n_0 = 8.49 \times 10^9 \text{ cm}^{-3}$ and $T_e = 2.11$ eV. Since the plasma parameters (I_{dis} , n_0 and T_e) were dependent on filament heating potential, so the parameters were varied by changing the filament heating potential.

In the main chamber, a substrate (SS disc of diameter 10.2 cm and thickness 0.4 cm) was mounted on a SS rod and the SS rod was fixed in the axis of the chamber. A high-voltage (HV) probe (Tektronix make 1000X probe) and a current transformer CT₁ (Bergoz make of sensitivity 1 volt/ampere) were mounted on the SS rod and were used to measure the pulse voltage and the current respectively. Such type of current transformers could measure the current from microamperes to 20 kilo ampere. To measure some of the properties of the displaced electrons from the ion matrix sheath during the bias period, a grounded extended

Chapter 3: Study of Electron Behavior in a Pulsed Ion Sheath

chamber (inner diameter 14 cm and length 30 cm) was attached to the main chamber, which was isolated from the main chamber by a metallic mesh (wire diameter 53 μm and aperture 74 μm) whose grid size was smaller than Debye length (λ_D). The mesh transparency was 34% and it was grounded. The distance between the mesh and the substrate was 20.6 cm. In the extended chamber, an axially movable disc probe (collector) of diameter 8 cm and thickness 0.4 cm was kept, which was grounded and in this path there was a current transformer (CT_2) as shown in Fig. 3.1. The collector was for the collection of the displaced electrons from the main chamber through the metallic mesh during the application of pulse and was placed at 0.5 cm behind the mesh for the optimal signal.

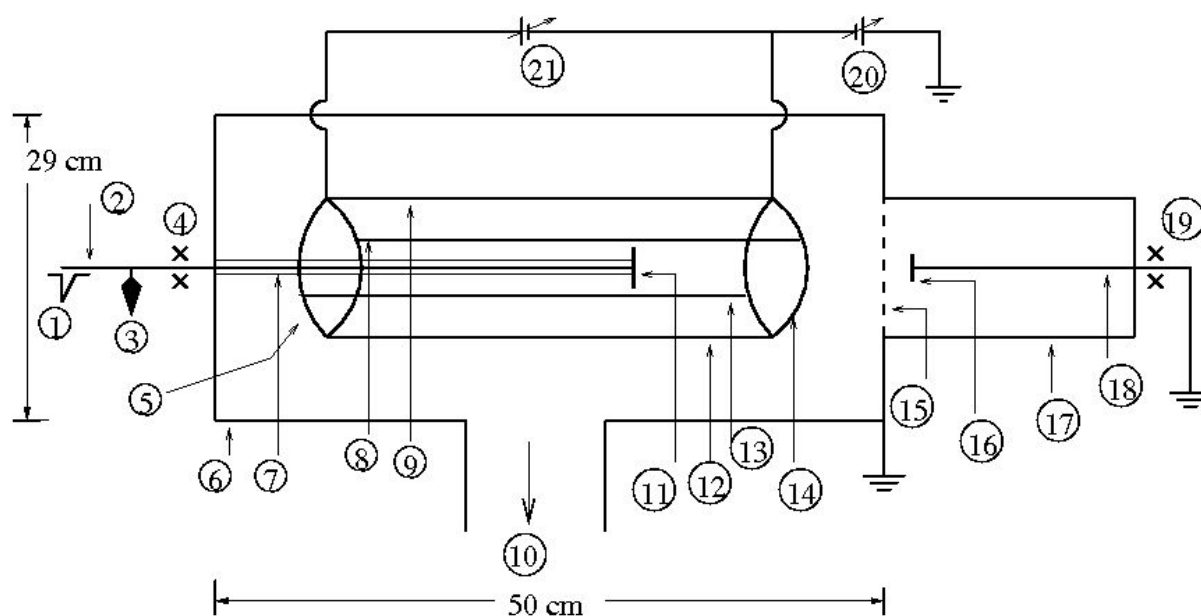


Figure 3.1 Schematic of the experimental set-up. (1) Applied negative voltage pulse. (2) and (18) are the SS rods. (3) high-voltage probe; to measure the voltage signal. (4) and (19) are Current transformers, CT_1 and CT_2 respectively; to measure the current signal. (5) and (14) are SS rings. (6) Main chamber or vacuum chamber. (7) Ceramic tube. (8),(9), (12) and (13) are the filaments. (10) Pumping system. (11) Stainless steel disc (substrate); on which bias is applied. (15) Metallic mesh. (16) Stainless steel disc (collector); to measure the electron current in the extended chamber during the bias period. (17) Extended chamber. (20) Discharge voltage. (21) Filament heating voltage.

The pulse-forming circuit is described in Sec. 2.6. The values of the capacitor (C) and the resistor (R_2) were adjusted in such a way that the pulse duration always satisfied the condition $\tau_i > \tau_p > \tau_e$ and the pulse height was decided by the voltage to which capacitor was charged. The value of the inductor was fixed. For varying the τ_p , capacitance of the capacitor and resistance of R_2 were adjusted.

3.4 Results and Discussions

Figure 3.2(a) shows the applied voltage pulse (solid line) and current (dotted line) on the electrode in presence of plasma for the pulse duration of 140 ns. This pulse duration is in between the electron and ion response times and is given in Table I for some plasma densities. The rise time of the voltage pulse is 40 ns with a comparatively slow fall time. The current signal (measured by CT₁) shows some fluctuations. Fig. 3.2(b) shows the collector signal (measured by CT₂) without plasma (dotted line) and in presence of plasma (solid line) during the bias period. It is seen that the collector signal in presence of plasma goes to zero earlier than the voltage pulse. It is assumed that on the application of the negative pulse bias (U_0) on the electrode, electrons are repelled instantaneously and isotropically from the vicinity of the electrode. The instantaneous repulsion of the electrons leads the collector signal goes to zero before voltage pulse. The fluctuations in the collector signal during the bias period are assumed to be due to electrostatic pickups.

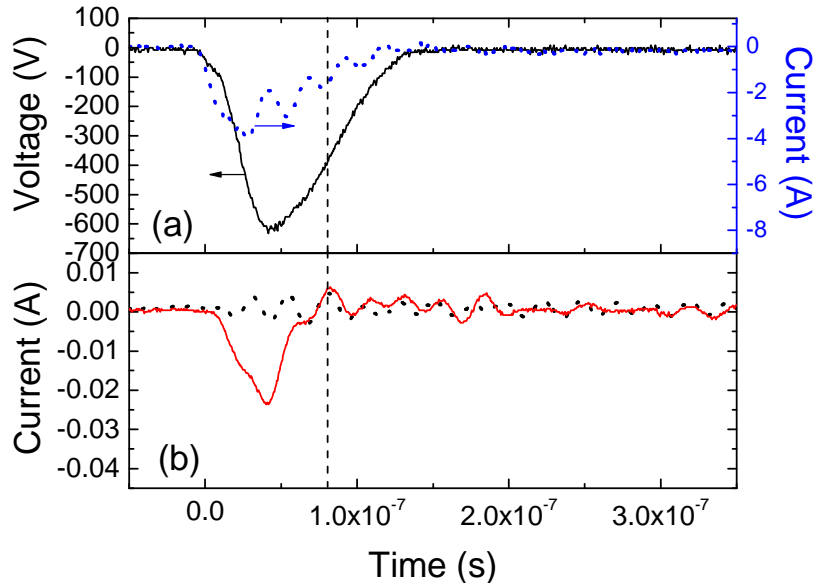


Figure 3.2(a) The applied negative voltage pulse (solid line) and current (dotted line) on the electrode. The arrows indicate the axis side. **(b)** The response of the collector without plasma (dotted line) and with plasma (solid line). The dashed line indicates the collector signal goes to zero before voltage. Here $U_0=-650$ V, $n_0=8.49\times 10^9$ cm⁻³ and $\tau_p=140$ ns.

Figure 3.3 and Fig. 3.4 show the applied voltage and current to the substrate and the signal of the collector for 250 ns and 300 ns respectively. In shorter pulse durations there are some fluctuations in the current signal and the collector signal (Fig. 3.2) than in the longer

Chapter 3: Study of Electron Behavior in a Pulsed Ion Sheath

pulse durations [Fig. 3.3 and Fig. 3.4]. There is no time delay of voltage and collector signal peaks.

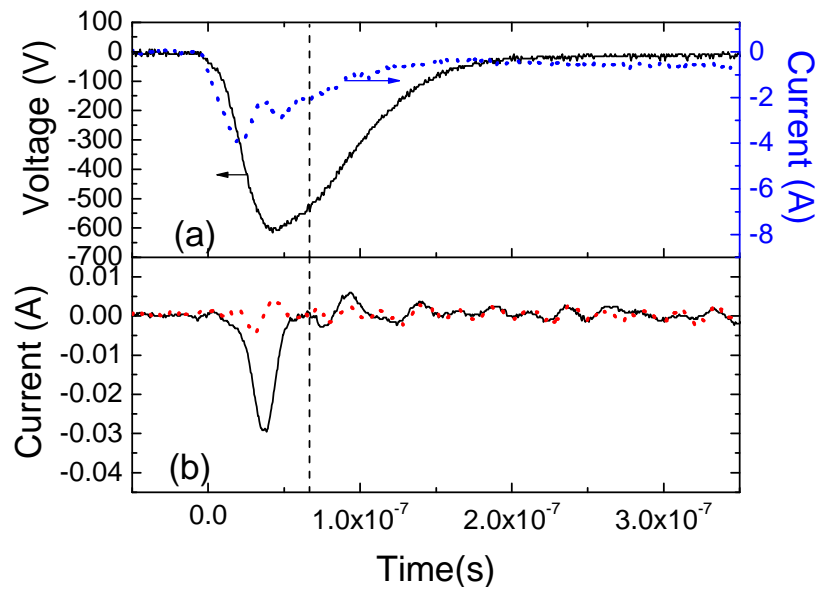


Figure 3.3 This plot is for a longer pulse duration, i.e., for 250 ns. Here $U_0 = -650$ V and $n_0 = 8.49 \times 10^9$ cm^{-3} .

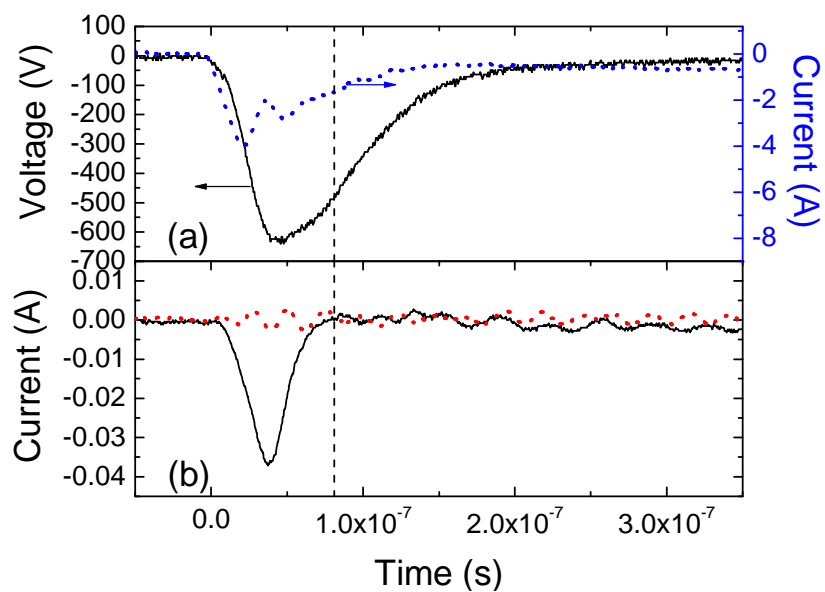


Figure 3.4 This plot is for pulse duration of 300 ns. Here $U_0 = -650$ V and $n_0 = 8.49 \times 10^9$ cm^{-3} .

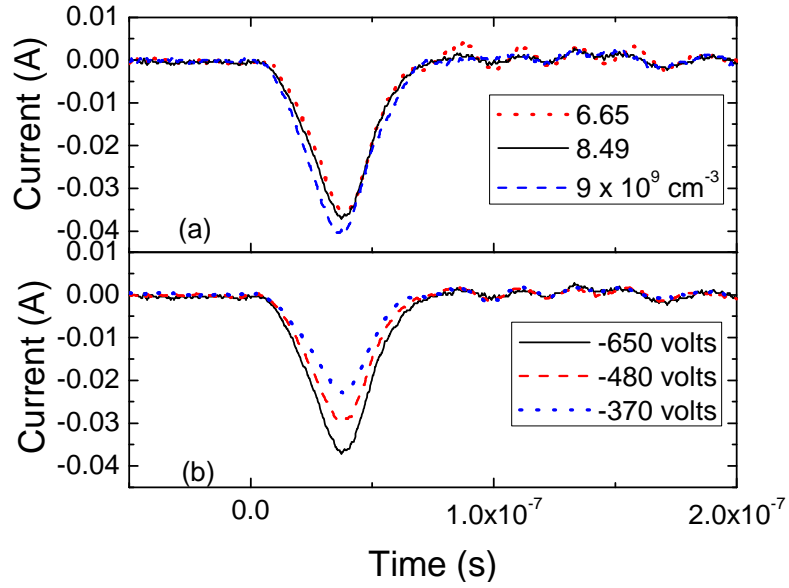


Figure 3.5 Collector signals for the pulse duration of 300 ns. **(a)** Shows for different densities and **(b)** shows for different applied voltages.

Figure 3.5 shows; there is no time delay between the peaks of the collector signal for various densities and applied voltages for constant pulse duration. This shows on increasing of plasma density and applied voltage, the magnitude of the collector signal increases.

The integral of the collector signal gives the total area under the curve. This area under the curve is a measure of the total number of electrons (N_c) ejected from the main chamber during the bias and collected by the collector, given in Eq. (3.1).

$$N_c = \frac{1}{e} \int_0^{\tau_c} I_c dt \quad (3.1)$$

where I_c is the collector current, e is the electron charge and τ_c is the collector signal duration. It is seen that more number of electrons are expelled from the main chamber on increasing electron density [Fig. 3.6(a)] and the applied pulse magnitude [Fig. 3.6(b)]. Fig. 3.6 shows more number of electrons is expelled for longer pulse widths.

On the application of a sudden negative voltage to an electrode [2, 11], the width s_0 of the ion matrix sheath for a planar geometry is

Chapter 3: Study of Electron Behavior in a Pulsed Ion Sheath

$$s_0 = \left(\frac{2\epsilon_0 U_0}{en_0} \right)^{1/2} \quad (3.2)$$

where U_0 is the voltage applied to the electrode. Thus the number of electrons displaced from the ion matrix sheath (N_s) is

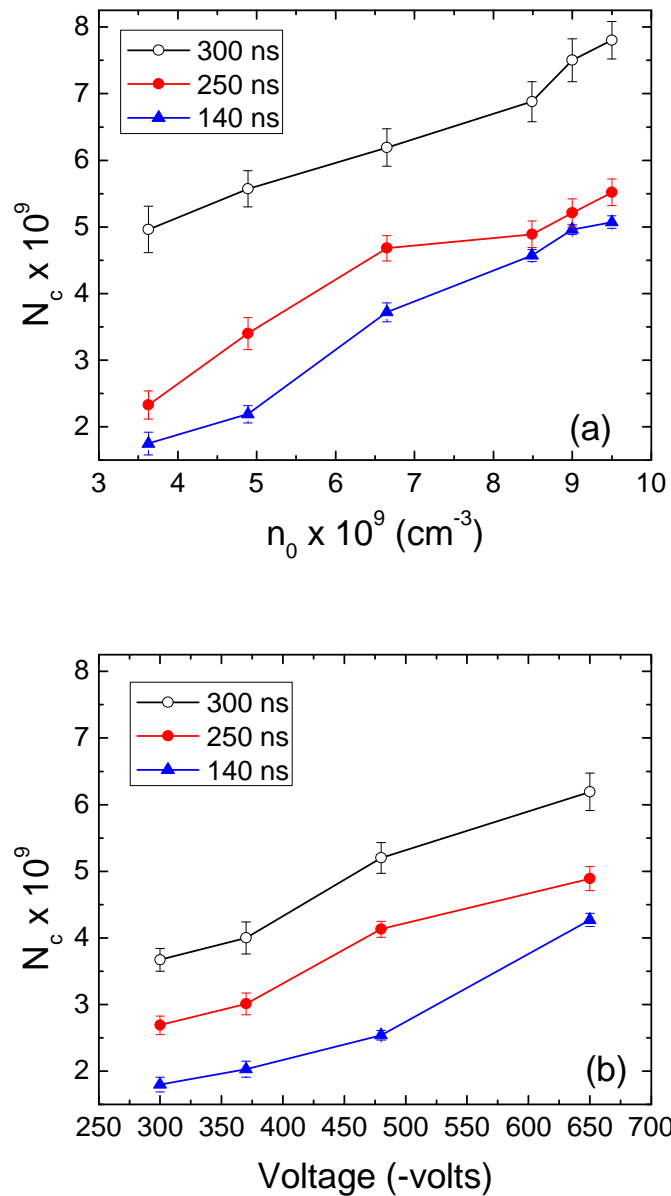


Figure 3.6 Number of electrons (expelled from the main chamber) collected by the collector are increased for various pulse durations. **(a)** Shows the number of electrons collected by the collector vs plasma density for a constant applied voltage of -650 V. **(b)** Shows the number of electrons collected by the collector vs applied voltage for a constant plasma density of $8.49 \times 10^9 \text{ cm}^{-3}$.

Chapter 3: Study of Electron Behavior in a Pulsed Ion Sheath

$$N_s = n_p V_s \quad (3.3)$$

where V_s is the volume of the ion matrix sheath during the bias period. V_s is calculated by multiplying the total substrate area (both sides) with the ion matrix sheath thickness.

To estimate the number of electrons lost to the walls, we have to calculate the number of electrons lost on the collector surface area (N_t) during the bias period as if there is no mesh, given in Eq. (3.4).

$$N_t = \frac{N_c}{T} \times 100 \quad (3.4)$$

where N_c is the number of electrons collected by the collector in presence of the mesh and T is the optical transparency of the mesh. Thus the total number of electrons lost to the inner surface area of the main chamber (N_{lost}) i.e., number of electrons lost to the walls is [37]

$$N_{lost} = \frac{N_t}{A_1} \times A_2 \quad (3.5)$$

where A_1 is the one sided area of the collector and A_2 is inner surface area of the main chamber. From Eq. (3.5) the total number of electrons lost to the walls of the main chamber during the bias period can be estimated.

Table I shows the number of electrons lost to the walls (N_{lost}) increases with plasma density for various applied bias for constant pulse duration. It is also seen that N_{lost} increases with applied bias for various plasma density for constant pulse duration. Here for various pulse durations, N_{lost} is larger than the N_s . This shows that the electrons lost to the walls come from the ion matrix sheath as well as from bulk plasma.

In Fig. 3.7, N_{lost} is plotted against N_s for various pulse durations. It is seen that N_{lost} increases with N_s . Assuming a linear dependency between N_{lost} and N_s , a relation can be written as

$$N_{lost} = kN_s \quad (3.6)$$

where k is a constant.

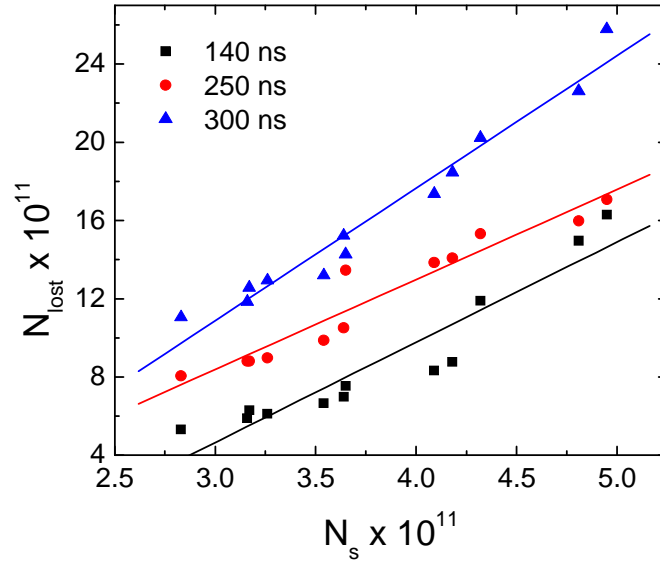


Figure 3.7 Number of electrons lost to the walls is plotted against the number of electrons displaced from the ion matrix sheath for different pulse durations. Number of electrons lost to the walls is increased linearly with the number of displaced electrons. Points are fitted by a straight line for better viewing.

$$N_{lost} = k \sqrt{\left(\frac{2\epsilon_0 U_0}{en_0} \right)} A_s n_0 \quad (3.7)$$

where A_s is taken as the electrode area. The number of plasma electrons N_p is

$$N_p = n_0 V_1 \quad (3.8)$$

where V_1 is the volume of the main chamber. Now a relation can be developed such that

$$\frac{N_{lost}}{N_p} = k_1 \sqrt{\left(\frac{U_0}{n_0} \right)} \quad (3.9)$$

where k_1 is another constant. The percentage (p) of electrons lost to the walls is

$$p = \frac{N_{lost}}{N_p} \times 100 \quad (3.10)$$

where N_p is the total number of plasma electrons which can be calculated from the Eq. (3.8).

Chapter 3: Study of Electron Behavior in a Pulsed Ion Sheath

Table I The sheath thickness, number of electrons displaced from the sheath, the number of electrons lost to the walls, ion plasma period for different pulse durations, applied bias and densities.

τ_p (ns)	Bias (U_0)	$n_0 \times 10^9$ (cm^{-3})	s (mm)	$N_s \times 10^{11}$	$N_{lost} \times 10^{11}$	τ_i (ns)	τ_e (ns)	
140	-300	6.65	2.23	2.83	5.31	369	1.36	
		8.49	1.97	3.16	5.88	327	1.20	
		9	1.92	3.26	6.11	317	1.17	
	-370	6.65	2.48	3.17	6.29	369	1.36	
		8.49	2.19	3.54	6.66	327	1.20	
		9	2.13	3.64	6.99	317	1.17	
	-480	6.65	2.82	3.65	7.54	369	1.36	
		8.49	2.50	4.09	8.32	327	1.20	
		9	2.42	4.18	8.77	317	1.17	
	-650	6.65	3.28	4.32	11.89	369	1.36	
		8.49	2.90	4.81	14.96	327	1.20	
		9	2.82	4.95	16.29	317	1.17	
	250	-300	6.65	2.23	2.83	8.05	369	1.36
			8.49	1.97	3.16	8.81	327	1.20
			9	1.92	3.26	8.98	317	1.17
-370		6.65	2.48	3.17	8.81	369	1.36	
		8.49	2.19	3.54	9.87	327	1.20	
		9	2.13	3.64	10.50	317	1.17	
-480		6.65	2.48	3.65	13.45	369	1.36	
		8.49	2.19	4.09	13.84	327	1.20	
		9	2.13	4.18	14.08	317	1.17	
-650		6.65	3.28	4.32	15.31	369	1.36	
		8.49	2.90	4.81	15.98	327	1.20	
		9	2.82	4.95	17.07	317	1.17	
300		-300	6.65	2.23	2.83	11.06	369	1.36
			8.49	1.97	3.16	11.85	327	1.20
			9	1.92	3.26	12.94	317	1.17
	-370	6.65	2.48	3.17	12.57	369	1.36	
		8.49	2.19	3.54	13.20	327	1.20	
		9	2.13	3.64	15.23	317	1.17	
	-480	6.65	2.82	3.65	14.27	369	1.36	
		8.49	2.50	4.09	17.37	327	1.20	
		9	2.42	4.18	18.46	317	1.17	
	-650	6.65	3.28	4.32	20.23	369	1.36	
		8.49	2.90	4.81	22.61	327	1.20	
		9	2.82	4.95	25.78	317	1.17	

In Fig. 3.8, the percentage of electron lost to the walls is plotted for $(n_0)^{-1/2}$ and $(U_0)^{1/2}$. Though the number of electrons lost to the walls is increased for plasma density and

Chapter 3: Study of Electron Behavior in a Pulsed Ion Sheath

applied voltage, but the percentage of electrons lost to the walls is decreased with plasma density (due to large N_p), which is followed the Eq. (3.9). So for lower densities, percentage of loss is more than the higher densities.

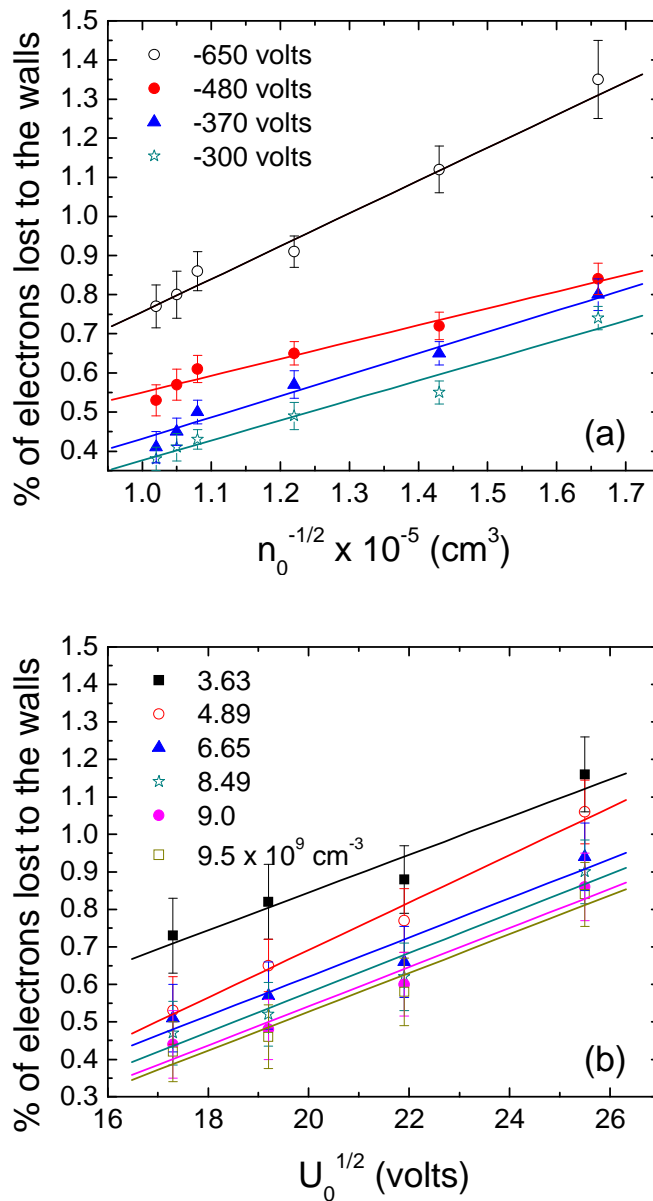


Figure 3.8 Percentage of electrons lost to the walls during the bias period for a pulse duration of 300 ns.

Figure 3.9 shows the number of electrons lost to the wall increases linearly with increase in plasma density for various electrode surface areas.

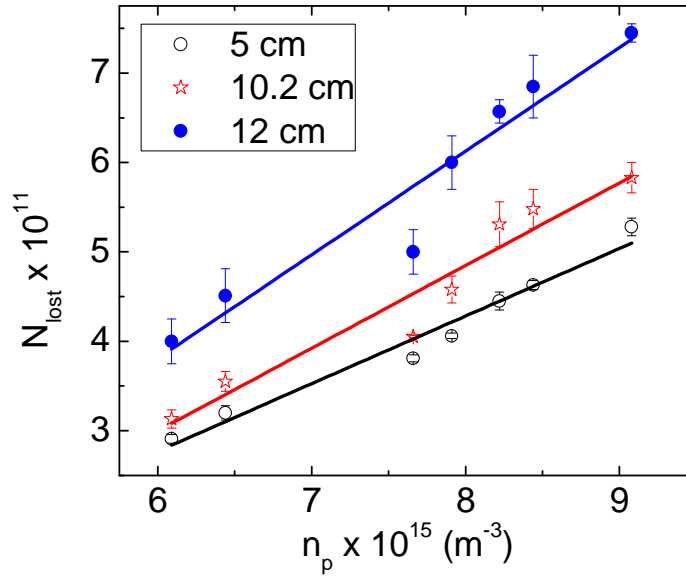


Figure 3.9 This shows for number of electrons lost to the wall versus plasma density for $U_0 = -550 \text{ V}$ and $\tau_p = 250 \text{ ns}$.

Figure 3.10 shows the collector current signals, when the disc electrode is set for various tilt angles (ϕ) to the collector. The electrode was set at a different tilt, which is the angle between the normal directions of the collector and the electrode (Figure 3.11). The tilt angles were set at 0° or 180° , 45° , 90° and 135° . The solid line shows the collector current signal for the horizontally (0° or 180°) mounted electrode to the collector. The dotted line shows, when the electrode is mounted perpendicularly (90°), that is the rod is mounted at a radial periphery of the electrode. The dashed line is for 45° . It is seen that for the horizontal position of the electrode to the collector, the time width of the collector current signal is more than the other two and the magnitude of current is less, i.e. on the increasing of the electrode angle to the collector, the time width of collector current signal decreases and the magnitude increases. But the total charge area under the curve is approximately same for all three conditions. So the number of electrons lost to the wall is approximately same for all, which is given in Table II. This shows that for above all three conditions, the number of electrons expelled during the bias period have the same plasma volume for the fixed plasma density, pulse magnitude and the pulse width. For 45° and 135° the collector current signal magnitude and the time width was approximately same.

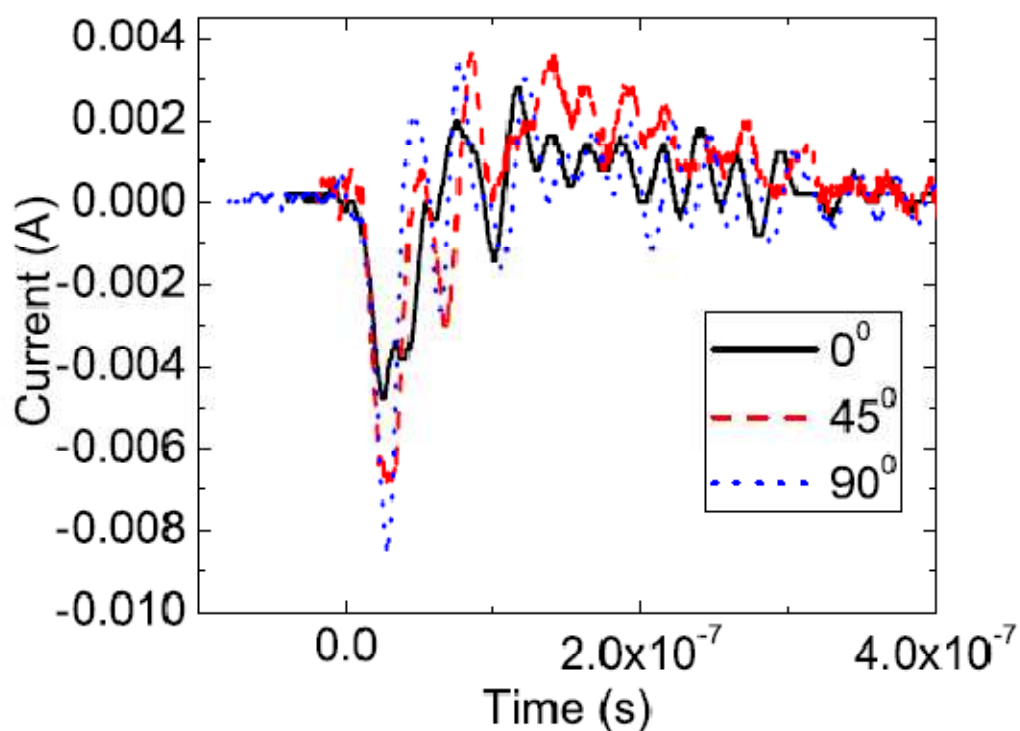


Figure 3.10 Collector current signals for various electrodes tilt angles to the collector. Here $U_0 = -550$ V, $n_p = 6.09 \times 10^9 \text{ cm}^{-3}$ and $\tau_p = 250$ ns. The electrode diameter is 5 cm. The electrostatic pick-ups are more for smaller electrode diameter.

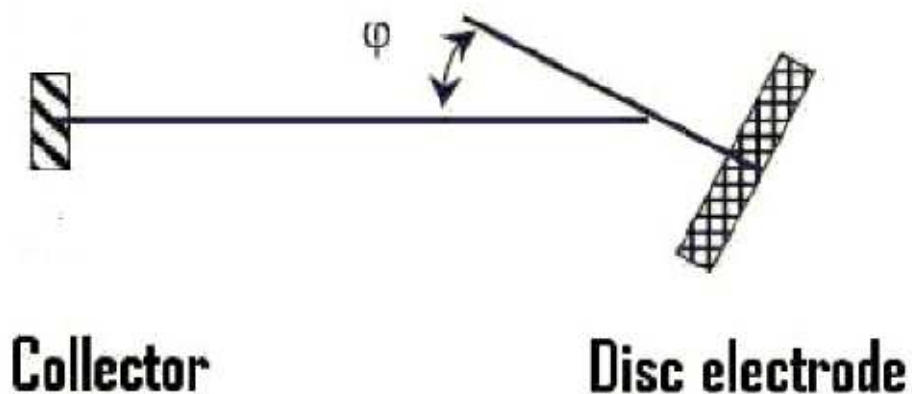


Figure 3.11 Schematic of disc electrode angle, which angle is between collectors and electrodes normal direction.

Chapter 3: Study of Electron Behavior in a Pulsed Ion Sheath

Table II Comparison of number of electrons lost to the wall for various electrode tilt angles. Here $U_0 = -550$ V, $\tau_p = 250$ ns and the electrode diameter is 5 cm.

$n_p \times 10^9$ (cm^{-3})	s (mm)	$N_s \times 10^{11}$	Number of electrons lost to the chamber wall (N_{lost}) $\times 10^{11}$		
			0°	45°	90°
6.09	3.13	0.87	2.67	2.39	2.68
6.44	3.03	0.89	3.13	3.24	3.06
7.66	2.78	0.97	3.55	3.81	3.67
7.91	2.74	0.99	4.05	4.14	3.97
8.22	2.69	1.0	4.58	4.98	4.50
8.44	2.65	1.1	5.08	5.18	4.75
9.08	2.56	1.5	5.48	5.75	5.54

When the electrode is horizontally mounted, then the collector sees a large surface area of the electrode. But on increasing angle of the electrode, the exposing area of the electrode to the collector is less. This may cause the decrease in time width of the collector signal when the electrode tilt angle increases to the collector. But the collector collects the approximately same number of electrons coming out from the same plasma volume for all three conditions. So if the time width decreases for larger angle, the magnitude of the current signal will increase. When negative bias is applied to a planar electrode, we normally apply 1-D planar model understanding. Then why should the same number of electrons collected by the collector even when the angle of the planar electrode with respect to the collector is changed, which is interesting. Even though the transient bias time scale is in between the ion and electron plasma periods, still the displaced electrons are able to modify the quasi-neutrality condition of the remaining plasma in the chamber, and the plasma is able to throw the excess electrons to the chamber wall. This is a new way of looking at transient sheath dynamics and electron interaction with bulk plasma.

The grid size of the mesh ensures that relatively there is no plasma inside the extended chamber, because density measurements at various positions in the extended chamber are below measurable limit. But the charged particles, with a directed velocity will penetrate the mesh. So those electrons are expelled from the main chamber, will enter into the extended chamber. The electrons which hit the mesh wires are lost, because the mesh is grounded. The electron-neutral collision mean free path is 39 cm. So the electrons which

enter this chamber retain their energies, because they are now moving in vacuum without any collision.

3.5 PDP1 Computer Simulation

PDP1 is a 1-D planar bounded plasma simulation code [38], which is described in detail by Birdsall [39]. The particle-in-cell (PIC) method [39-40] is implemented in PDP1 to solve for motions of the particle and is based on the simultaneous solution of the Newton motion equations $m_i \vec{a}_i = q_i \vec{E}$ ($i = 1, 2, 3, \dots, N$, where N is the number of charged particles in the system) and the Poisson equation $\nabla^2 \phi = -\frac{\rho}{\epsilon_0}$. Charged particles of finite size are placed in a grided system, which will move about due to forces of their own and applied fields. Here the physics comes from two parts,

- (a) Field produced by the particles \rightarrow this is obtained from Maxwell's equations.
- (b) Motion produced by the fields \rightarrow this is obtained by solving Newton-Lorentz equation of motion.

In a 1-D model, all physical quantities vary along x-axis; there are no variations in y or z axes.

From the particle positions and velocities, charge densities are calculated at the grid points. Using these charge densities as sources, electric field is calculated by solving Maxwell's equation on the grid. Once the electric field is known at the grid points, the forces on the particles are calculated. Using these forces, the new particle velocities and positions are calculated; and this whole cycle is repeated for many time steps.

PDP1 employs general series *RLC* circuit [41] solvers as shown in Fig. 3.12 to handle the full range of external circuit parameters, including open circuit, short circuit and current drives circuit which is shown in figure. The general circuit equation is used to advance the capacitor charge Q :

$$L \frac{d^2 Q}{dt^2} + R \frac{dQ}{dt} + \frac{Q}{C} = V(t) + \phi_{nc} - \phi_0 \quad (3.11)$$

where nc is number of cells from 0 to nc .

Chapter 3: Study of Electron Behavior in a Pulsed Ion Sheath

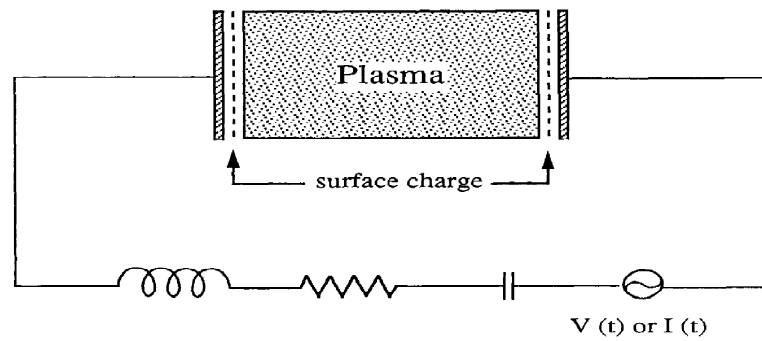


Figure 3.12 Simulation plasma system including the external R-L-C circuit for the planar geometry.

The PDP1 code also uses a Monte-Carlo (MC) scheme to model charged and neutral particle collisions, such as the elastic, excitation and ionization collisions are considered for the electrons and the scattering and charge transfer collisions for the ions.

In this study, the plasma is initially Maxwellian and the electrode is assumed to be perfectly absorbing. Throughout the simulation, we use the typical parameters of experimental results. For most of the simulations presented here, the pressure of the neutral gas was set to 1×10^{-3} mbar, hence the plasma was assumed to be collisionless. The important parameters (experimental parameters) are as follows:

Gas = argon,

Plasma length = 0.5 m

Electrode area = 0.008 m^2 (planar)

Electron temperature = 0.9 – 2.5 eV

Ion temperature = 0.2 eV

Time step = 1×10^{-10} s

Pulse width = 300 ns

Pulse rise time = 50 ns

Number of particles = 4000

Pulse voltages (U) = -300 V, -370 V, -480 V & -650 V

Plasma density = $3.63 \times 10^{15} \text{ m}^{-3}$ to $9.5 \times 10^{15} \text{ m}^{-3}$

3.5.1 Simulation Results

The PDP1 code is run with similar shape of potential (Figure 3.2(a)) which is applied on the left electrode. We have set the applied voltages for a ramping time at 50 ns. The rise time of the applied signal is equal to $DC/Ramp$. Figure 3.13 shows the uniform velocity distribution of electrons without bias.

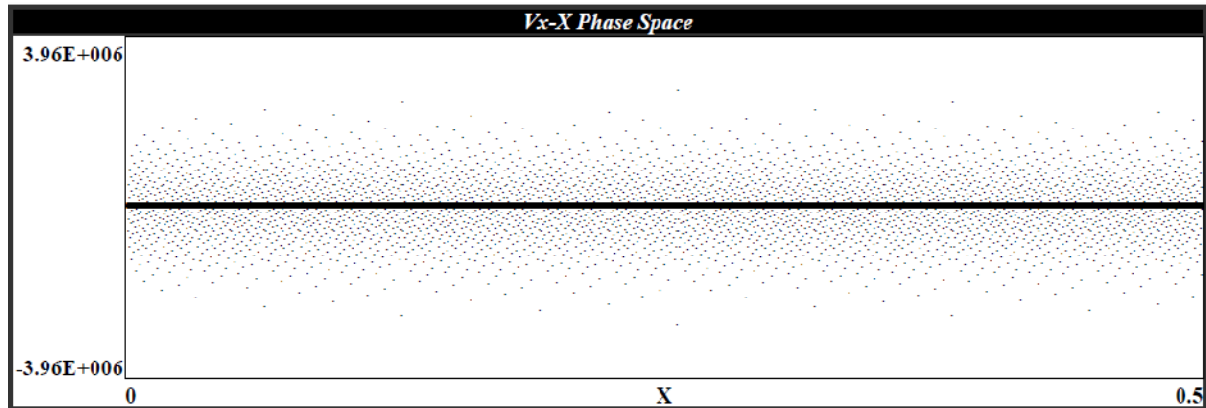


Figure 3.13 Results from PDP1 regarding the phase space (y-axis corresponds to the velocity and x-axis is the distance between left electrode and right electrode). All units are in SI. The thick centre line is the ion distribution and dots are electron distribution. This is for at $t = 0$ and at density of $3.63 \times 10^{15} \text{ m}^{-3}$.

Figure 3.14 shows the velocity distribution of electrons when the voltage is applied on the left electrode after the rise time (50 ns). The mean velocity of electrons does not change, i.e., the width of electron distribution is same in both positive and negative axes. On the application of negative voltage, mobile electrons are expelled, causing an ion matrix sheath. The ion matrix sheath thickness can be measured from this figure and also from the potential profile (Fig. 3.15). The obtained sheath thickness is very close to the thickness calculated from Eq. (3.2). It is seen that in the ion matrix region, there is a slightly small break (circle mark) in the thick centre line, i.e., some ions are lost to the negative biased electrode, which can be seen more clearly in Figs. 3.14(b) and 3.16.

Chapter 3: Study of Electron Behavior in a Pulsed Ion Sheath

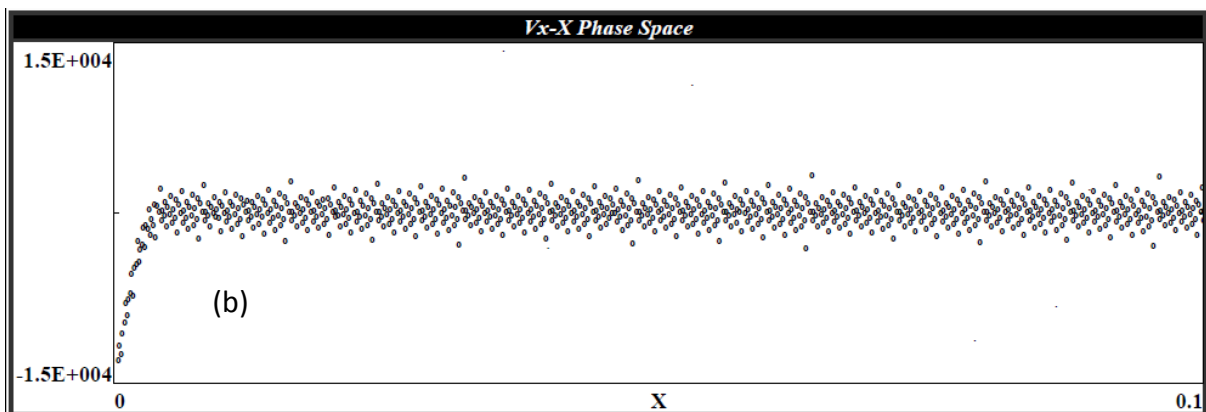
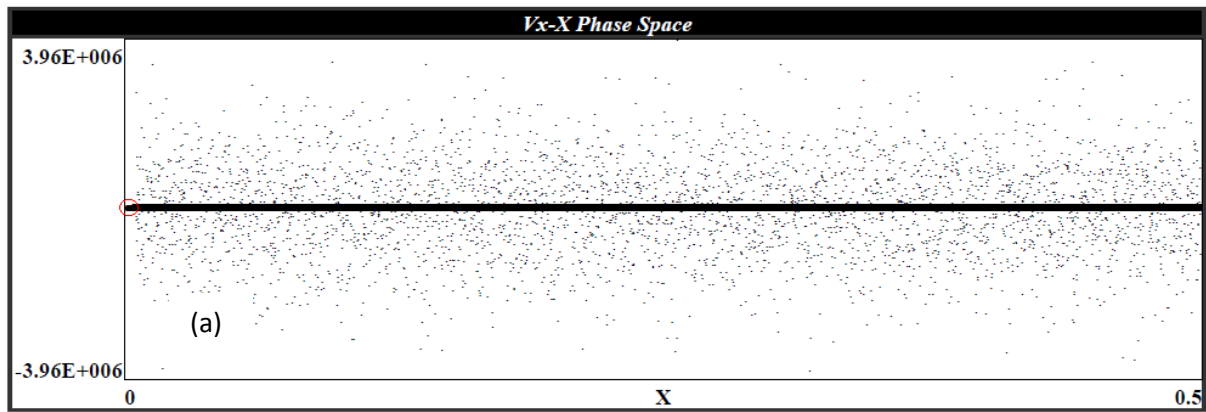


Figure 3.14 (a) The left electrode is biased by a ramp such that its bias reaches -300 V in 50 ns. It is seen that the entire electron distribution is given a uniform velocity much similar to Fig. 3.13, but forming an ion matrix sheath. (b) Zoom of Fig. (a).

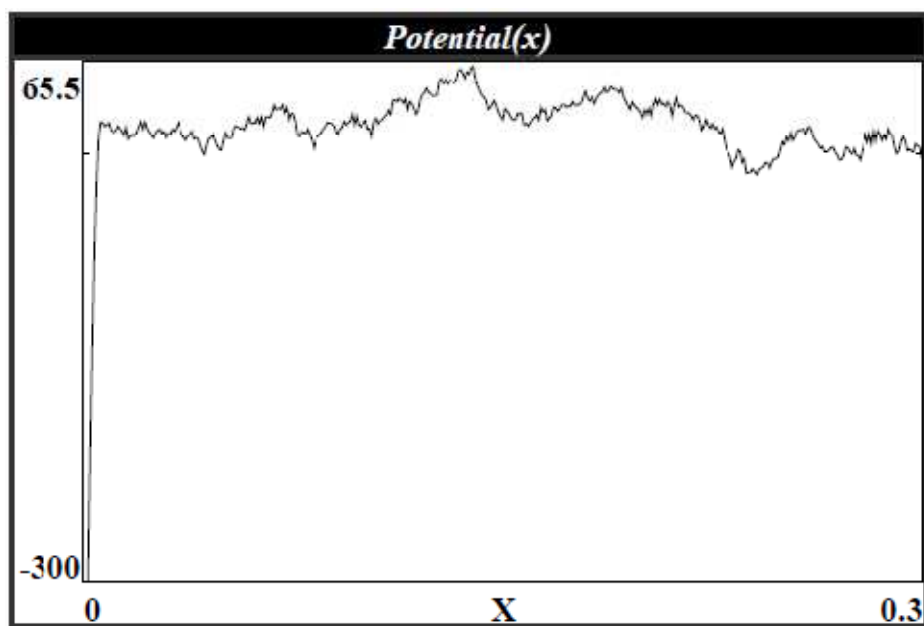


Figure 3.15 Potential profile which shows the sheath thickness at the left electrode.

Chapter 3: Study of Electron Behavior in a Pulsed Ion Sheath

Figure 3.16 shows the number of electrons lost to the right electrode (chamber wall in the experiment). The electrons which are lost from the simulation region are not the ones displaced from regions closer to the biased electrode, but also electrons closer to the right electrode and a small break down in ion curve is shown (ellipse mark). This shows that a delay in ion response comparison to electron response. The simulation is run for the rise time of the pulse (50 ns) at which the bias reaches its maximum value. So, even if, the applied pulse width is less than the ion plasma period, some ions can be lost ballistically to the negative biased electrode, which is clearly shown in Fig. 3.14(b). We measure the electrons lost to the electrode only on rise time of the pulse, not on the fall time. Because on the fall time of pulse plasma should remains it's quasi-neutrality, and the number of electrons will increase. When the voltage pulse reaches its zero value, the plasma would be quasi-neutral, which is shown in Fig. 3.17.

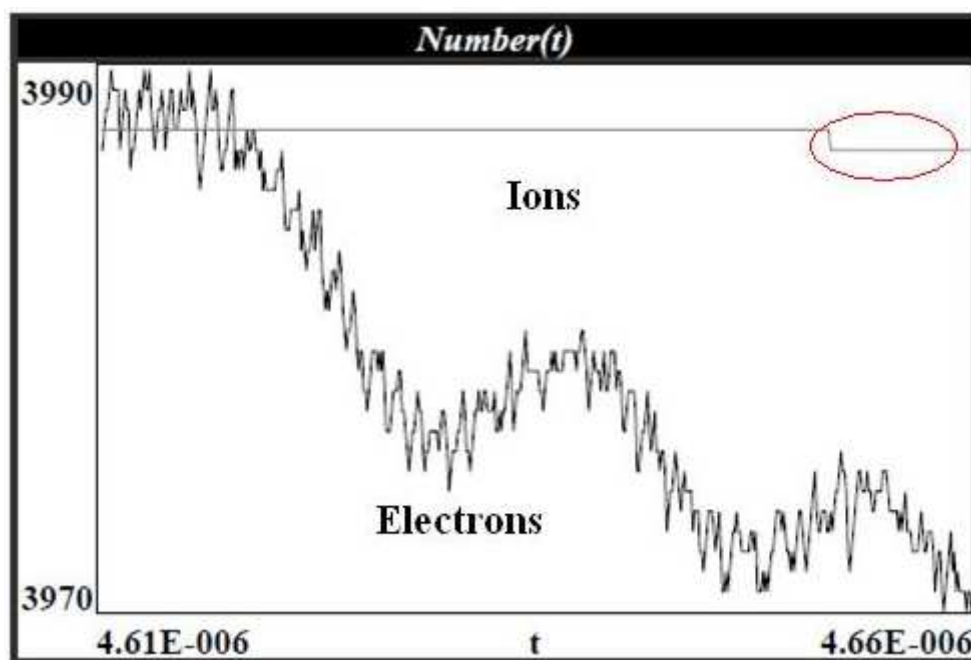


Figure 3.16 The number of electrons lost to the right electrode after 50 ns when the bias reaches its maximum value. Initially the code was run up to 4.61 μ s for better accuracy of electron and ion distributions. During this time 10 numbers of particles have lost.

Figure 3.18 shows the simulated ion and electron densities at 50 ns. The left hand side ($x=0$) represents the electrode to which a negative pulse is applied. At this moment the ion

Chapter 3: Study of Electron Behavior in a Pulsed Ion Sheath

matrix sheath thickness is 3.5 mm. In this figure, a pre-sheath can be seen between $x \approx 3.5$ and $x \approx 5.7$ mm from electron and ion spatial profiles.

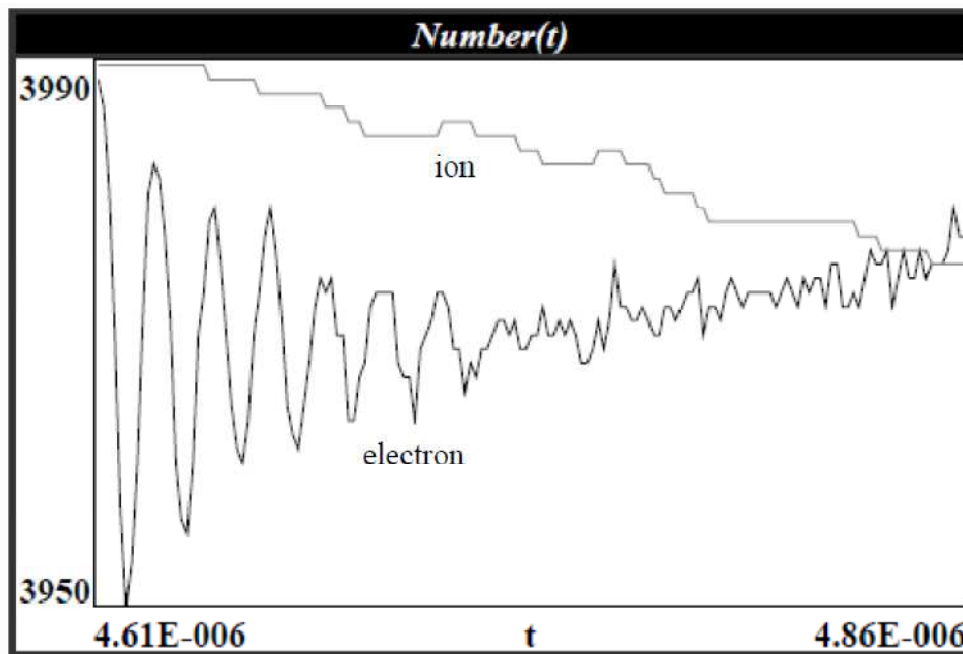


Figure 3.17 This profile shows for number of particles during fall time of the applied voltage pulse. The fall time was 250 ns. This graph shows that, when voltage pulse goes to zero (after 250 ns) the number of electrons and ions are approximately same.

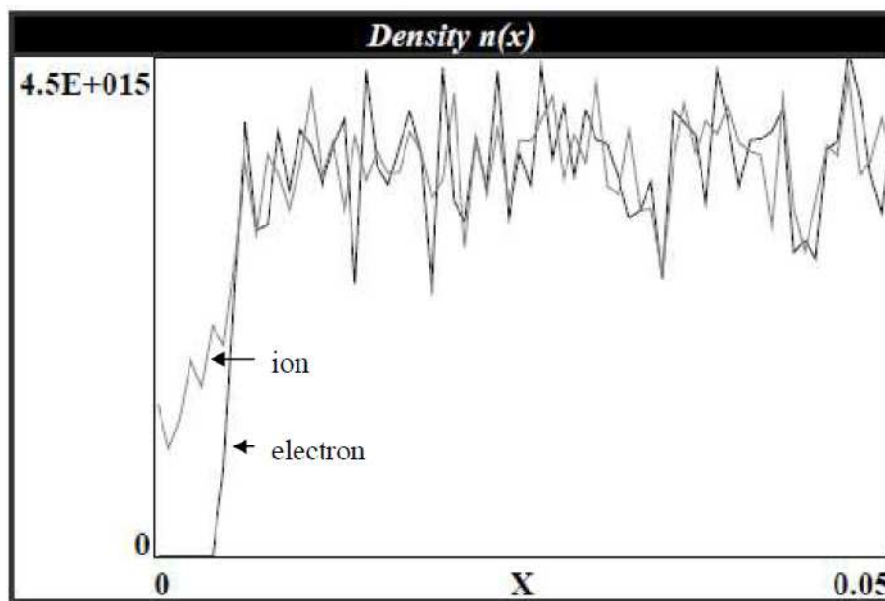


Figure 3.18 Density profile for ions and electrons for $U_0 = -300$ V and $n_0 = 3.63 \times 10^9$ cm⁻³ after 50 ns. This graph is zoomed for better view.

Chapter 3: Study of Electron Behavior in a Pulsed Ion Sheath

The results obtained from the PDP1 simulation is agreed closely with the experimental value, which is given in Table III. Though the number of electrons lost to the walls increases with increase in plasma density and voltage, but the percentage of electrons lost to the wall decreases with increase in plasma density. Because N_{lost} increases slowly with larger plasma densities (larger N_p).

Table III Comparison of the percentage of electron loss to the wall between PDP1 simulation and experimental results for various plasma densities and applied voltages. Here 'S' indicates the simulation values and 'E' the experimental values.

Density (m^{-3}) \times 10^{15}	% of electron lost to the wall			
	-300 V	-370 V	-480 V	- 650 V
3.63	0.625 (S)	0.75 (S)	0.85 (S)	1.075 (S)
	0.729 (E)	0.802 (E)	0.88 (E)	1.16 (E)
4.89	0.576 (S)	0.6716 (S)	0.825 (S)	1 (S)
	0.53 (E)	0.65 (E)	0.769 (E)	1.05 (E)
6.65	0.55 (S)	0.64 (S)	0.75 (S)	0.95 (S)
	0.50 (E)	0.572 (E)	0.66 (E)	0.938 (E)
8.49	0.504 (S)	0.605 (S)	0.712 (S)	0.9023 (S)
	0.465 (E)	0.52 (E)	0.62 (E)	0.898 (E)
9	0.5 (S)	0.5514 (S)	0.6766 (E)	0.8902 (S)
	0.443 (E)	0.48 (E)	0.6 (E)	0.856 (E)
9.5	0.476 (S)	0.536 (S)	0.645 (S)	0.814 (S)
	0.42(E)	0.458 (E)	0.58 (E)	0.83 (E)

3.6 Conclusions

The present investigation estimates the number of electrons lost to the walls and the origin of these electrons during the bias period (for $\tau_i > \tau_p > \tau_e$) for different applied voltages, densities and pulse durations in collisionless plasma. The experimental results are closely agreed with PDP1 simulation results. In summary,

- (a) the higher the substrate potential the higher the sheath thickness implies the more number of electrons displaced from the ion matrix sheath and more electron loss occurs,
- (b) increase in plasma density reduces the sheath thickness, again more number of electrons displaced from the ion matrix sheath and more electron loss occurs,

Chapter 3: Study of Electron Behavior in a Pulsed Ion Sheath

- (c) for increased pulse durations, though the number of electrons displaced from the ion matrix sheath is same, but the number of electrons lost to the walls is more for a constant applied bias and the plasma density,
- (d) the origin of the electrons, those are lost to the walls during the bias period is from the ion matrix sheath and probably from the bulk plasma as well,
- (e) with various angles between the biased planar electrode and collector, the width and magnitude of the collector current is depends on the angle; however the total number of electrons (area under the curve) lost to the chamber wall is same,
- (f) the fluctuations in the current signal (measured by CT_1) are assumed to be due to the ion matrix sheath oscillations or some non-thermal ions responding faster than τ_i , which brings the electrons back into the ion matrix sheath. These fluctuations are dependent upon τ_i/τ_p ,
- (g) PDP1 simulation results are well agreed with experimental results.

The above conditions indicate that even for pulse durations lesser than ion plasma period, the time independent ion matrix sheath understanding needs to be relooked at to find out the number of displaced electrons for the matrix sheath and their dynamics.

➤ Part of the work presented in this Chapter is published in
S. Kar and S. Mukherjee, Phys. Plasmas 15, 063504 (2008).

3.7 References

- [1] J. R. Conrad, J. L. Radtke, R. A. Dodd, F. J. Worzala, and N. C. Tran, *J. Appl. Phys.* **62**, 4591 (1987).
- [2] M. A. Lieberman, *J. Appl. Phys.* **66**, 2926 (1989).
- [3] K. G. Kostov, J. J. Barroso, and M. Ueda, *Braz. J. Phys.* **34**, 1689 (2004).
- [4] M. Shamim, J. T. Scheuer, and J. R. Conrad, *J. Appl. Phys.* **69**, 2904 (1991).
- [5] R. A. Stewart and M. Lieberman, *J. Appl. Phys.* **70**, 3481 (1991).
- [6] B. P. Wood, *J. Appl. Phys.* **73**, 4770 (1993).
- [7] B. Briehl and H. M. Urbassek, *Surf. Coat. Technol.* **156**, 131 (2002).
- [8] D. Israel, K. -U. Riemann, and L. Tsendin, *J. Appl. Phys.* **95**, 4565 (2004).
- [9] K. Yukimura, X. Ma, and T. Ikehata, *Surf. Coat. Technol.* **186**, 73 (2004).
- [10] J. R. Conrad, *J. Appl. Phys.* **62**, 777 (1987).
- [11] J. T. Scheuer, M. Shamim, and J. R. Conrad, *J. Appl. Phys.* **67**, 1241 (1990).
- [12] S. Radovanov, L. Godet, R. Dorai, Z. Fang, B. W. Koo, C. Cardinaud, G. Cartry, D. Lenoble, and A. Grouillet, *J. Appl. Phys.* **98**, 113307 (2005).
- [13] S. Mukherjee, M. Ranjan, R. Rane, N. Vaghela, A. Phukan, and K. S. Suraj, *Surf. Coat. Technol.* **201**, 6502 (2007).
- [14] J. Brutscher, R. Gunzel, and W. Moller, *Surf. Coat. Technol.* **93**, 197 (1997).
- [15] Y. X. Huang, X. B. Tian, S. Q. Yang, R. K. Y. Fu, and P. K. Chu, *Surf. Coat. Technol.* **201**, 5458 (2007).
- [16] N. Hershkowitz, "Plasma Diagnostics-Discharge Parameters and Chemistry", edited by O. Auciello and D. L. Flamm, Academic Press, New York, **1**, 113 (1989).
- [17] M. J. Mayberg, R. I. Pinstler, C. C. Petty, M. Porkolab, S. C. Chiu, W. P. Cory and R. Prater, *Nucl. Fusion* **33**, 267 (1993).
- [18] T. J. Sommerer, M. S. Barnes, J. H. Keller, M. C. McCaughey and M. J. Kushner, *Appl. Phys. Lett.* **59**, 638 (1991).
- [19] S. Quin, and C. Chan, *J. Vac. Sci. Technol. B* **12**, 962 (1994).
- [20] D. Bohm, "The characteristics of Electrical Discharges in Magnetic Fields" edited by A. Guthry and R. K. Wakerling, McGraw-Hill, New York, ch 3, p 77 (1959).
- [21] R. R. Speth, G. A. Emmert and M. J. Goekner, *Appl. Phys. Lett.* **65**, 2272 (1994).
- [22] M. M. Shamim, J. T. Scheuer, R. P. Fetherston and J. R. Conrad, *J. Appl. Phys.* **70**, 4756 (1991).

Chapter 3: Study of Electron Behavior in a Pulsed Ion Sheath

- [23] D. J. Rej, B. P. Wood, R. J. Faehl and H. H. Fleischmann, *J. Vac. Sci. Technol. B* **12**, 861 (1994).
- [24] K. Nakamura, M. Tanaka and H. Sugai, *Surf. Coat. Technol.* **156**, 83 (2002).
- [25] A. Anders and G. Y. Yushkov, *Surf. Coat. Technol.* **136**, 111 (2001).
- [26] M. Yatsuzuka, S. Miki, R. Morita, K. Azuma and E. Fujiwara, *Surf. Coat. Technol.* **136**, 93 (2001).
- [27] S. Han, Y. Lee, H. Kim, G. H. Kim, J. Lee, J. H. Yoon, and G. Kim, *Surf. Coat. Technol.* **93**, 261 (1997).
- [28] X. Tian, S. Yang, Y. Huang, and P. K. Chu, *J. Phys. D: Appl. Phys.* **37**, 50 (2004).
- [29] I. H. Tan, M. Ueda, R. S. Dallaqua, J. O. Rossi, A. F. Beloto, M. H. Tabacniks, N. R. Demarquette, and Y. Inoue, *Surf. Coat. Technol.* **186**, 234 (2004).
- [30] X. C. Li, and Y. N. Wang, *Surf. Coat. Technol.* **201**, 6569 (2007).
- [31] L. Schiesko, M. Carrere, G. Cartry, and J. M. Layet, *J. Nucl. Mater.* **363-365**, 1016 (2007).
- [32] R. Günzel and J. Brutscher, *Surf. Coat. Technol.* **85**, 98 (1996).
- [33] R. Rosa, *J. Phys. A: Gen. Phys.* **4**, 934 (1971).
- [34] K. E. Longren and I. Alexeff, *Phys. Plasmas* **15**, 093505 (2008).
- [35] K.-U. Riemann and T. Daube, *J. Appl. Phys.* **86**, 1202 (1999).
- [36] S. Mukherjee, K. Avinash and P. I. John, *Pramana-J. Phys.* **44**, 263 (1995).
- [37] S. Kar and S. Mukherjee, *Phys. Plasmas* **15**, 063504 (2008).
- [38] Codes available from Industrial Liaison Program, EECS Department, UC Berkely, CA 94720.
- [39] C. K. Birdsall, *IEEE Ttrans. Plasma Sci.* **19**, 65 (1991).
- [40] C. K. Birdsall and A. B. Langdon: *Plasma Physics via Computer Simulation* (M C Graw-Hill, NewYork, 1985).
- [41] J. P. Verboncoeur, *Journal of Computational Physics* **104**, 321 (1993).

CHAPTER 4

4 Excitation of Ion Rarefaction Waves in a Low Pressure Plasma by Applying a Short High Negative Voltage Pulse

4.1 Motivation

In the last Chapter, we measured the properties of the displaced electrons to the chamber wall, when a metallic plate is negatively pulsed biased for pulse duration in between the ion and electron plasma response times. In that case no attention was given to the wave propagation in plasma.

The present Chapter reports the experimental observation of the propagation of ion rarefaction waves, though the applied pulse duration (τ_p) is less than the ion plasma period (τ_i). The experiments are performed for single pulse excitation and the pulse magnitude is much greater than the electron plasma temperature. Such a pulse duration is chosen so that ions are collectively undisturbed and according to general understanding no force is given to ions. Hence no ion rarefaction wave should be excited. But contrary to the general understanding, excitation of ion rarefaction wave is observed. The results indicate that the speed of the ion rarefaction wave is sonic. After a distance from the exciter (biased plate), typically three-fourth of the exciter diameter, the rarefaction waves also develop a compressive part. The experimental results indicate that even though the bias durations are shorter than the ion plasma period, if the bias magnitude is large enough; some collective plasma behavior can still be excited.

An overview of the previous works is given in Sec. 4.2. The experimental setup is explained in Sec. 4.3 followed by observed results in Sec. 4.4. The experimental results are discussed in Sec. 4.5 and finally summary is given in Sec. 4.6.

4.2 An overview of Previous Works

The earliest prediction on ionic sound waves in plasmas is done by Tonks et al. [1]. The propagation characteristics of linear ($\frac{e\phi}{kT_e} \ll 1$) and nonlinear ($\frac{e\phi}{kT_e} \approx 1$) ion acoustic waves have been reported in a number of works both experimentally [2-8] and theoretically [8-10]. The experiments based on ion acoustic waves are roughly divided into two groups. One is on spontaneously excited ion acoustic waves [11, 12] in current carrying plasma, and the other [2-8] on externally excited ion acoustic waves in plasma with or without currents.

Widner et al. [8] have reported the ion acoustic wave excitation with transient ion sheath evolution. They report that the ion acoustic wave breaks away from the sheath, depends upon the launching plate geometry and the ion-neutral collisions. In experiments by Saxena et al. [6,13], a rarefactive pulse is found to fission into several pulses. Recently Oksuz et al. [14] have measured the phase velocity of ion acoustic wave near the presheath and sheath boundary in a weakly collisional plasma. Okutsu and Nakamura [15] have carried out a numerical and experimental study of the temporal development of weakly nonlinear, broad ion acoustic pulses. They used three kinds of initial perturbations for excitation of ion acoustic pulses, like pure compressive, pure rarefactive and one-cycle sinusoidal pulse in which the rarefactive leading part is followed by a compressive part. Honzawa [16] has observed solitary structures close to the grid in a double plasma device by applying a negative potential pulse. Characteristics of linear ion acoustic response of a plasma to an impulse temporal disturbance is investigated by Ikezi et al. [2]. They report that plate excitation method cannot be used to measure the dispersion of ion acoustic waves. Recently a lot of work has been carried on quantum ion acoustic wave [17-20]. Also the dust acoustic waves are observed in dusty plasmas [21-24]. Some researchers [25-27] have described the properties of ion rarefaction wave for various launching plate geometry. Nishihara et al. and Ludwig et al. [28-29] show the existence of rarefaction solitons in a two-electron-temperature plasma.

Chapter 4: Excitation of Ion Rarefaction Waves in a Low Pressure Plasma...

When the electrode potential is much more negative than the kT_e/e , an ion matrix or transient sheath forms initially around the electrode and the sheath expands far into the plasma. The first details of the sheath evolution were revealed by Alexeff et al [30] in an experiment in which an ion acoustic wave was launched by application of a -250 V pulse to an electrode in a low pressure xenon plasma. By solving Poisson's equation for a negative biased planar electrode, they showed that the transient or ion matrix sheath thickness (s_0) is

$$s_0 = \left(\frac{2\epsilon_0 U_0}{n_0 e} \right)^{1/2}.$$

The total sheath thickness (s_c) can be obtained from the quasistatic Child-Langmuir law [31]

$$s_c = \frac{\sqrt{2}}{3} \left(\frac{2eU_0}{kT_e} \right)^{3/4} \lambda_D.$$

This assumes that ions are stationary, and suddenly they see the sheath electric field and get accelerated. However, we know for stability of a steady state sheath, ions need to enter the sheath with a velocity defined by the Bohm sheath criterion [32].

Widner et al [8] observed the propagation of a rarefying disturbance from the ion matrix sheath boundary into the plasma, on the application of negative pulse of ~100 V to the electrode. Initially, this disturbance moved out rapidly from the ion matrix sheath and after several ion plasma periods, slow down to ion acoustic speed. Murakami et al. [33] pointed out that when the sheath propagation velocity is greater than the ion acoustic speed (supersonic regime, where the dynamic sheath thickness $s < s_c$), the initial pre-sheath is buried and the ions at the sheath edge are still stationary when the sheath comes by, i.e., any perturbation cannot propagate ahead of it. When the sheath propagation velocity drops below the ion acoustic speed (subsonic regime, where $s > s_c$), a rarefaction wave is lunched ahead of it, i.e., the rarefaction wave sets up a pre-sheath in plasma which starts accelerating the ions toward the ion acoustic speed. Wickens et al. [34] reported that the compressive like features can be generated by a contracting sheath introducing an ionization term in their model. The inclusion of this ionization term introduces an additional degree of freedom that allows a self-consistent steady state model, with the ionization balancing the wall losses. Similar compressive waves are also modeled by Daube et al. [35] experimentally. Collins et al [36] observed that the plasma potential decreases outside of the sheath on application of a

high negative pulse. In most of the above experiments and theoretical models, ion acoustic or rarefaction waves are excited externally in a double plasma device using grid and the applied pulse duration is greater than the ion plasma response time. To the best of our knowledge, there are no experimental or theoretical explanations available for the ion acoustic waves or the ion rarefactions waves for high voltage and the applied pulse width less than the ion plasma period.

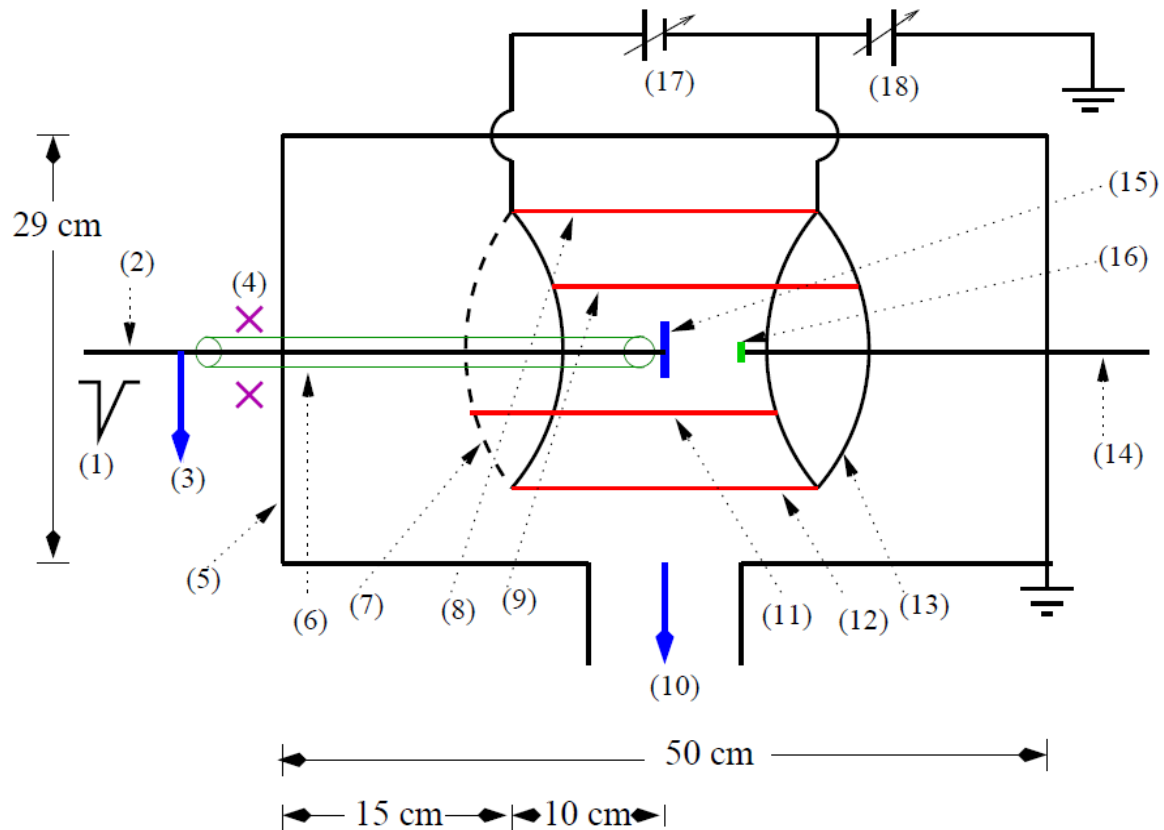


Figure 4.1 Schematic of the experimental setup. (1) Applied negative voltage pulse. (2) and (14) are the SS rods. (3) High-voltage probe; to measure the voltage signal. (4) Current transformer CT; to measure the current signal. (5) Main chamber. (6) Ceramic tube which covers the SS rod. (7) and (13) are SS rings. (8), (9), (11) and (12) are the filaments. (10) Pumping system. (15) Exciter (SS disc plate); on which pulse is applied. (16) Detecting probe (SS disc plate); to detect rarefaction disturbances, this can move axially. (17) Filament heating voltage. (18) Discharge voltage.

4.3 Experimental Setup

The schematic diagram of the system is shown in Fig. 4.1. The experiment was performed in a grounded cylindrical chamber of stainless steel (SS) 304 with an inner diameter of 29 cm and a length of 50 cm. The chamber was evacuated by using a

Chapter 4: Excitation of Ion Rarefaction Waves in a Low Pressure Plasma...

combination of rotary and diffusion pumps and the base pressure was 5×10^{-5} mbar. The plasma was generated by impact ionization of gas neutrals by primary electrons coming out from dc biased hot thoriated tungsten filaments of diameter 0.25 mm. The filaments were mounted on two SS rings. The diameter of the SS rings was 23 cm and the length of each filament was 20 cm. The distance between the inside of the radial chamber wall and the filaments were 3 cm. The filament bias potential was -65 V. The working gas was argon (99.999% pure) at pressure of 1×10^{-3} mbar. The plasma density (n_0) and electron temperature (T_e) were determined with Langmuir probe for various axial and radial positions. The plasma was uniform throughout the main chamber. For a fixed discharge current (I_{dis}), n_0 and T_e were uniform for relevant locations i.e., for $I_d = 0.4$ A, $n_0 = 3.92 \times 10^9 \text{ cm}^{-3}$ and $T_e = 6$ eV. The experiments were performed with plasma density $8.9 \times 10^8 - 4 \times 10^9 \text{ cm}^{-3}$ with electron temperature $T_e \sim 0.9-6$ eV. Since the plasma parameters (I_{dis} , n_0 and T_e) were dependent on filament heating potential (V_f). The plasma parameters were varied by changing V_f , as shown in Table I.

Table I The plasma parameters are varied with filament heating voltage. Here the filament bias potential was -65 V and pressure was 1×10^{-3} mbar.

V_f (V)	I_d (A)	T_e (eV)	$n_0 \times 10^9 \text{ cm}^{-3}$
17.3	0.05	0.9	0.89
18	0.1	1.4	1.55
18.4	0.15	1.8	1.9
19.3	0.3	4.96	3.32
20.1	0.4	6	3.92

Rarefaction disturbances were excited by applying a large negative voltage pulse (pulse magnitude $U_0 \gg kT_e/e$) to a metal plate (exciter) inserted in a low pressure argon plasma. The pulse magnitudes were -600 V to -1.5 kV and the pulse durations were 140 to 300 ns. These pulse durations were in between the ion and electron response times. The ion response times were 480-950 ns and the electron response times (τ_e) were 2-4 ns, determined by the plasma density. The pulse forming circuit is described in Sec. 2.6. In the main chamber, the metal plate (SS disc of diameter 12 cm and thickness 0.4 cm) was mounted on a

SS rod and the SS rod was fixed along the axis of the chamber. A high-voltage (HV) probe (Tektronix make 1000X probe) and a current transformer CT (Bergoz make of sensitivity 1 V/A) were mounted on the SS rod and were used to measure the pulse voltage and the current respectively.

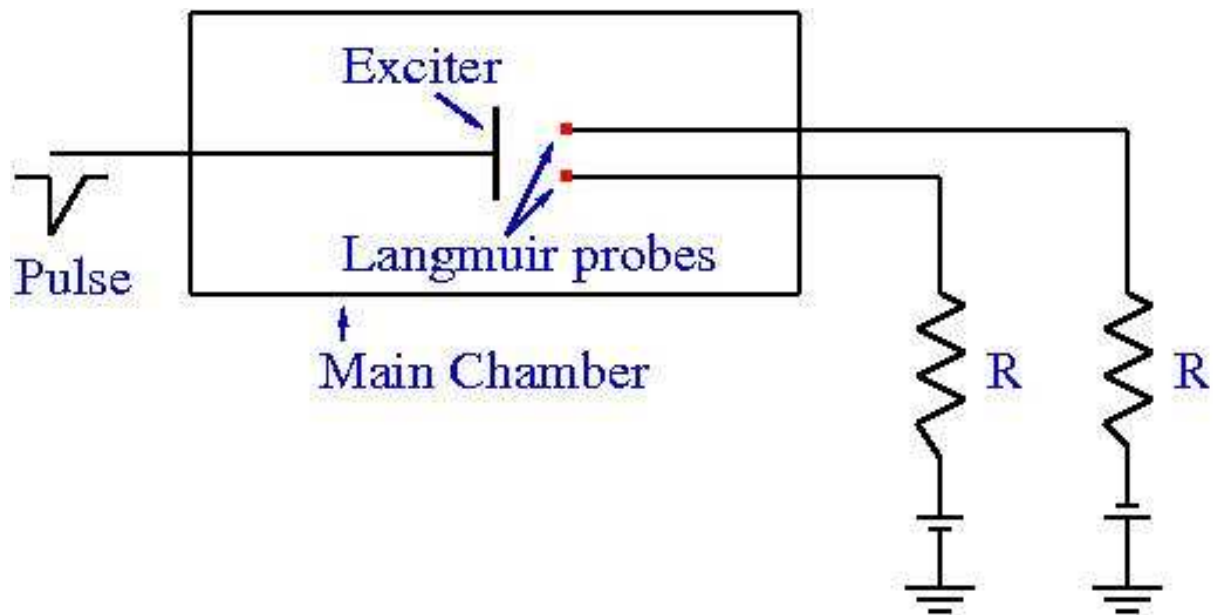


Figure 4.2 Simultaneous measurement of ion and electron saturation currents using two Langmuir probes.

To detect the propagation of rarefaction disturbances, three types of measurements were taken: floating potential measurements, ion saturation current and electron saturation current measurements. For floating potential measurements, one axially movable probe (detecting probe) of diameter 7 cm and thickness 0.4 cm was introduced. The detecting probe was kept floating and the propagating signal was directly observed on an oscilloscope. For ion and electron saturation current measurements simultaneously, two disc Langmuir probes of radius (r_p) 4.5 mm were biased with negative (-100 V) and positive (+50 V) voltage respectively, across a 10 k Ω resistor as shown in Fig. 4.2. Such type of disc (planar) Langmuir probe is often used for large collecting area (compared with a long thin wire), which makes easier to characterize low density plasmas. A very general requirement for Langmuir probe construction is

$$\lambda_m \gg r_p \gg \lambda_D \quad (4.1)$$

where λ_m is the electron-neutral collision mean free path and λ_D is the Debye length. For planar Langmuir probes [37] the below condition should be satisfied:

$$10 < r_p / \lambda_D < 45. \quad (4.2)$$

In our case, all the conditions are satisfied, hence the disc probe of radius 4.5 mm can be used for ion and electron saturation current measurements.

4.4 Experimental Results

Figure 4.3 shows the applied voltage pulse (solid line) and current (dotted line) on the metal plate in the presence of plasma for the pulse duration of 140 ns. The rise time of the voltage pulse is fast comparatively with fall time. The time duration of the pulse is measured from zero to at which voltage of the tail part goes to zero.

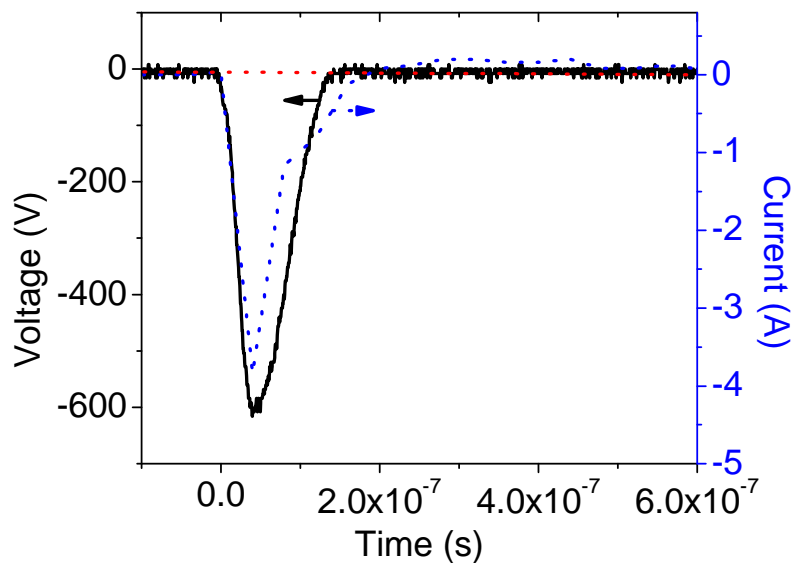


Figure 4.3 The applied voltage pulse (solid line) and current (dotted line) on the metal plate. The arrows indicate the axis side. Here $n_0 = 1.55 \times 10^9 \text{ cm}^{-3}$.

The perturbation signals in the floating potential, ion and electron saturation current measurements are shown in the following figures. The floating potential signals comprise of a very fast propagating component and a slow propagating component. The discussion primarily focuses on the slow propagating component.

The observed floating potential perturbations are shown in Fig. 4.4 for two detecting probe positions from the exciter. In the Y-axis the floating potential perturbation magnitude (ϕ) is normalized to kT_e/e . The signals were for the applied pulse width (300 ns) less than the inverse of ion plasma frequency ($f_i^{-1} \sim 770$ ns). Similar signals are also observed for lower pulse widths like 140 ns. The detecting probe detects first a large amplitude negative pulse, followed much later (typically after the end of the pulse) by the arrival of a small amplitude rarefaction pulse (second pulse, which is indicated by an arrow). The small amplitude rarefaction pulse propagates in to plasma with distance from the exciter.

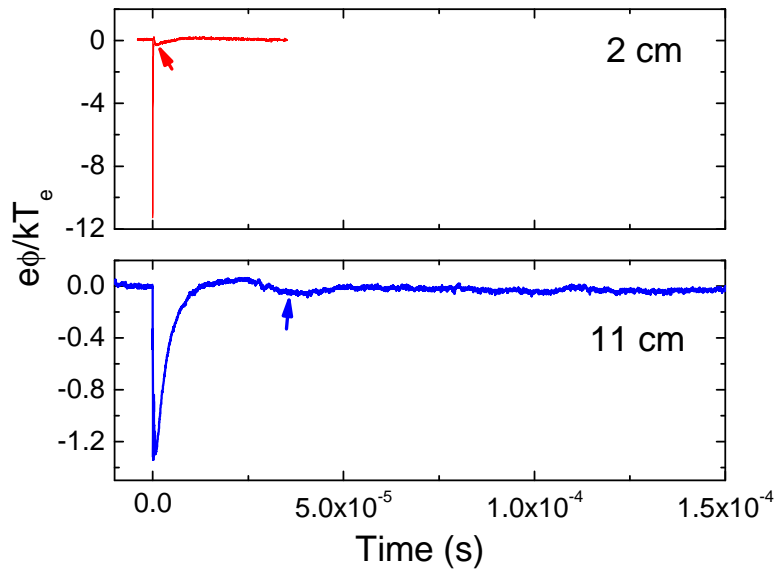


Figure 4.4 Oscilloscope traces (floating potential measurements) of the rarefaction disturbances for two detector positions from the exciter, when a single negative pulse is applied. Here $U_0 = -600$ V, $n_0 = 1.55 \times 10^9$ cm⁻³ and $\tau_p = 300$ ns. ϕ is the amplitude of the perturbed potential.

In Fig. 4.5(a) the first large amplitude negative pulse is zoomed for various distances from the exciter. In this figure, the slow propagating small amplitude rarefaction waves are not shown. The signals indicated inside a rectangular box are the electrostatic coupling signals during the application of negative pulse to the exciter and the amplitude of these signals are decreased with distance from the exciter. After the electrostatic coupling signal, a fast moving signal (marked by arrows in Fig. 4.5(a)) is observed with decreasing amplitude. Figure 4.5(b) shows the time-of flight plot for the fast moving signals which propagates with the phase speed of $0.54v_e$, where v_e is the electron thermal speed.

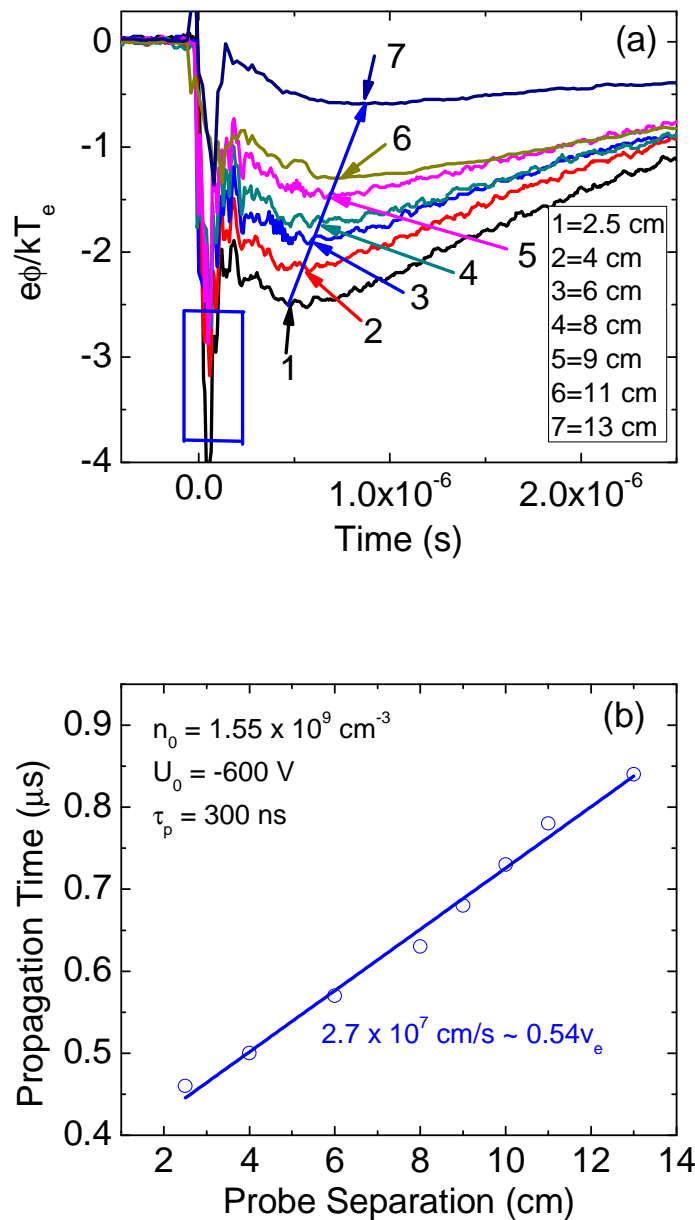


Figure 4.5 (a) The first large negative pulse is zoomed for various distances from the exciter, consisting an electrostatic coupled signal (rectangular box marked) and a fast propagating wave (marked by a long blue color arrow). **(b)** The time-of-flight plot for the fast moving waves.

The fast large negative pulse is followed much later by a slow propagating second pulse (small amplitude rarefaction waves) into the plasma. The normalized rarefaction waves are plotted in Fig. 4.6 for different positions of the detecting probe from the excitation plate. To show the small amplitude rarefaction pulses clearly in the figure, the full structure of the first peak is not shown in. The rarefaction pulses are indicated by arrows; they have a large

time delay when they move away from the exciter. The amplitude of these disturbances decreases with distances from the exciter. At longer distances (i.e., after three-fourth of the exciter diameter) from the exciter, a compressive part is observed.

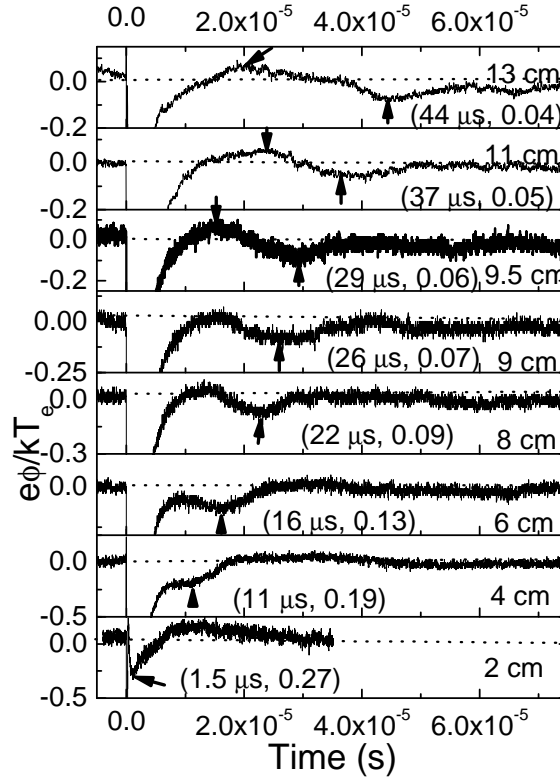


Figure 4.6 Oscilloscope traces (floating potential measurements) of the rarefaction disturbances observed at various distances from the exciter, when a single negative pulse is applied. Here $U_0 = -600$ V, $n_0 = 1.55 \times 10^9$ cm⁻³ and $\tau_p = 300$ ns. The arrows show the rarefactive and compressive parts. Scale of Y-axis is taken different to show the low amplitude rarefaction waves. The bracketed values are the time delay and amplitude of the rarefaction waves. ϕ is the amplitude of the perturbed potential.

Spatial plots for the rarefactive disturbances (normalized floating potential perturbations to electron temperature) at different times are shown in Fig. 4.7. The data points for various detecting probe positions are extracted from Fig. 4.6 for particular times. This figure illustrates clearly the formation of rarefaction disturbances and for some time periods compressive part is also shown. Further the spatial widths of the disturbances are approximately constant ($\approx 190 \lambda_D$).

The speed of the observed disturbances is calculated from the slope of the time delay versus the detecting probe position, as shown in Fig. 4.8 (floating potential measurement). This figure is plotted for various plasma densities. The phase speed for various plasma densities is normalized to ion acoustic speed. It is seen that the speed of the waves is

comparable to ion acoustic wave (IAW) speed. The error bars (1-3 μs) are within the symbols (circles or the squares).

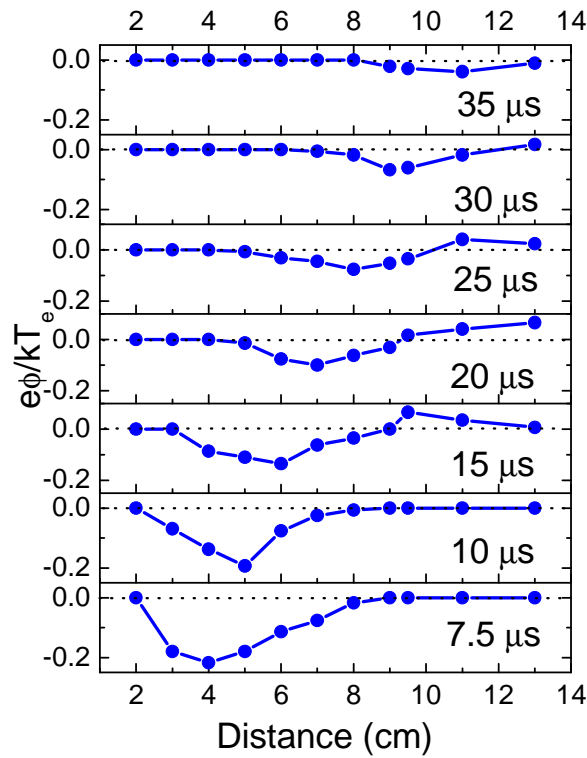


Figure 4.7 Spatial developments of the rarefaction waves. Here $U_0 = -600 \text{ V}$, $n_0 = 1.55 \times 10^9 \text{ cm}^{-3}$ and $\tau_p = 300 \text{ ns}$.

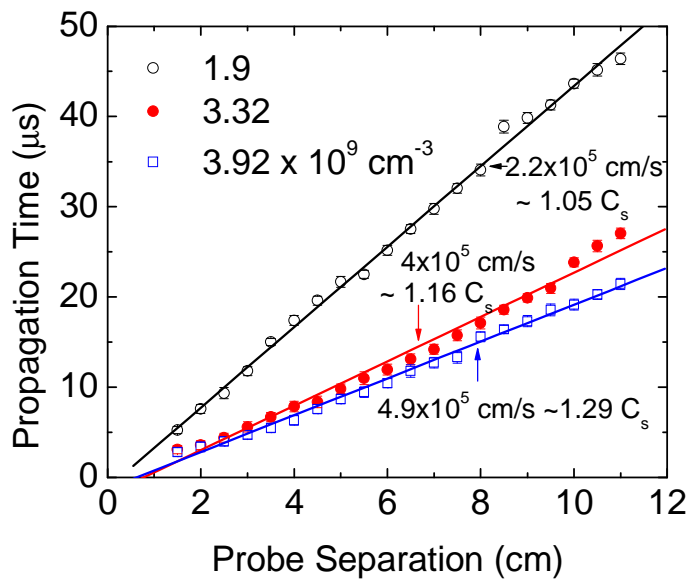


Figure 4.8 Probe separation versus time delay showing the rarefaction wave speed dependence on plasma density. Here $U_0 = -800 \text{ V}$ and $\tau_p = 300 \text{ ns}$.

Figure 4.9 shows the time of flight plots of potential perturbations for various applied pulse voltage to the exciter. It is seen that on increasing the pulse magnitude, the speed of the rarefaction waves increases and comparable to the IAW speed.

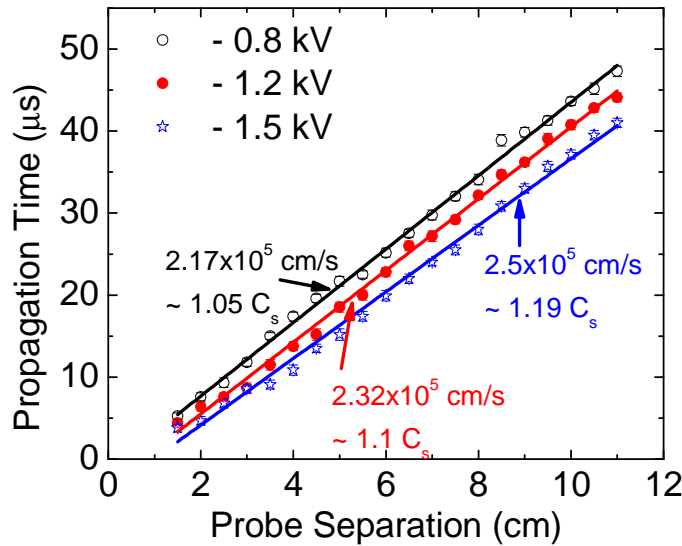


Figure 4.9 Probe separation versus time delay showing the rarefaction wave speed dependence on pulse amplitude. Here $n_0 = 1.9 \times 10^9 \text{ cm}^{-3}$ and $\tau_p = 300 \text{ ns}$.

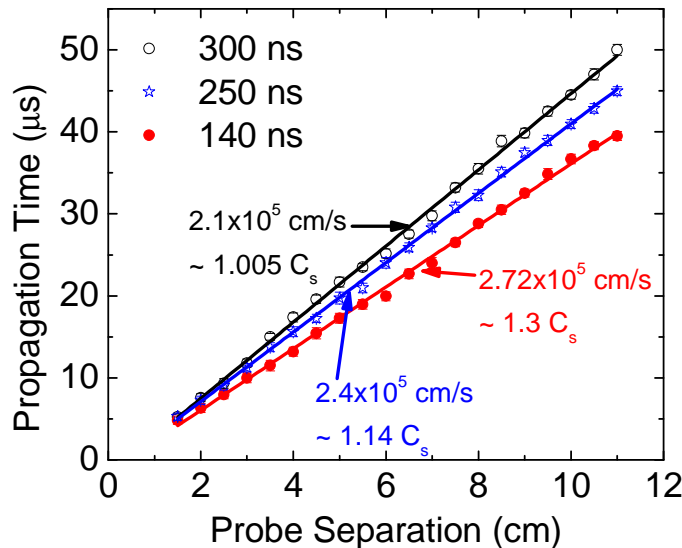


Figure 4.10 Probe separation versus time delay showing the rarefaction wave speed dependence on pulse duration. Here $U_0 = -800 \text{ V}$ and $n_0 = 1.9 \times 10^9 \text{ cm}^{-3}$.

Figure 4.10 shows the time of flight plots of potential perturbations for various applied pulse durations. This shows the speed of the rarefaction waves decreases on

increasing pulse duration, keeping however the pulse duration between inverse of ion and electron response frequencies. Here the pulse durations are 140–300 ns. So the speed of the disturbances depends upon the pulse duration of the applied negative voltage pulse.

Again we have measured the ion saturation current (negative biased Langmuir probe) and the electron saturation current (positive biased Langmuir probe) for various probe positions from the exciter. These measurements are taken through two Langmuir probes simultaneously during the application of voltage pulse to the exciter, which is shown in Fig. 4.11. Assuming no variation of temperature during the application of pulse to the exciter, we

can say $\frac{\delta I_{is}}{I_{is}} = \frac{\delta I_{es}}{I_{es}} = \frac{\delta n}{n_0}$. Here the ion as well as electron density perturbations show a

reduction in density and hence both ions and electrons have a rarefactive response and they are in phase with each other. Here also the rarefaction waves (indicated by arrows) propagate with decreasing amplitude with distance from the exciter. In Fig. 4.11, Y-axes scales are different to show the small amplitude waves. The solid line shows the ion density perturbation and the dotted line shows the electron density perturbations. The bracketed values show the amplitude of the waves and the value in between the arrows shows the time delay. Here the rarefaction waves are not measurable for longer distances from the exciter due to much decaying of wave amplitude. The ion and electron density perturbations are moving with ion acoustic speed ($1.08C_s$).

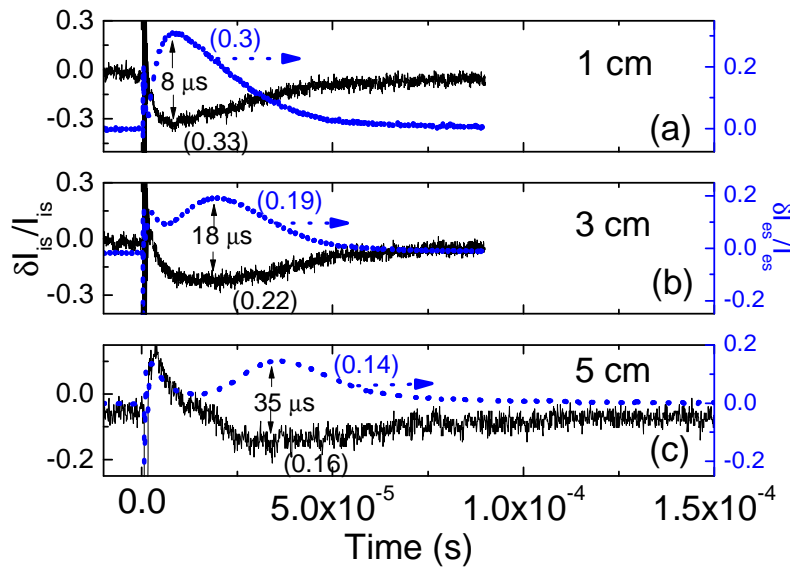


Figure 4.11 Ion and electron density perturbations for various probe positions from the exciter. Y-axes scales are taken different. Here $U_0 = -800$ V, $n_0 = 8.9 \times 10^8$ cm⁻³ and $\tau_p = 300$ ns.

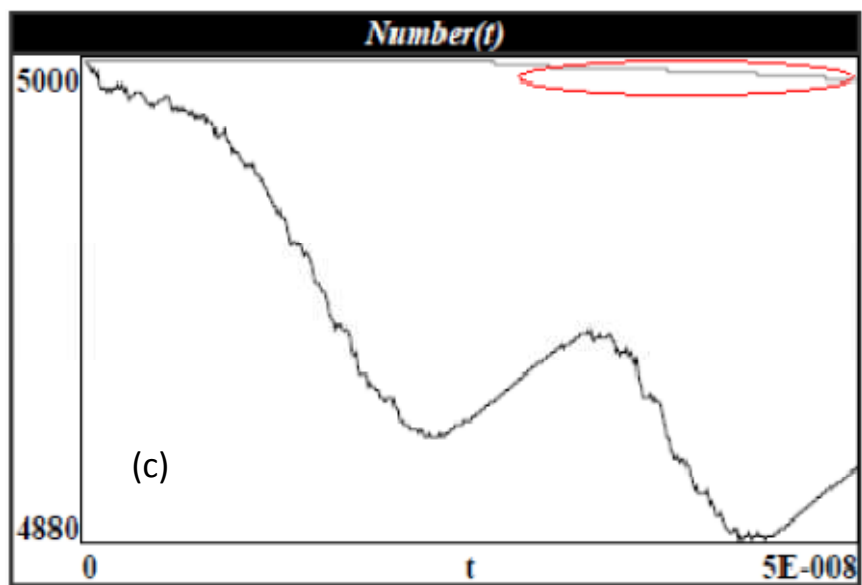
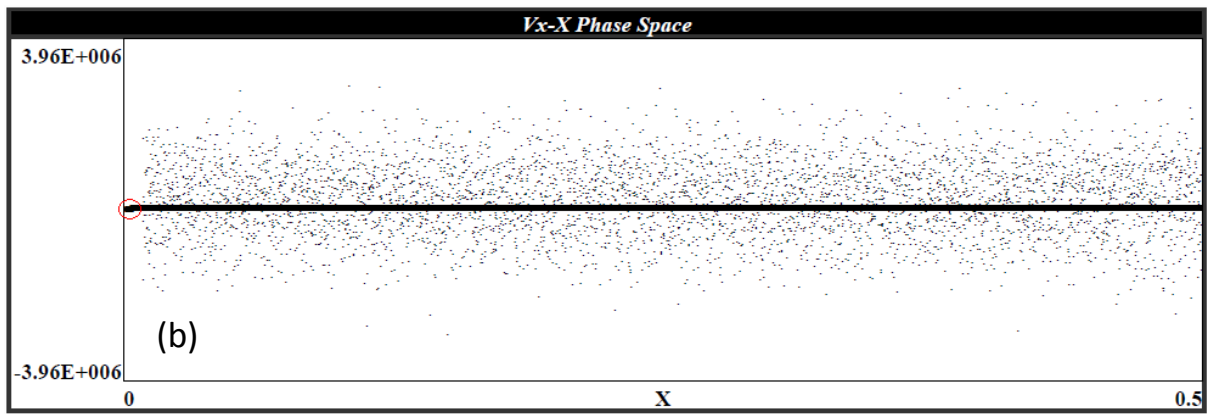
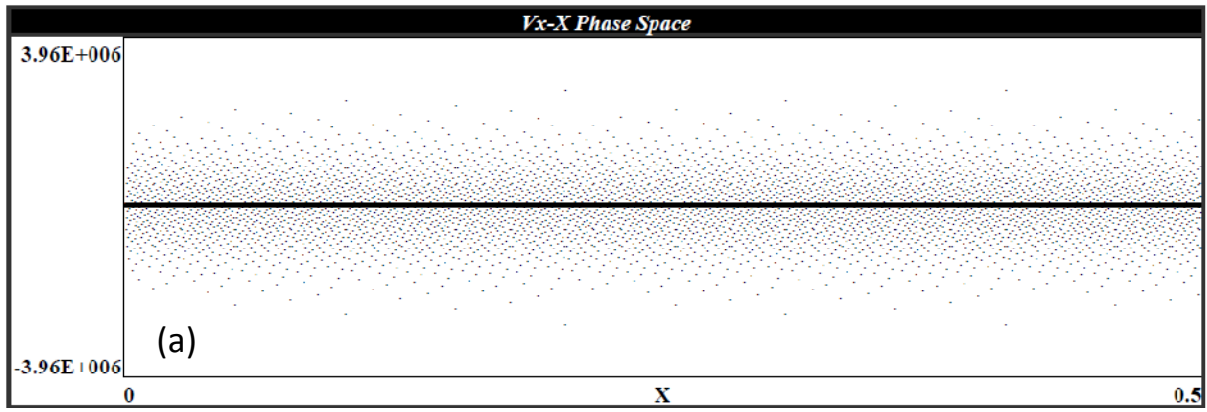
4.5 Discussions

The total current on the plate (Fig. 4.3) is the mix of three currents, i.e., displacement current, electron current and ion current. Here the contribution from ion current will be very small comparable to electron current. Though the applied pulse width is less than the ion plasma period, but a few numbers of ions within the ion matrix sheath respond ballistically and are lost to exciter [38]. This statement can be supported by the PDP1 simulation, a one dimensional planar bounded plasma simulation code [39], based on particle-in-cell (PIC) method [40, 41] and is described in detail by Birdsall [40]. PDP1 employs general series RLC circuit solvers to handle the full range of external circuit parameters, including open circuit, short circuit and current drives circuit which is shown in Fig. 3.12 and the complete simulation system is given by Verboncoeur et al. [42]. In the PDP1 simulation, the plasma is initially Maxwellian and the electrode is assumed to be perfectly absorbing. The PDP1 simulation is explained detailed in Sec. 3.5.

The PDP1 code is run with similar shape of potential (Fig. 4.3) which is applied on the left electrode. The rise time of the pulse is set 50 ns for the 300 ns pulse. Fig. 4.12(a) shows the uniform velocity distribution of electrons without bias. The thick centre line is the ion distribution and dots are electron distribution. Fig. 4.12(b) shows the velocity distribution of electrons when the voltage pulse is applied on the left electrode after the rise time. On the application of negative pulse on the left electrode, electrons are expelled, causing an ion matrix sheath, which is clearly shown in Fig. 4.12(b). It is seen that in the ion matrix region, there is a slightly small break in the thick centre line (circle mark), i.e., some ions are lost to the negative biased electrode, which can be seen more clearly in Fig. 4.12(c). Fig. 4.12(c) shows the number of electrons lost to the right electrode (chamber wall in the experiment) and shows a small break down in ion curve (ellipse mark). This shows that a delay in ion response comparison to electron response (assumed that electrons are lost instantaneously). This simulation is run for the rise time of the pulse (50 ns) at which the bias reaches its maximum value. So, even if, the applied pulse width is less than the ion plasma period, some ions can lost ballistically to the negative biased electrode. These ions can come from the vicinity of the electrode or from the sheath edge, which can be seen from Fig. 4. 12(d).

In floating potential measurement (Fig. 4.5(a)), the first negative pulse (indicated in the rectangular box) does not propagate with distance from the exciter, but the amplitude

Chapter 4: Excitation of Ion Rarefaction Waves in a Low Pressure Plasma...



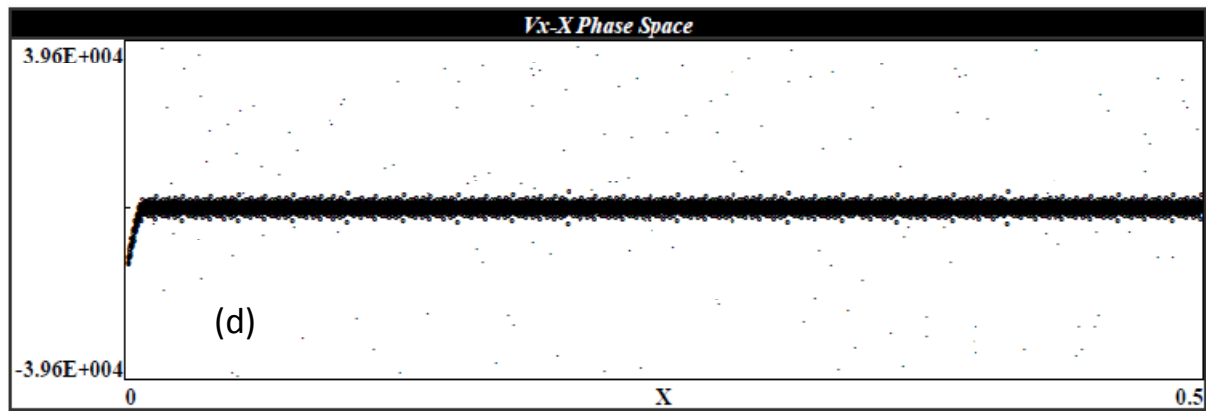


Figure 4.12 (a) Phase space plot for electron and ion distributions at $t = 0$ for the plasma density of $1.55 \times 10^9 \text{ cm}^{-3}$. X-axis is the distance between left electrode and right electrode, i.e., 0.5 m and the area of electrode is 0.008 m^2 . **(b)** The left electrode is biased by a ramp such that its bias reaches -600 V in 50 ns. It is seen that the entire electron distribution is given a uniform velocity much similar to Fig. (a), but forming an ion matrix sheath. **(c)** The number of electrons and ions lost after 50 ns when the bias reaches its maximum value. The number 5000 is the computer super particles. It shows that even if at 50 ns, a small number of ions are lost to the negative biased electrode. **(d)** Zoom of Fig. (b).

decreases with increasing distance. This non-propagating pulse may result from either an electrostatic pick-up or transient response of the plasma and exciter circuit or a combination of these effects. Similar observations have been made earlier in connection to wave launching experiments [43]. A fast pulse, propagating at the speed of $0.54v_e$, where v_e is the electron thermal speed, is observed following the non-propagating electrostatic coupled signal. Stix [44] observed the electron acoustic waves (EAWs) propagating at the phase speed of $1.31v_e$. Schamel et al. [45-48] have shown that EAWs can propagate at velocities between 0 to v_e , depending upon the status of particle trapping. Generally, the EAWs (electrostatic potential pulses) are in the form of negative potential structures [49-50], but also many researchers have observed the positive potential signature [49, 51-52]. The fast propagating pulse in present experiment may be speculated as EAW. We have, however, not investigated this further as the focus of the present chapter is on propagation of small amplitude, slow propagating rarefaction pulse.

The rarefaction waves are, normally, excited when ions move towards the negative biased exciter and electrons repelled from the exciter. In the present experiment the pulse duration is kept below the ion plasma period. Although no ion motion to the exciter plate is expected during the excitation, due to narrow perturbation pulse, still a rarefaction disturbance is created in our experiment. The disturbances are excited after the pulse goes off,

so the mechanism for ion expulsion to the plate should be discussed. A large proportion of exciting negative pulse bias U_0 appear across a thin sheath surrounding the plate which was formed on the time scale of electron motion. When $U_0 \gg kT_e/e$ ($eU_0/kT_e \approx 100-1500$), the shielding effect is not perfect and the negative potential penetrates into the quasi-neutral plasma region (“pre-sheath”) where the ions are accelerated. In our case, the ion matrix sheath doesn’t evolve within the applied pulse duration. Though the applied pulse width is less than the ion plasma period, but some ions respond ballistically very close to the exciter and are lost to the exciter [38]. A pre-sheath, therefore, starts forming from the ion matrix sheath edge which leads the acceleration of ions with ion acoustic velocity, resulting in the excitation of a nonlinear ion rarefaction wave [53]. This propagates as a rarefactive pulse as observed in this experiment. In other words the rarefaction wave is the precursor of the pre-sheath that would eventually exist at steady state.

We can relate the excitation of these rarefaction waves to nonambipolar diffusion. Nonambipolar diffusion [54], in which essentially all positive ions leave the plasma to only one boundary while essentially all electrons are lost to a different boundary. The bulk plasma remains quasi-neutral even when all the electrons are lost to only one physically small location. Nonambipolar flow is entirely a sheath effect. Baalrud et al. [54] have shown the global nonambipolar flow for a positive biased electrode. In our case, the electrode is negatively biased. The electrons are repelled from the vicinity of the electrode and lost to the chamber wall, while some ions lost to the electrode ballistically. Here electrons and ions are lost on two different boundaries. After the pulse goes off, during the fill-up process, ion rarefaction waves are excited.

When the electrode is biased with a high negative single pulse, an ion matrix sheath is formed at $t = \tau_e$. When the high voltage pulse is switched off, at $t = \tau_e$ due to small time scale the electrons adjust themselves instantaneously to the new electrode potential and build a quasi-neutral fill up region. For $t > \tau_i$ ions are refilled into this region. Due to a small ion current available for this process, this takes a longer time, i.e., several ion plasma periods. As ion density increases in the fill-up region, a rarefaction wave propagates in the pre-sheath region of the plasma. The relaxation phases are sketched in Fig. 4.13.

In most of the investigations of ion acoustic waves, the finite electron mass is neglected and the isothermal electrons with constant temperature (T_e) are considered. In many

cases, however, the drift motion of the electrons considerably influences the properties of ion acoustic waves, which is not negligible [55]. The momentum transfer by ion-neutral collisions [43] may be the cause of damping of the rarefaction pulses, shown in Fig. 4.14. It is apparent that the establishment of the pre-sheath and the ionization rate [26] in the surrounding plasma need to be considered in any realistic model of sheath formation and propagation of ion rarefaction wave. Indeed, particle balance considerations will affect the structure of the pre-sheath [36].

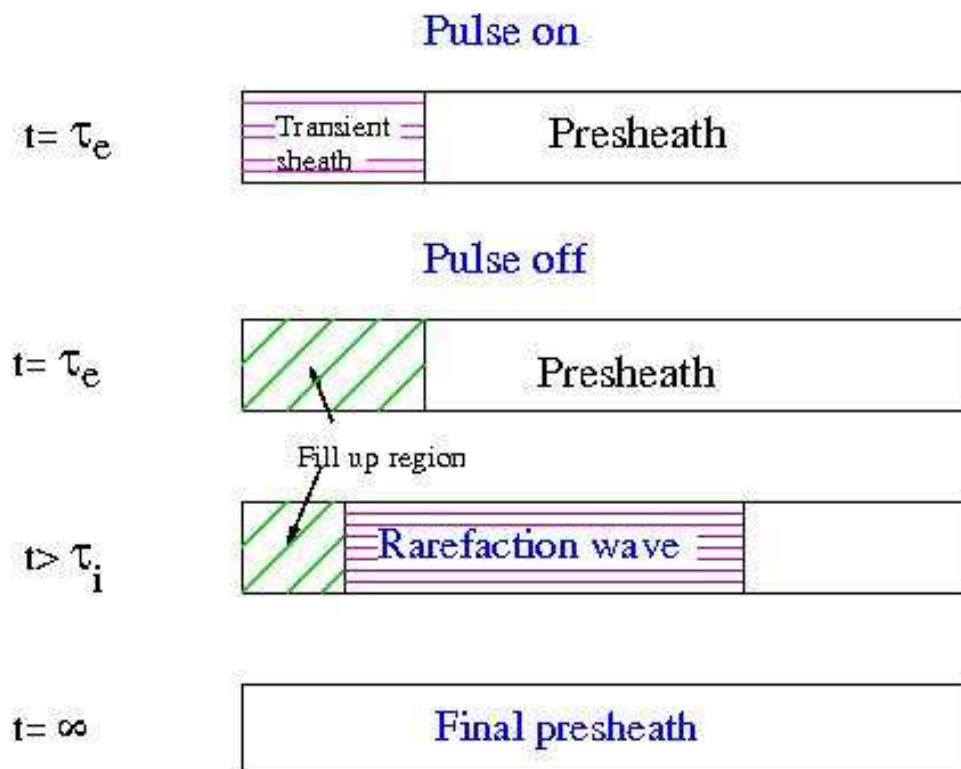


Figure 4.13 The sketching of the phase of the plasma relaxation (for different times like at $t = \tau_e$ and $t = \tau_i$) for switching on and off a high negative electrode voltage.

Hansen et. al. [56] has excited the rarefactive waves with short rf pulses. The waves evolving from the initial density cavity (caviton) to a large amplitude ion sound rarefactive waves after the decay of the rf pulse. Large amplitude and changing shape (leading edge of the wave flattened and trailing edge is steepened) leads to a strongly non-linear effect. In our experiment, no density cavity is observed during the pulse bias to the exciter. The small amplitude ($\frac{e\phi}{kT_e} = \frac{\delta n}{n_0} < 1$) rarefaction waves approximately have the similar shape (Fig. 4.7)

and the same spatial widths. Also there is neither narrowness nor splitting into smaller pulses of these rarefactive waves.

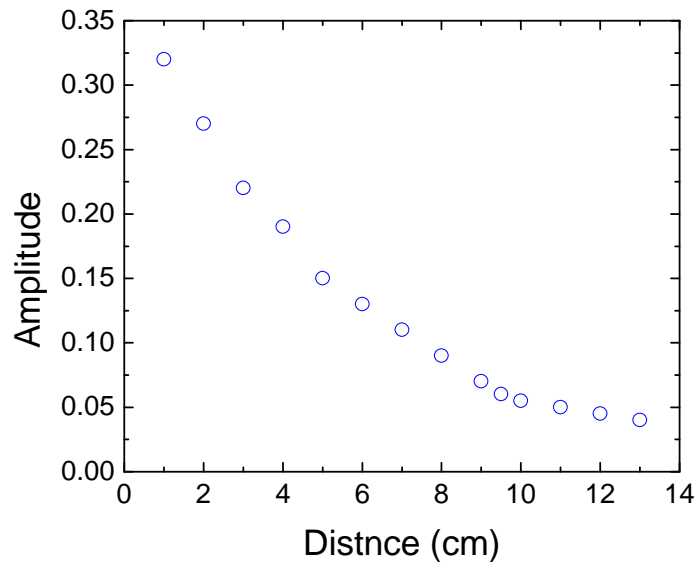


Figure 4.14 Variation of amplitude of the rarefaction waves with distance from the exciter for the floating potential measurement. Here $U_0 = -600$ V, $n_0 = 1.55 \times 10^9$ cm⁻³ and $\tau_p = 300$ ns.

One important observation is the accompanying of a compressive wave with the rarefaction wave after a distance of three-fourth of the exciter diameter [57]. Experimentally, Widner et al. [8] have verified that the ion rarefaction also becomes an ion acoustic wave at a distance of half of the disc diameter in planar geometry for longer applied pulse duration. In this work it is seen that the rarefaction disturbances are turned to ion acoustic wave after a distance of three-fourth of the exciter diameter for shorter pulse duration. The experiment is verified for 5 cm and 8 cm diameter exciter. The transition process of rarefaction waves to ion acoustic waves depends upon the neutral background and geometry of the exciter [8]. The position of the separation is close for the smaller electrode. Our experiments were performed, keeping the fix ion-neutral collision mean free path as 5 cm, which is greater than the transient sheath thickness (0.4-1.3 cm) and less than the experimental chamber dimension (29 cm diameter and 50 cm in length). So the ion-neutral collisions will be effective in the bulk plasma. A collision causes the loss of an ion that has been accelerated in the pre-sheath electric field. This ion is replaced by a new ion that is approximately at rest. Thus collisions can be modeled as a sink for moving particles and a source for new particles and the ion loss

rate reduces by ion-neutral collisions [58]. Due to these ion-neutral collisions the shape of the rarefaction pulses changes to ion acoustic waves and at further distances, these low amplitude waves are damped. In Fig. 4.6 the shape and the time width of the rarefaction disturbances are changed with distance although the amplitude itself decreases. Tanaka [59] and Amagishi et al. [60] have shown experimentally that ion-neutral collision exhibits heavy amplitude damping and profile deformation with anomalous time delay.

After the pulse goes to zero, plasma retains its quasi-neutrality. To answer this question we need to know the loss of electrons to the chamber wall during the pulse bias. In our previous paper [38], we have estimated the number of electrons lost to the chamber wall, when a metal plate is negatively pulsed biased for pulse duration in between the ion and electron plasma response times. It is seen that the percentage of lost electrons is around 1%. For a particular plasma parameter $U_0 = -600$ V, $n_0 = 3.32 \times 10^9$ cm⁻³ and $\tau_p = 300$ ns, the total charge lost to the chamber wall during the pulse is $Q_{\text{lost}} = 8.18 \times 10^{-8}$ Coulomb. For a particular filament heating voltage (19.3 V) and current (24 A), we can find the final filament temperature (2366 K) from Stefan's law. Corresponding to the filament heating voltage and current, the plasma density is $n_0 = 3.32 \times 10^9$ cm⁻³ and the emission current from four filaments is $I_{\text{em}} = 1.43 \times 10^{-3}$ A, which can be calculated from Richardson-Dushman equation. Hence the plasma relaxation time will be $Q_{\text{lost}} / I_{\text{em}}$, i.e., 57 μ s. During the plasma relaxation process ion rarefaction waves are excited in the pre-sheath region. For the above plasma condition, in our experiment, the rarefaction waves sustain (i.e., plasma relaxation time) up to 50 μ s, which close to 57 μ s.

4.6 Summary

The present investigation shows the excitation of ion rarefaction waves even when the applied pulse duration is kept intermediate of electron and ion plasma response times. In summary,

- (a) two electrostatic modes are excited, when a conducting disc electrode is negatively biased. One is the electron acoustic wave, which is followed much later by an ion rarefaction wave,

Chapter 4: Excitation of Ion Rarefaction Waves in a Low Pressure Plasma...

- (b) rarefaction waves are excited in the pre-sheath region due to large amplitude of applied voltage pulse and nonambipolar diffusion, though the applied pulse duration is less than the ion plasma response time,
- (c) the rarefaction waves are propagated with IAW speed,
- (d) after a distance of $3/4$ of plate diameter from the plate, the rarefaction waves turned to ion acoustic waves,
- (e) the higher the applied pulse amplitude, the higher the speed of the rarefaction waves,
- (f) for increasing applied pulse durations, speed of the rarefaction waves decreases,
- (g) after the applied pulse goes to zero, plasma relaxes to its quasi-neutrality after some time and rarefaction waves are excited during the plasma relaxation in the pre-sheath region.

➤ The work presented in this Chapter is published in

S. Kar, S. Mukherjee and Y. C. Sxaena, Phys. Plasmas **18**, 053506 (2011).

4.7 References

- [1] L. Tonks and I. Langmuir, Phys. Rev. **33**, 195 (1929).
- [2] H. Ikezi, Y. Kiwamoto and K. E. Lonngren, Plasma Phys. **15**, 1141 (1973).
- [3] R. C. Cross, Plasma Phys. **25**, 1377 (1983).
- [4] I. Alexeff and R. V. Neidigh, Phys. Rev. Lett. **7**, 223 (1961).
- [5] K. E. Longren, M. Khazei, E. F. Gable and J. M. Bulson, Plasma Phys. **24**, 1483 (1982).
- [6] A. K. Singh and Y. C. Saxena, J. Plasma Phys. **58**, 623 (1996).
- [7] Y. F. Li, J. X. Ma, Y. R. Li, D. L. Xiao and K. E. Lonngren, Phys. Lett. **358A**, 297 (2006).
- [8] M. Widner, I. Alexeff, W. D. Jones and K. E. Lonngren, Phys. Fluids **13**, 2532 (1970).
- [9] P. K. Kaw and J. M. Dawson, Phys. Fluids **14**, 792 (1971).
- [10] N. Chakrabarti and M. S. Janaki, Phys. Lett. **305A**, 393 (2002).
- [11] H. Tanaca, M. Koganei and A. Hirose, Phys. Rev. Lett. **16**, 1079 (1966).
- [12] S. Watanabe and H. Tanaca, J. Phys. Soc. Japan **27**, 517 (1969).
- [13] Y. C. Saxena, S. K. Mattoo, A. N. Sekar and V. Chandna, Phys. Lett. **84A**, 71 (1981).
- [14] L. Oksuz, D. Lee and N. Hershkowitz, Plasma Sources Sci. Technol. **17**, 015012 (2008).
- [15] E. Okutsu and Y. Nakamura, Plasma Phys. **21**, 1053 (1979).
- [16] T. Honzawa, Plasma Phys. Controlled Fusion **26**, 1251 (1984).
- [17] B. Sahu and R. Roychoudhury, Phys. Plasmas **14**, 012304 (2007).
- [18] L. Wei and Y. N. Wang, Phys. Rev. **B 75**, 193407 (2007).
- [19] S. Ali, W. M. Moslem, P. K. Shukla and R. Schlickeiser, Phys. Plasmas **14**, 082307 (2007).
- [20] S. A. Khan and W. Masood, Phys. Plasmas **15**, 062301 (2008).
- [21] A. Barkan, R. L. Merlino and N. D'Angelo, Phys. Plasmas **2**, 3563 (1995).
- [22] S. Ghosh, S. Sarkar, M. Khan and M. R. Gupta, Phys. Plasmas **9**, 1150 (2002).
- [23] N. X. Wei and J. K. Xue, Phys. Plasmas **13**, 052101 (2006).
- [24] M. J. Lee, Phys. Plasmas **14**, 032112 (2007).
- [25] J. T. Scheuer, M. Shamim and J. R. Conrad, J. Appl. Phys. **67**, 1241 (1990).
- [26] G. J. Andrews and A. J. Shrapnel, Phys. Fluids **15**, 2271 (1972).
- [27] J. K. Chester, J. Sci. Technol. **37**, 2 (1970).
- [28] K. Nishihara and M. Tajiri, J. Phys. Soc. Japan **50**, 4047 (1981).
- [29] G. O. Ludwig, J. L. Ferreira and Y. Nakamura, Phys. Rev. Lett. **52**, 275 (1984).

- [30] I. Alexeff, W. D. Jones, K. E. Lonngren and D. Montgomery, *Phys. Fluids* **12**, 345 (1969).
- [31] I. Langmuir, *Phys. Rev.* **21**, 4 (1923).
- [32] D. Bohm, in *Characteristics of Electrical Discharges in Magnetic Fields*, edited by A. Guthrie and R. K. Wakering (McGraw-Hill, New York, 1949), Chap. 3.
- [33] M. Murakami and K. Nishihara, *Phys. Fluids* **5B**, 3441 (1993).
- [34] L. M. Wickens, N. St. J. Braithwaite and A. J. Coates, *Phys. Lett.* **88A**, 147 (1982).
- [35] Th. Daube, P. Meyer, K. –U. Riemann and H. Schmitz, *J. Appl. Phys.* **91**, 1787 (2002).
- [36] G. A. Collins and J. Tendys, *Plasma Sources Sci. Technol.* **3**, 10 (1994).
- [37] T. E. Sheridan, *Phys. Plasmas* **7**, 3084 (2000).
- [38] S. Kar and S. Mukherjee, *Phys. Plasmas* **15**, 063504 (2008).
- [39] Codes available from Industrial Liaison Program, EECS Department, UC Berkeley, CA 94720.
- [40] C. K. Birdsall, *IEEE Trans. Plasma Sci.* **19**, 65 (1991).
- [41] C. K. Birdsall and A. B. Langdon, in *Plasma Physics via Computer Simulation* (McGraw-Hill, New York, 1985).
- [42] J. P. Verboncoeur, *J. Computational Phys.* **104**, 321 (1993).
- [43] I. Alexeff, W. D. Jones and D. Montgomery, *Phys. Fluids* **11**, 167 (1968).
- [44] T. H. Stix, *The Theory of Plasma Waves* (McGraw-Hill, New York, 1962), p218.
- [45] H. Schamel, *Phy. Scr.* **20**, 336 (1979).
- [46] A. Luque and H. Schamel, *Phys. Rep.* **415**, 261 (2005).
- [47] H. Schamel and S. Bujarbarua, *Phys. Fluids* **23**, 2498 (1980).
- [48] H. Scamel, *Phys. Plasmas* **7**, 4831 (2000).
- [49] M. Berthomier, R. Potelette, M. Malingre and Y. Khotyaintsev, *Phys. Plasmas* **7**, 2987 (2000).
- [50] F. Valentini, T. M. O’Neil and D. E. Dubin. *Phys. Plasmas* **13**, 052303 (2006).
- [51] F. Verheest, T. Cattaert and M. A. Hellberg, *Space Sci. Rev.* **121**, 299 (2005).
- [52] A. P. Kakad, S. V. Singh, R. V. Reddy, G. S. Lakhina and S. G. Tagare, *Adv. Space Res.* **43**, 1945 (2009).
- [53] H. Y. Chang, C. Lien, A. Seyhounzadeh, P. Forsling and K. E. Lonngren, *IEEE Trans. Plasma Sci.* **16**, 50 (1988).
- [54] S. D. Baalrud, N. Hershkowitz and B. Longmier, *Phys. Plasmas* **14**, 042109 (2007).
- [55] B. C. Kalita, M. K. Kalita and J Chutia, *J. Phys. A: Math. Gen.* **19**, 3559 (1986).
- [56] K. Hansen and A. Piel, *Contrib. Plasma Phys.* **37**, 13 (1997).

Chapter 4: Excitation of Ion Rarefaction Waves in a Low Pressure Plasma...

[57] S. Kar, S. Mukherjee and Y. C. Saxena, Phys. Plasmas **18**, 053506 (2011).

[58] Z. Sternovsky, K. Downum and S. Robertson, Phys. Rev. **70E**, 026408 (2004).

[59] M. Tanaka, Plasma Phys. Control. Fusion **31**, 1049 (1989).

[60] Y. Amagishi and M. Tanaka, Phys. Rev. Lett. **71**, 360 (1993).

CHAPTER 5

5 Excitation of Solitary Electron Holes in a Laboratory Plasma

5.1 Motivation

In the last Chapter, we discussed about the excitation and propagation of ion rarefaction waves through a negative biased disc electrode, though the applied pulse width was less than the ion plasma period. Many experiments have been done for the excitation of electrostatic waves, such that ion acoustic waves [1-3] or solitons [4-6] and electron acoustic waves [7-11] or solitons [12-13]. Mainly all these waves are excited using mesh grids and in double plasma (DP) devices mostly. The obtained results are same for both negative and positive bias to the grid [14-15]. In Chapter 4, we have observed the ion rarefaction waves for the negative bias to a metallic disc electrode. In the present Chapter, when the disc electrode is positively biased, totally different results are obtained, i.e., solitary electron holes (EHs).

Solitary electron hole (EH) structures are special class of cnoidal hole solutions (CHSs) of Vlasov-Poisson (VP) system of equations representing special trapping situation. CHSs are nonlinear, undamped, low frequency, weak amplitude electrostatic plasma waves, distinct from any linear wave solution, such as ion acoustic waves. Depending on the status of trapping, they are known to propagate at velocities between zero and electron thermal velocity v_e , covering the whole velocity range. They hence can be subsonic or supersonic with respect to ion acoustic speed C_s , which depends upon electron trapping in the potential humps (maxima) and of ion trapping in the potential dips (minima). CHSs are stationary solutions of the full set of VP equations and, therefore, not subject to Landau damping [16], since Landau's linear approach doesn't apply to these waves.

In the present investigation, EHs are excited by a sudden perturbation at large amplitude to a disc metal plate inside a homogeneous electron-ion plasma. When positive voltage pulse is applied to the exciter, the plasma potential is forced to increase, resulting in a hole formation. Here the applied pulse width (τ_p) is varied from less than ion plasma period (f_i^{-1}) to greater than thrice of ion plasma period. The distinctive feature of this experiment is the observation of the presence of a virtual source for pulse widths less than $3f_i^{-1}$. An overview of the previous works is given in Sec. 5.2. The experimental setup is explained in Sec. 5.3 followed by observed results in Sec. 5.4. The experimental results are discussed in Sec. 5.5 and finally conclusions are given in Sec. 5.6.

5.2 An Overview of Previous Works

A number of pioneering theoretical studies on CHSs in a collisionless and unmagnetized plasma has been carried out by Schamel and coworkers [8-11, 17-22], using a physically acceptable method of construction different from that of Bernstein-Greene-Kruskal (BGK) [23]. The class of cnoidal electron hole solutions (CEHSs) [8, 11, 20, 22] has two different limits, the solitary electron hole (EH) limit, when $k_0 = 0$, and the harmonic wave limit, when $k_0 = k$, where k_0 is a system parameter, which controls the wavelength of the structure, and k is the actual wave number. In a thermal, nondrifting background plasma two expressions characterize this CEHSs class [11]: the nonlinear dispersion relation (NDR)

$$k_0^2 - \frac{1}{2} Z_r' \left(\frac{v_0}{\sqrt{2}} \right) = B_e \quad (5.1)$$

and the classical potential

$$-V(\phi) = \frac{k_0^2}{2} \phi(\psi - \phi) + \frac{B_e}{2} \phi^2 \left(1 - \sqrt{\frac{\phi}{\psi}} \right) \quad (5.2)$$

In the above expressions v_0 is the actual phase velocity (normalized by the electron thermal velocity), which is determined by the NDR, assuming ions are immobile, and B_e is a parameter, which represents the status of the trapped electrons. The function $-\frac{1}{2} Z_r' (v_0/\sqrt{2})$ is zero at $(v_0/\sqrt{2}) = 0.924$ and at $(v_0/\sqrt{2}) \rightarrow \infty$ and negative in between. The NDR, therefore has for $B_e = 0$ and $k_0 = k \ll 1$, i.e. in the long wavelength limit, two solutions: one is the

Chapter 5: Excitation of Solitary Electron Holes in a Laboratory Plasma

Langmuir branch ($v_0/\sqrt{2} \rightarrow \infty$), and another is the slow electron acoustic waves (SEAWs) at ($v_0/\sqrt{2}$) = 0.924. ϕ is the electric potential and ψ is the perturbation amplitude. Historically, Vlasov [24] has proposed the above dispersion relation with $B_e = 0$ at first.

In a situation when ion trapping comes into play the CHSs are seen to move with lower phase velocities. As analyzed by Luque et al [9], an ion contribution B_i has to be added to the NDR. This 3 parameter (k_0, B_e, B_i) class of solutions now involves cnoidal ion holes, as well as, being characterized by ion trapping in the potential minima and includes the solitary ion hole (IH) as a special case, first discovered and described by Bujarbarua and Schamel [10, 21]. Also Franck et al. [25] has excited the propagating periodic ion holes.

So EHs are the special class of CEHSs for $k_0 = 0$ and nonzero B_e . By the way, k_0 decides about the kind of a structure, not B_e . Many theoretical models [19, 26-27] explain the solitary EH in plasma as a positive hump like potential in which a population of electrons is trapped and the propagation velocity of the order of the thermal electron velocity. First Schamel [8, 19] has derived analytically the phase (propagation) velocity of EHs in the range of $v_p \leq 1.31v_e$. Kono et al. [28] showed that the EH formation is possible only when the $v_p > 1.73v_e$. Later Califano et al. [27] showed that the propagating velocities of EHs can range from a fraction of v_e up to $2v_e$.

Theoretically, first Schamel in [8] presented the theory of EHs [9, 11, 19-21], where a hollow vortex distribution is assigned for the trapped electrons. When the EHs move slow enough, a slight ion density bump accompanies the EHs or an ion density cavity or an ion acoustic wave create [26-27, 29]. EHs are existed in the computer simulation of two stream instability [30]. Recently EHs have received substantial attention in space plasma with higher dimensions rather than one-dimensional (1D) theory [31-34].

The first experimental observation of the special member of CHSs, namely the solitary electron hole (together with the Gould-Trivelpiece mode), has been made by Lynov et al. [35]. For the excitation of EHs, Saeki et al. [36] has developed a relation that the excitation potential should be exceeds a critical value ϕ_c , i.e.

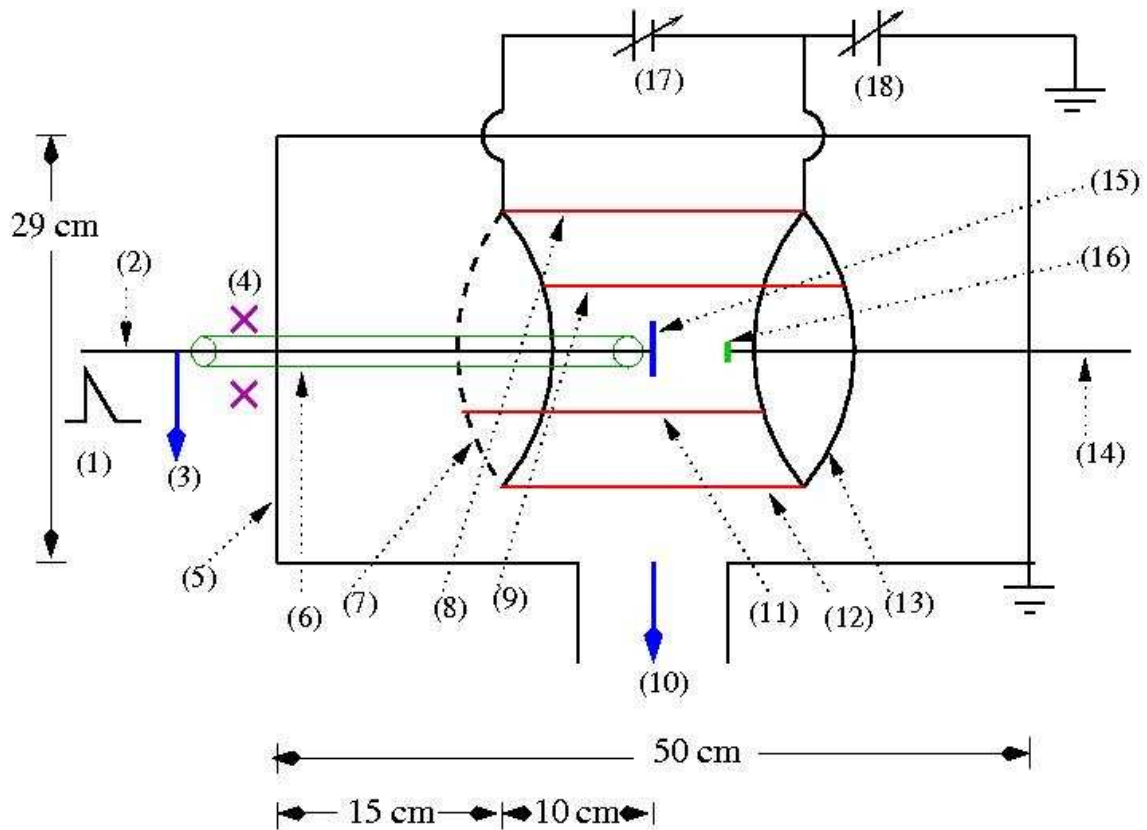
$$\phi_c = \frac{1}{2} \frac{m}{e} \left(\omega_{pe} \frac{a}{2.4} \right)^2 \quad (5.3)$$

where m is the electron mass, ω_{pe} is the angular electron plasma frequency and a is the plasma radius. Iizuka et al. [37] has observed the EHs in the early stage of evolution of moving double layers in a single ended plasma device. EHs are also created during magnetic reconnection [38]. Recently, a laser-created EH is observed by Sarri et al. [39].

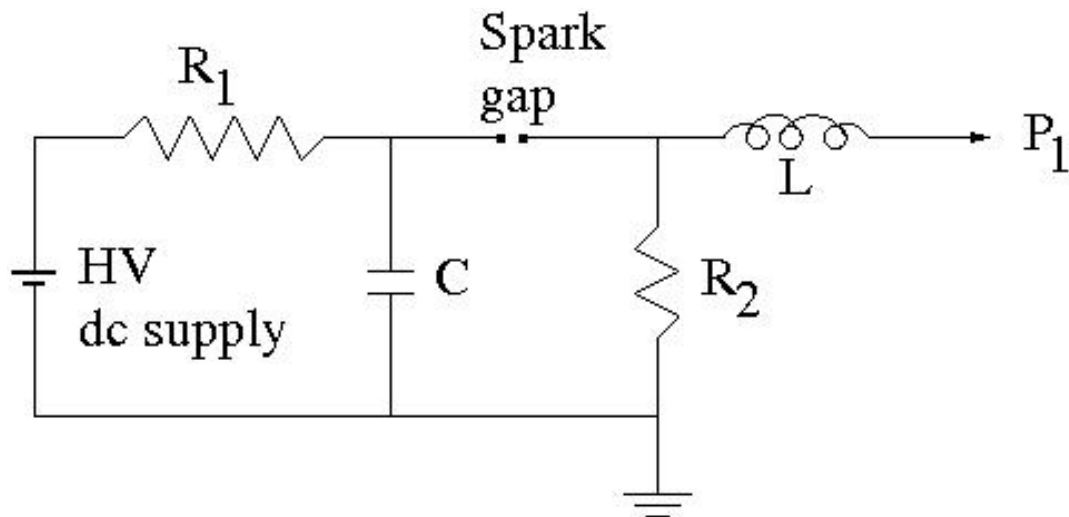
5.3 Experimental Setup

The schematic diagram of the system is shown in Fig. 5.1(a). The experiment was performed in a grounded cylindrical chamber of stainless steel (SS) 304 with an inner diameter of 29 cm and a length of 50 cm. The chamber was evacuated by using a combination of rotary and diffusion pumps and the base pressure was about 5×10^{-5} mbar. The plasma was generated by impact ionization of argon, at pressure of 1×10^{-3} mbar, by primary electrons coming out from dc biased hot thoriated tungsten filaments of diameter 0.25 mm. The filaments were mounted on two SS rings, and biased to a potential of -60 V. The plasma density (n_p) and electron temperature (T_e) was determined using Langmuir probe for various axial and radial positions. For a fixed discharge current (I_{dis}), n_0 and T_e were found to be uniform throughout the main chamber. The experiments were performed with plasma densities $1-5 \times 10^9 \text{ cm}^{-3}$, electron temperatures $T_e \sim 0.5-2 \text{ eV}$ and the cold ion temperature $T_i \sim 0.2 \text{ eV}$.

Plasma disturbances were excited by applying a large positive voltage pulse to a metal plate (exciter) inserted in a low pressure argon plasma. The pulse magnitudes and durations were in the range of 0.4 - 1 kV and 0.14 - 10 μs respectively. In the main chamber, the metal plate (SS disc of diameter 10.2 cm and thickness 0.4 cm) was mounted on a SS rod and the SS rod was fixed along the axis of the chamber. A high-voltage (HV) probe (Tektronix make 1000X probe) and a current transformer CT (Bergoz make of sensitivity 1 V/A) were mounted on the SS rod and were used to measure the pulse voltage and the current respectively. Such type of current transformers could measure the current from microamperes to 20 kA. One axially movable probe (detecting or the receiving probe) of diameter 7 cm and thickness 0.4 cm was introduced to detect the propagation of plasma disturbances. The detecting probe was kept floating and the propagating signal was observed directly on an oscilloscope.



(a)



(b)

Figure 5.1(a) Schematic of the experimental setup. (1) Applied positive pulse. (2) and (15) are the SS rods. (3) High-voltage probe; to measure the voltage signal. (4) Current transformer CT; to measure the current signal. (5) and (14) are SS rings. (6) Main chamber. (7) Ceramic tube. (8), (9), (12) and (13) are the filaments. (10) Pumping system. (11) Stainless steel disc (metal plate or the exciter); on which pulse is applied. (16) Stainless steel disc (detecting probe); to detect potential disturbances. (17) Filament supply voltage. (18) Discharge voltage. **(b)** The pulse forming circuit. [HV dc Supply = high voltage dc supply (1.5 kV, 500 mA), R_1 = resistor (3 k Ω), C = capacitor, R_2 = load resistor, L = inductor (320 nH), P_1 = metal plate or the exciter].

The positive pulse forming circuit is shown in Fig. 5.1(b). The details of the pulse forming circuit are described in Sec. 2.6. Experiments have been carried out for various applied pulse widths τ_p ranging from less than $3f_i^{-1}$ to greater than $3f_i^{-1}$.

5.4 Experimental Results

Figure 5.2 and 5.3 show the applied positive voltage pulses to the metal plate for different widths of very fast rise times. During the application of pulse the current drawn by the metal plate is very high (around 15-20A), which is much greater than the discharge current (0.1-0.4 A). In order to calculate the number of electrons lost to the metal plate, the integral of the current pulse is taken, i.e.

$$N = \frac{1}{e} \int_0^{\tau} I dt \quad (5.4)$$

where e is the electron charge, I is the electrode current and τ is the current pulse duration. From the above integral, the percentage of electron density lost to the metal plate can be calculated to be around 10% to 40% of the unperturbed plasma density for pulse width in the range of $0.5f_i^{-1} < \tau_p < 4f_i^{-1}$.

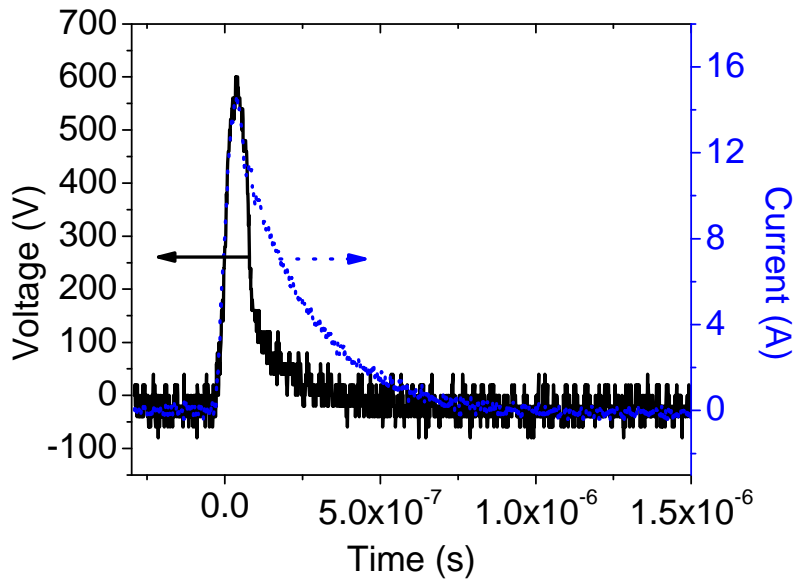


Figure 5.2 The applied voltage (solid line) and current (dotted line) pulse to the exciter. Here the pulse width $\tau_p=350$ ns ($\tau_p < 3f_i^{-1}$), $U_0=625$ V and $n_0=4 \times 10^9$ cm⁻³.

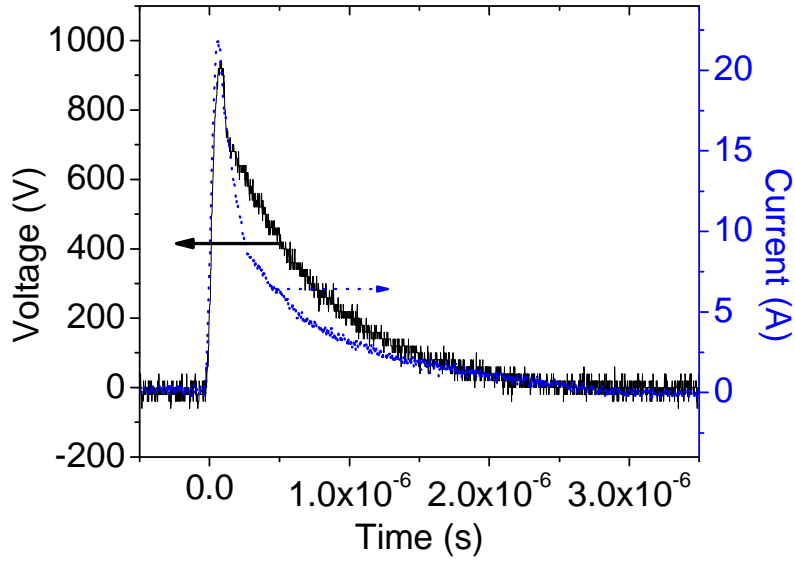


Figure 5.3 The applied voltage (solid line) and current (dotted line) pulse to the exciter. Here the pulse width $\tau_p=2 \mu\text{s}$ ($\tau_p > 3f_i^{-1}$), $U_0=1000 \text{ V}$ and $n_0=4 \times 10^9 \text{ cm}^{-3}$.

Figure 5.4 shows the floating potential signals of the detecting or the receiving probe at various distances from the metal plate or the exciter. The signals were for the applied pulse width (350 ns) less than the thrice of the inverse of ion plasma frequency ($f_i^{-1} \sim 480 \text{ ns}$). The first peak doesn't propagate with distance, but the second peak propagates with distance. The first peak is the electrostatic coupled signals [40] during the application of positive pulse to the electrode. However, the second peak shows interesting characteristics; potential disturbances propagate in two opposite directions from a location (around 3 cm from the exciter), indicating the presence of a virtual source. Interestingly only the rear edge of the second peak flattens (i.e., the steepness flattens) and all the signals fall in a line. The point of potential depression between the two peaks doesn't vary with distance. The amplitude of the signals increase, when the signals move towards the exciter and the signal damps as it moves away from the exciter.

Similar results are obtained with pulse width $\sim f_i^{-1}$. However as the pulse width is increased further, strikingly different results are obtained at pulse width $\sim 3f_i^{-1}$. Figure 5.5 shows the potential signals of the receiving probe for the applied pulse width (2 μs) greater than $3f_i^{-1}$. Here the second peak propagates away from the metal plate with distance in one direction only. Here also the point of potential depression between the two peaks doesn't vary with distance, but the depression region (distance between two peaks) is decreased with

increase in pulse width. The amplitude of the potential disturbances decreases away from the metal plate. This may be due to the collisions between electrons and neutral atoms leading to an increasing damping rate for the amplitude [41].

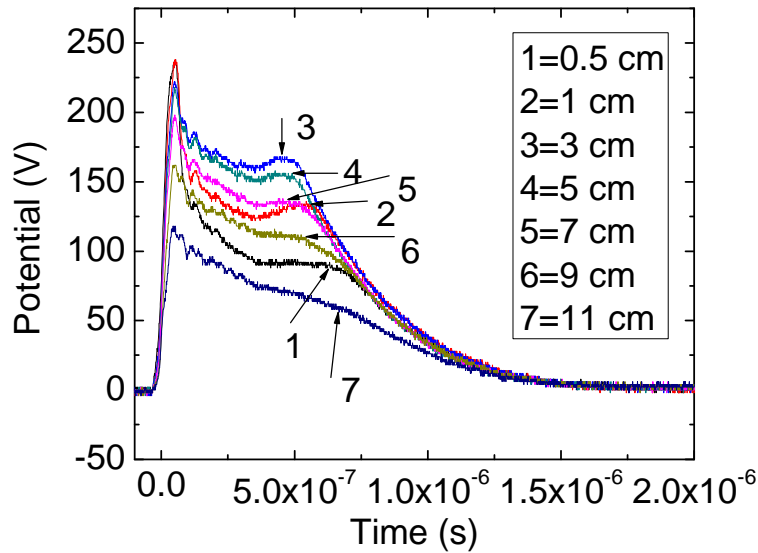


Figure 5.4 Oscilloscope traces of the potential disturbances measured by the detector from the positive biased exciter. It shows only the second peak propagates with distance from the exciter. The numbers 1-7 show the distances from the exciter. Here pulse width is 350 ns ($\tau_p < 3f_i^{-1}$), $U_0=625$ V and $n_0=4 \times 10^9$ cm⁻³.

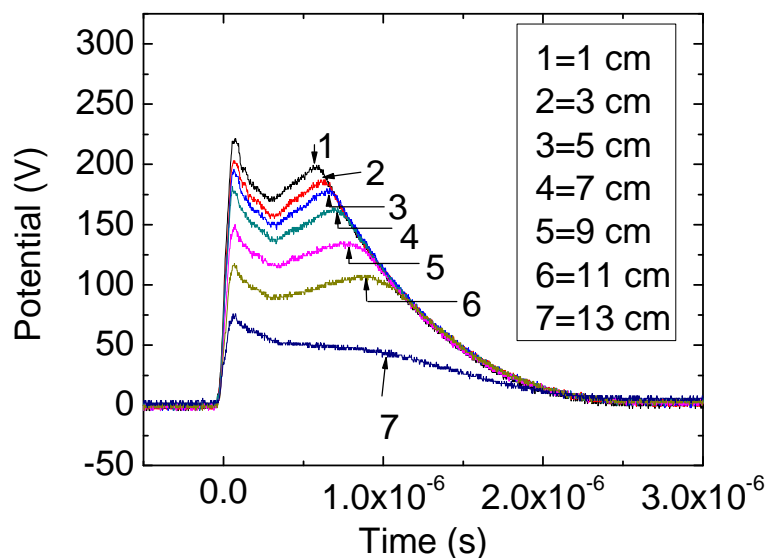


Figure 5.5 Oscilloscope traces of the potential disturbances for a longer applied pulse width. The numbers 1-7 show the distances from the exciter. Here the pulse width is 2 μ s ($\tau_p > 3f_i^{-1}$), $U_0=625$ V and $n_0=4 \times 10^9$ cm⁻³.

Chapter 5: Excitation of Solitary Electron Holes in a Laboratory Plasma

It appears from the above results that the transition of the potential perturbations from two-way to unidirectional propagation depends upon the pulse width transition from $< f_i^{-1}$ to $\geq 3f_i^{-1}$. This is reminiscent of some kind of a virtual source for the potential perturbations. To probe this further, a plot of the virtual source location versus a time normalized constant ($\tau_p f_i$) is shown in Figure 5.6. When the applied pulse width is increased, the virtual source distance is decreased. The virtual source distance is independent of the plasma density and applied pulse magnitude. Pulse width, equal or greater than $\sim 3f_i^{-1}$, the virtual source distance is approximately zero. The virtual source distance depends upon only on the applied pulse widths.

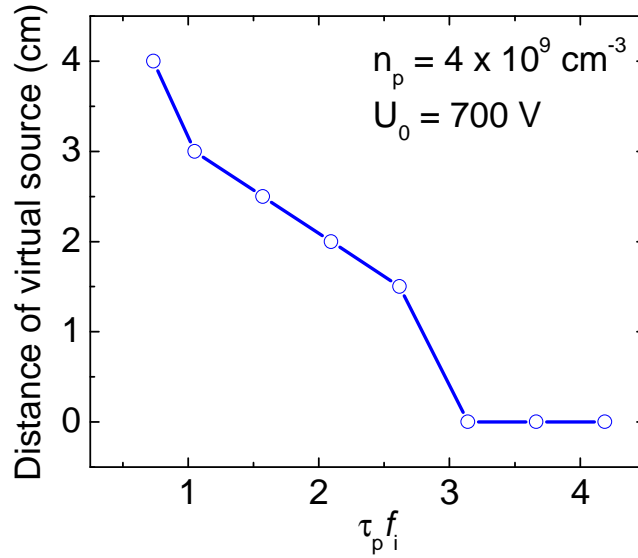


Figure 5.6 A plot of distance of virtual source from the exciter as a function of pulse width. Distance of virtual source decreases with increasing pulse width till $\tau_p f_i \approx 3$ and then goes to zero.

Figure 5.7 shows the phase velocity plot for $\tau_p < 3f_i^{-1}$. The plot shows two phase velocities: with a phase velocity of $0.26-0.37v_e$ towards the exciter and with another phase velocity of $1.25-1.36v_e$ away from the exciter. Such type of nature indicates the presence of a virtual source. The virtual source distance doesn't depend upon plasma density. Here also on increasing the plasma density, the speed of the signals increases.

Figure 5.8 shows the time delay of the second peak versus the distance between the exciter plate and the receiver for $\tau_p > 3f_i^{-1}$. The time-of-flight phase velocity curve shows two slopes. The first slope is up to 8 cm from the exciter moving with $v_p = 1.32-1.47v_e$. And the

Chapter 5: Excitation of Solitary Electron Holes in a Laboratory Plasma

second slope shows the velocity $v_p = 0.25-0.3v_e$. It is seen that on increasing the plasma density, the speed of the signals increases.

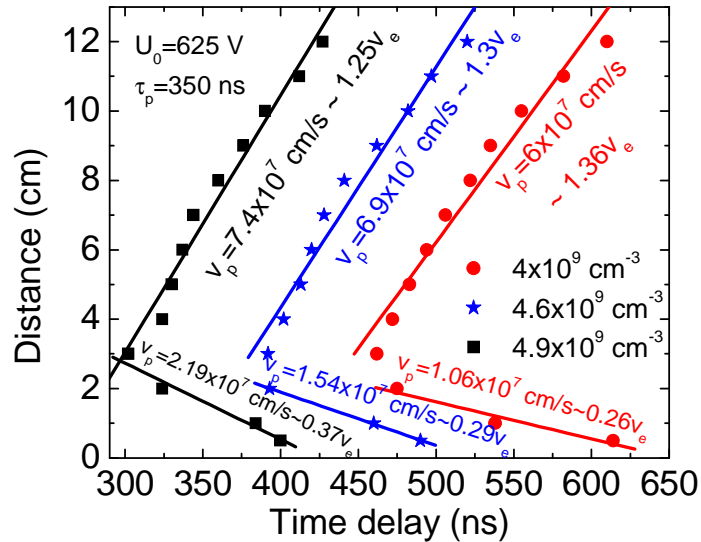


Figure 5.7 Time delay vs the detector position for $\tau_p < 3f_i^{-1}$. This plot is for various plasma densities and shows two slopes. It indicates a virtual source around 3 cm from the exciter. It shows that the phase velocity increases with increase in plasma density.

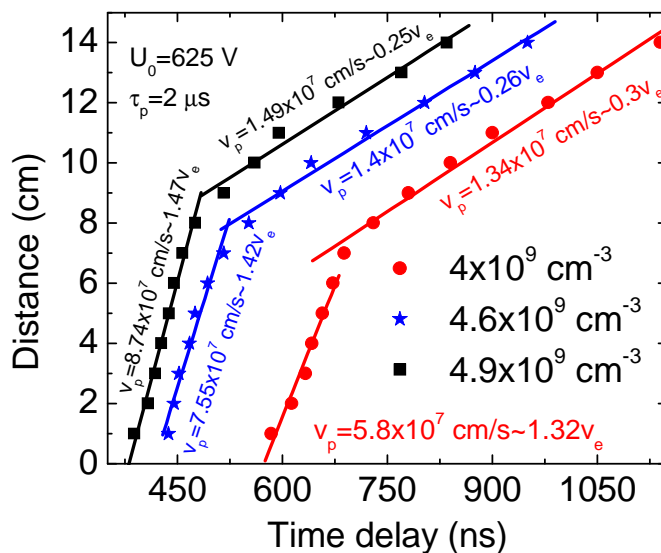


Figure 5.8 Time delay vs the detector position for $\tau_p > 3f_i^{-1}$. This is for various plasma densities and also shows two slopes. Here is no indication of virtual source.

Chapter 5: Excitation of Solitary Electron Holes in a Laboratory Plasma

Figures 5.9 and 5.10 show the phase velocity of the signals for various applied pulse magnitudes to the exciter plate. The signals move with $v_p = 1.28-1.38v_e$ and $0.25-0.55v_e$. Here it is seen that the speed of the signals doesn't depend upon on increasing the pulse magnitude.

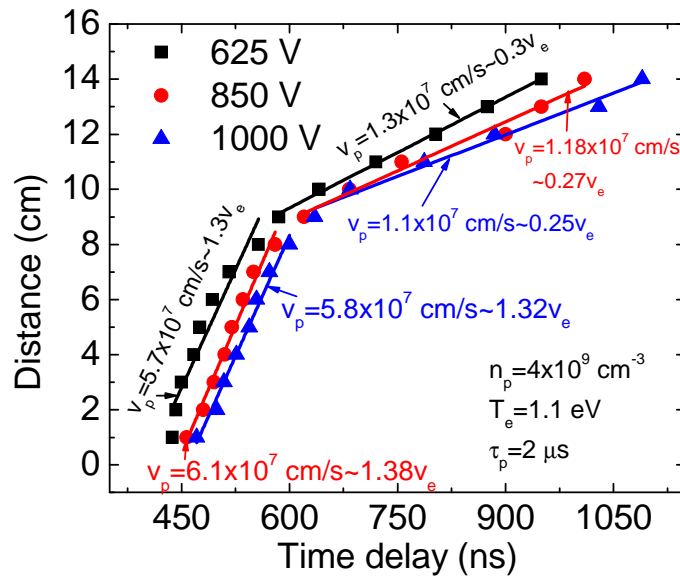


Figure 5.9 Time delay vs detector position for various applied pulse magnitude and the pulse width is greater than the thrice of ion plasma response time. It shows the phase velocity is independent of applied pulse magnitude.

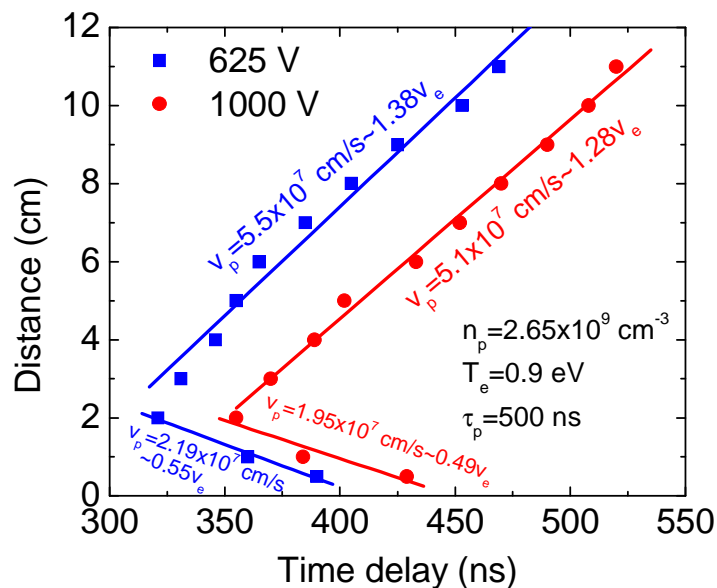


Figure 5.10 Time delay vs detector position for various applied pulse magnitude and the pulse width is less than the thrice of ion response time.

Chapter 5: Excitation of Solitary Electron Holes in a Laboratory Plasma

Figures 5.11 and 5.12 show the spatial variations of the signals for pulse widths less than and greater than the $3f_i^{-1}$ respectively. Here the metallic disc electrode (anode) is biased to a positive potential and the chamber wall is kept ground. The axial distance between the biased electrode and the wall was 18 cm. So the potential at the wall (18 cm) will be zero, while some potential difference exists at the biased electrode for various times during the pulse bias. The potential disturbances restore the unperturbed plasma potential after a long time $\approx 3-4$ times of f_i^{-1} . In Figure 5.11 ($\tau_p < 3f_i^{-1}$), at the very early times (just after the rising time of the potential disturbance) a potential well is observed near to the electrode. These potential wells may have trapped ions. For $\tau_p f_i \geq 3$, however, no potential wells are formed (Fig. 5.12).

When a positive pulse is applied to a metallic electrode, then plasma potential is more positive. This larger plasma potential produces more energetic filament electrons, resulting in a larger plasma density [42]. In our experiments, the density of these energetic filament electrons is not taken into account.

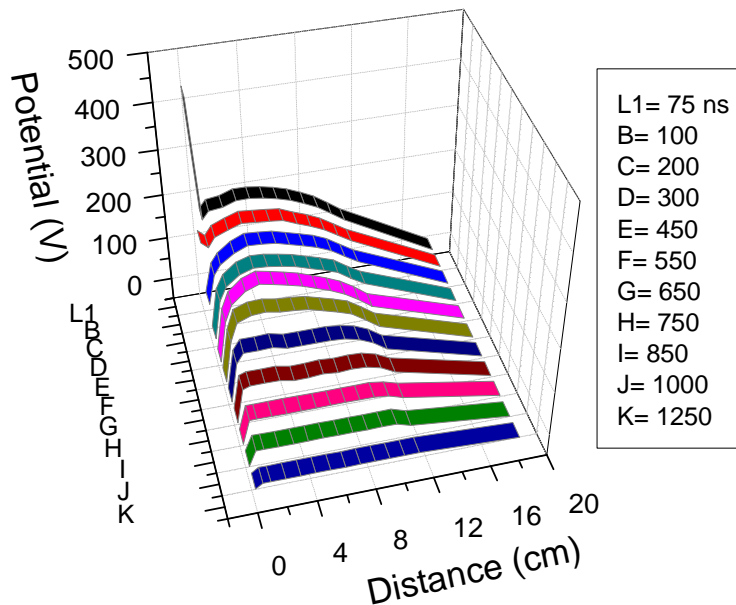


Figure 5.11 Spatial variation of the disturbances for 350 ns pulse width, which is less than thrice of the ion plasma period. Here $U_0=625$ V and $n_0=4 \times 10^9$ cm⁻³. Potential well structures are observed for L1 and B time scales.

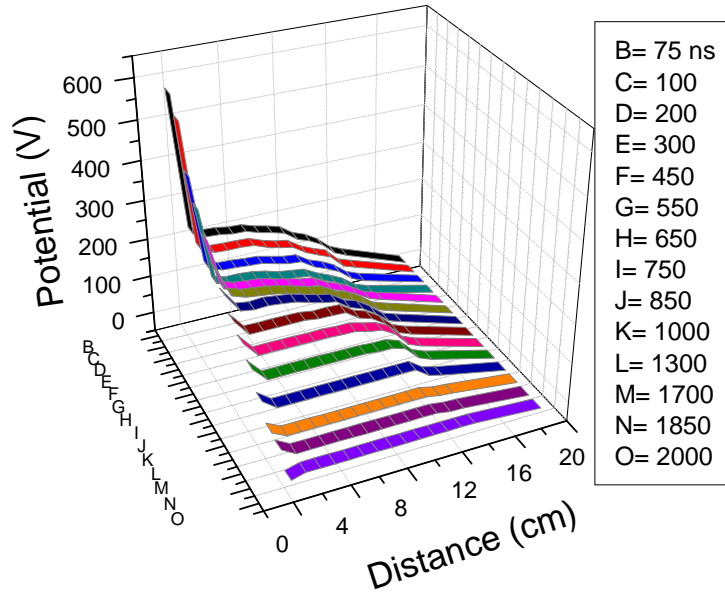


Figure 5.12 Spatial variation of the disturbances for 2 μ s pulse width, which is greater than the thrice of ion plasma period. Here $U_0=625$ V and $n_0=4 \times 10^9$ cm⁻³.

5.5 Discussions

In summary the experimental observations are;

- (h) Virtual sources are present for the pulse width less than $3f_i^{-1}$. Here the disturbances propagate with two speeds. The disturbances propagate towards the exciter with the speed of $0.4 \pm 0.15v_e$ and away from the plate with the speed of $1.36 \pm 0.11v_e$. Virtual sources are only dependent on applied pulse widths. Formation of a potential well structure is seen near the vicinity of the biased electrode. This potential well structure seems to exist for very early times during the application of the pulse.
- (i) There is no virtual source present for the pulse width equal or greater than the $3f_i^{-1}$. Here the disturbances propagate away from the plate with two speeds. From the plate up to some distances, the disturbances move with the speed of $1.36 \pm 0.11v_e$, and after longer distances from the exciter they move with the speed of around $0.4 \pm 0.15v_e$. In this case no potential well structures are observed.
- (j) The speed of the disturbances increases with increase in plasma density.
- (k) The speed of the disturbances is independent of applied pulse magnitude.

Chapter 5: Excitation of Solitary Electron Holes in a Laboratory Plasma

The most important observation is the virtual source. The virtual source is observed for $\tau_p < 3f_i^{-1}$, but not for $\tau_p \geq 3f_i^{-1}$. Lieberman [43] has derived for plasma immersion ion implantation cases that all the ions will be implanted in the time scale of $\omega_i t \sim 3$. In our case, one possible thing is, may be all the ions can reflect back from the vicinity of the exciter after $3f_i^{-1}$. When $\tau_p < 3f_i^{-1}$, an ion rich region is present there, which may attracts the solitary electron holes. When τ_p approaches $3f_i^{-1}$, all the ions reflect back and hence no indication of virtual source (Fig. 5.6).

According to Saeki et al. [36], the solitary electron hole will be only excited when the excitation potential exceeds a critical value φ_c (Eq. 5.3). In our case the critical value is [44]

$$\varphi_c = \frac{1}{2} \frac{m}{e} \left(\frac{\omega_{pe}}{2\pi} \frac{a}{2.4} \right)^2. \quad (5.5)$$

Here a is taken as the exciter radius. Because the potential perturbations are observed only in the axial direction and in the diameter region of the exciter. In our experimental set up, $\varphi_c \approx 400\text{V}$ for a particular plasma density. So it is expected that the EHs can be excited above this critical value.

Chan et al. [45] has observed the multiple electrostatic ion-acoustic shock-like density perturbations when a large amplitude positive pulse is applied to a square metal plate. The pulse duration in their experiment is of the order of $\sim f_i^{-1}$. The velocities of these shocks don't depend upon the applied pulse magnitude to the exciter plate. The potential disturbances in our experiment are excited by applying a positive voltage pulse to a disc metallic plate. These disturbances propagate with two phase velocities: $v_p = 1.36v_e$ and another is $0.4v_e$, not at ion acoustic shock speed and also the phase speed doesn't depend upon the pulse magnitude. Further these potential disturbances are excited for an applied pulse magnitude geater than the critical value φ_c . According to previous literature [19, 26-27], a solitary structure in plasma is identified as an EH by a positive hump like potential & a depletion in the electron density at the potential peak. Some other theoretical and experimental studies [19, 21, 27, 28, 35] show that the EHs propagate with the phase speed of $v_p = 1.31v_e$ or from a fraction of v_e up to $2v_e$. Our experimental results shown in Figs. 5.4-5.5, 5.7-5.10 satisfy all the conditions expressed above. We, therefore, speculate that the excited disturbances are the nonlinear solitary electron holes.

Chapter 5: Excitation of Solitary Electron Holes in a Laboratory Plasma

In Figures 5.7 and 5.10, where $\tau_p < 3f_i^{-1}$, the potential disturbances move with two phase velocities: with a phase velocity of $0.4 \pm 0.15v_e$ from a location in front of the exciter (around 3 cm) towards the exciter and with a phase velocity of $1.36 \pm 0.11v_e$ away from the exciter. This type of nature indicates a virtual source is present at 3cm from the exciter, at which two waves propagate in opposite directions. Also the distinct difference between two phase velocities shows simultaneous existence of two propagating waves in opposite directions. Taking 3cm as the source point, the amplitude of both the phase velocity waves decreases (Fig. 5.4). The trapping conditions in the two wave propagating regions ($0.4v_e$ phase velocity wave or the left propagating wave moves towards the exciter, i.e., near to the exciter and $1.36v_e$ phase velocity wave or the right propagating wave moves away from exciter) are different. First the origin of the left propagating wave should be discussed. Near to the exciter, a less number of electrons will be trapped and an ion rich region is present there. So the EH interaction with ions may lead to a slower phase velocity. The $0.4v_e$ phase velocity perturbation is accompanied by a small amplitude potential well seen in Fig. 5.11, resembling an ion hole. The right propagating wave propagates from the virtual source position with a phase velocity of $1.36v_e$ with decrease in amplitude. Here the number of trapped electrons will be greater than the region of left propagating wave. So the speed of the right propagating wave conforms an EH.

In Figures 5.8 and 5.9, where $\tau_p > 3f_i^{-1}$, the disturbances move away from the exciter in a one direction with two phase speeds of $1.36 \pm 0.11v_e$ (8cm from the exciter) and $0.4 \pm 0.15v_e$ (far away from the exciter). In this case, initially (nearer to the exciter) the wave propagates with a faster phase velocity and far away from the exciter a sudden slowing down of phase velocity occurs. In 1D plasma problem, the penetration speed of the exciter potential will be suppressed by the shielding effect of the radial boundary. In this experiment the EHs are excited at the exciter by a sudden subtraction of electrons in front of the exciter. So the EHs have a positive potential shape propagating with a speed comparable to v_e , initially up to some distances and determined mainly by electron trappings. On later distance, when collisions have the dominant effect, this wave ceases to exist. But instead of extinguishing the structure, the plasma dissipation in connection with ion mobility may give rise to a coherent dissipative EH structure, as proposed by the second paper of [9] and in [20], resulting in a sudden lowering of the phase velocity.

5.5 Conclusions

The present investigation shows the excitation of solitary electron holes using a metal disc electrode in a homogeneous electron-ion plasma. A virtual source is present during the EH excitation, when $\tau_p < 3f_i^{-1}$, an observation not reported in earlier experiments. Two branches of holes are found: one is EH moving with the phase velocity of $1.36v_e$ and the other is a coupling of EH and ions moving with $0.4v_e$ phase velocity. The speed of the EHs increases with increase in plasma density and independent of applied pulse magnitude.

➤ The work presented in this Chapter is published as
S. Kar, S. Mukherjee, G. Ravi and Y. C. Saxena, Phys. Plasmas 17, 102113 (2010).

5.6 References

- [1] M. Widner, I. Alexeff, W. D. Jones and K. E. Lonngren, *Phys. Fluids* **13**, 2532 (1970).
- [2] H. Ikezi, Y. Kiwamoto and K. E. Lonngren, *Plasma Phys.* **15**, 1141 (1973).
- [3] R. C. Cross, *Plasma Phys.* **25**, 1377 (1983).
- [4] T. E. Sheridan, S. Yi and K. E. Lonngren, *Phys. Plasmas* **5**, 3165 (1998).
- [5] K. E. Lonngren, *Plasma Phys.* **25**, 943 (1983).
- [6] Y. El-Zein, T. E. Sheridan, K. E. Lonngren and W. Horton, *J. Plasma Phys.* **61**, 161 (1999).
- [7] T. H. Stix, *The Theory of Plasma Waves* (McGraw-Hill, New York, 1962), p218.
- [8] H. Schamel, *Phy. Scr.* **20**, 336 (1979).
- [9] A. Luque and H. Schamel, *Phys. Rep.* **415**, 261 (2005).
- [10] H. Schamel and S. Bujarbarua, *Phys. Fluids* **23**, 2498 (1980).
- [11] H. Scamel, *Phys. Plasmas* **7**, 4831 (2000).
- [12] M. Berthomier, R. Pottelette, M. Malingre and Y. Khotyaintsev, *Phys. Plasmas* **7**, 2987 (2000).
- [13] J. F. McKenzie, *J. Plasma Phys.* **69**, 199 (2003).
- [14] H. Ikezi, P. J. Barrett, R. B. White and Y. Wong, *Phys. Fluids* **14**, 1997 (1971).
- [15] K. Saeki, P. Michelsen, H. L. Pécseli and J. J. Rasmussen, *Phys. Rev. Lett.* **42**, 501 (1979).
- [16] L. D. Landau, *J. Phys. U. S. S. R.* **10**, 25 (1946).
- [17] H. Schamel, *Plasma Phys.* **14**, 905 (1972).
- [18] H. Schamel, *J. Plasma Phys.* **13**, 139 (1975).
- [19] H. Schamel, *Phys. Reports* **140**, 161 (1986).
- [20] J. Korn and H. Schamel, *J. Plasma Phys.* **56**, 307 (1996); *ibid* **56**, 339 (1996).
- [21] S. Bujarbarua and H. Schamel, *J. Plasma Phys.* **25**, 515 (1981).
- [22] H. Schamel and A. Luque, *New J. Phys.* **7**, 69 (2005).
- [23] I. B. Bernstein, J. M. Greene and M. D. Kruskal, *Phys. Rev.* **108**, 546 (1957).
- [24] A. A. Vlasov, *J. Phys. U. S. S. R.* **9**, 25 (1945).
- [25] C. Franck, T. Klinger, A. Piel and H. Schamel, *Phys. Plasmas* **8**, 4271 (2001).
- [26] B. Eliasson and P. K. Shukla, *Phys. Rev. Lett.* **93**, 045001 (2004).
- [27] F. Califano and M. Lontano, *Phys. Rev. Lett.* **95**, 245002 (2005).
- [28] M. Kono and M. Tanaka, *Physica Scripta* **34**, 235 (1986).
- [29] J. M. Dawson, *Phys. Plasmas* **2**, 2189 (1995).

Chapter 5: Excitation of Solitary Electron Holes in a Laboratory Plasma

- [30] M. E. Dieckmann, P. K. Shukla and B. Eliasson, *New J. Phys.* **8**, 225 (2006).
- [31] M. Oppenheim, D. L. Newman and M. V. Goldman, *Phys. Rev. Lett.* **83**, 2344 (1999).
- [32] C. S. Ng and A. Bhattacharjee, *Phys. Plasmas* **13**, 055903 (2006).
- [33] M. V. Goldman, D. L. Newman and A. Mangeney, *Phys. Rev. Lett.* **99**, 145002 (2007).
- [34] M. Berthomier, G. Dubois and L. Muschietti, *Phys Plasmas* **15**, 112901 (2008).
- [35] J. P. Lynov, P. Michelsen, H. L. Pecseli, J. J. Rasmussen, K. Saeki and V. A. Turikov, *Physica Scripta* **20**, 328 (1979).
- [36] K. Saeki, P. Michelsen, H. L. Pecseli and J. J. Rasmussen, *Phys. Rev. Lett.* **42**, 501 (1979).
- [37] S. Iizuka and H. Tanaca, *Phys. Lett.* **103A**, 57 (1984).
- [38] W. Fox, M. Porkolab, J. Egedal, N. Katz and A. Le, *Phys Rev. Lett.* **101**, 255003 (2008).
- [39] G. Sarri, M. E. Dieckmann, C. R. D. Brown, C. A. Cecchetti, D. J. Hoarty, S. F. James, R. Jung, I. K. Kourakis, H. Schamel, O. Willi and M. Borghesi, *Phys. Plasmas* **17**, 010701 (2010).
- [40] I. Alexeff, W. D. Jones and D. Montgomery, *Phys. Fluids* **11**, 167 (1968).
- [41] T. Kawabe, Y. Kawai, O. Saka and Y. Nakamura, *Phys Rev. Lett.* **28**, 889 (1972).
- [42] S. D. Baalrud, N. Hershkowitz and B. Longmier, *Phys. Plasmas* **14**, 042109 (2007).
- [43] M. A. Lieberman, *J. Appl. Phys.* **66**, 2926 (1989).
- [44] S. Kar, S. Mukherjee, G. Ravi and Y. C. Sxaena, *Phys. Plasmas* **17**, 102113 (2010).
- [45] C. Chan, M. Khazei and K. E. Lonngren, *Phys. Fluids* **24**, 1452 (1981).

CHAPTER 6

6 Excitation of Electrostatic Waves Using Pulsed Capacitive Process

6.1 Motivation

In the last Chapters, we discussed about the ion rarefaction waves and the solitary electron holes. In Chapter 4, ion rarefaction waves are excited using a conducting electrode, biased with a high negative pulse whose width is less than the ion plasma period. In Chapter 5, solitary electron holes are excited through a conducting material by applying a high positive voltage pulse, where the pulse width is varied from less than the ion plasma period to greater than ion plasma period. In this Chapter, in lieu of a conducting material, a dielectric electrode (a conducting electrode covered by a dielectric film) is used to excite some electrostatic waves. Here both the positive and negative pulses are used for various dielectric thicknesses. According to dielectric thickness solitary electron holes or solitary ion holes are excited for positive pulse bias and for negative pulse bias ion rarefaction waves are excited. An overview of previous literature is given in Sec. 6.2. The experimental setup is described in Sec. 6.3 followed by the observed results and discussions presented in Sec. 6.4. And finally conclusions are given in Sec. 6.5.

6.2 An Overview of Previous Works

Many experiments or theoretical models have been studied for the basic plasma physics point of view, when a metallic electrode or a metallic mesh grid is immersed inside plasma [1-2]. When the electrode or the mesh grid is biased with positive or negative pulses,

Chapter 6: Excitation of Electrostatic Waves Using Pulsed Capacitive Process

the ion acoustic waves [2], ion shocks [3], ion acoustic solitons [4], electron plasma waves [5], electron acoustic waves [6], electron acoustic solitons [7] or solitary electron holes [8] can be excited. Generally these linear or non-linear waves are propagated from the sheath edge [2].

One of the major applications that have been developed using pulsed bias on the electrode is plasma immersion ion implantation (PIII). PIII is a novel technique for surface modification and has mostly been applied to conducting materials [9-11] or semiconductors [12]. In PIII, a metallic electrode is immersed in a low pressure plasma and is biased with high negative voltage pulses. In general, the applied negative pulse bias magnitude (U_0) is much greater than the electron temperature, such that in the time scale of inverse electron plasma frequency f_e^{-1} , electrons are depleted from the vicinity of the electrode, leaving behind a uniform density of ion matrix sheath in which ions are stationary. Subsequently, in the time scale of inverse ion plasma frequency f_i^{-1} , ions are accelerated towards the electrode and implanted into the surface of the electrode. In typical PIII, the pulse duration (τ_p) is much larger than the ion response time and hence the ion matrix sheath or the transient sheath expands and ion implantation happens on the biased electrode. Also an experiment has done for PIII using positive bias [13] to the electrode. However, in PIII, both positive and negative bias is used depending on the application.

As an advanced technique for surface modification, PIII of insulating materials [14-17] has been used to modify the surface properties of dielectric materials (e.g. polymer), giving an improvement in qualities, like hardness, conductivity, wetting property and also used for protection against atomic oxygen degradation in space environment. PIII of dielectric materials is quite challenging because of surface charging, capacitance effects and poor conductivity. The dielectric material is positioned on a conducting target holder. During PIII, charges will accumulate on the dielectric surface and produce a charge layer because of the low electrical conductivity of the dielectric. The charge layer in turn builds up an opposing electric field that decreases the surface potential of the dielectric (i.e., the dielectric surface cannot rise to the full pulse bias potential that is applied to the metal target holder on which the insulating sample is placed) and change the profile of the sheath [18]. So the energy of the incident charge particles is less than that expected from the pulse bias voltage. The shorter the applied pulse rise time the larger is the charge dose accumulated on the dielectric surface. It would decrease the surface potential and hence the lower ion impact energy at the later stage of the pulse. A combination of short pulse duration, high pulse

frequency, high pulse magnitude and low plasma density can be beneficial for the dielectric in PIII [16].

Many researchers have explained the charging effect [14-16], incident charge particle energy distribution [19], effect of applied pulse duration and plasma density and the dielectric film characteristics (thickness and permittivity) [17] for PIII of dielectrics. But no experiments or theoretical models have been reported whether some kind of electrostatic plasma waves are excited in such cases. In this report, the experiments are performed for the excitation of electrostatic plasma waves from a positive and negative pulse biased dielectric covered metallic electrode. All the experiments are performed for single pulse excitation.

6.3 Experimental Set-up

The schematic diagram of the system is similar as Figures 4.1 and 5.1(a). The experiments were performed in a grounded cylindrical chamber of stainless steel (SS 304) with an inner diameter 29 cm and a length of 50 cm. The chamber was evacuated by using combination of rotary pump and diffusion pump and the base pressure was about 5×10^{-5} mbar. The plasma was generated by impact ionization of gas neutral by primary electron coming out from the dc biased hot tungsten filaments of diameter 0.25 mm. The filaments were mounted on two SS rings and filament bias potential was -65 V. The working gas was argon (99.999% pure) at pressure of 1×10^{-3} mbar. Plasma density (n_0), electron temperature (T_e) was determined with a Langmuir probe for various axial and radial positions. For fixed discharge current (I_{dis}), plasma density and electron temperature were found to be uniform throughout the main chamber. The experiments were performed with the plasma density of order 10^9 cm^{-3} , electron temperature 0.6 – 2 eV and the ions are considered as cold, i.e., 0.2 eV.

In the chamber, a dielectric covered metallic electrode was mounted on a SS rod and the SS rod was fixed in the axis of the chamber. Here the metallic electrode (diameter 12 cm) was covered by various dielectric (Kapton) thicknesses, shown in Figure 6.1. Here the metallic electrode, dielectric and plasma acted like a capacitor. A high voltage (HV) probe (1000X) and a current transformer (CT) were mounted on the SS rod and were used to measure the pulse voltage and the current respectively. The direction of the CT was such that it will give a positive signal when electrons are collected by the biased electrode. In the

chamber, an axially movable disk probe (receiver or detector) of diameter 7 cm and thickness 0.4 cm was introduced to detect the propagation of plasma perturbations. The detecting probe was kept floating and the propagating signals were directly observed on an oscilloscope. The details of the pulse forming circuit are described in Sec. 2.6.

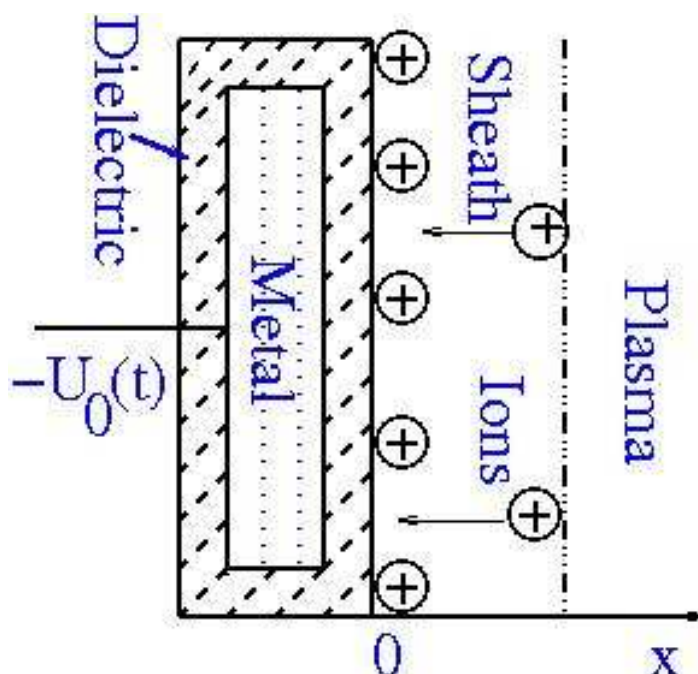


Figure 6.1 Schematic of the dielectric layer over a metallic electrode, on which the pulse bias is given.

6.4 Experimental Results and Discussions

6.4.1 Charging Effect

Figure 6.2(a) is the applied negative voltage pulse (solid line) and current pulse (dotted line) to the metal electrode, which is covered by a dielectric film in the presence of plasma. Here the applied pulse width is greater than the ion plasma period ($1 \mu\text{s}$). The current shown in this figure, is the mix of displacement current, electron current and ion current. Figure 6.2(b) shows the total current in presence of plasma (which is also shown in Fig. 6.2(a)), vacuum current (the capacitive current in the absence of plasma) and the subtracted current from total current to vacuum current. This vacuum current is the derivative of the applied voltage pulse. In the subtracted current pulse, first a negative current (ion current (I_i)) and later a positive current (electron current (I_e)) is shown. For increasing plasma density,

Chapter 6: Excitation of Electrostatic Waves Using Pulsed Capacitive Process

applied voltage pulse magnitude and the pulse width, the ion and electron currents are increased. We can calculate ion and electron charges from the integration of the current pulse, i.e., the area under the curve. Table I shows ion and electron charges for one particular plasma condition.

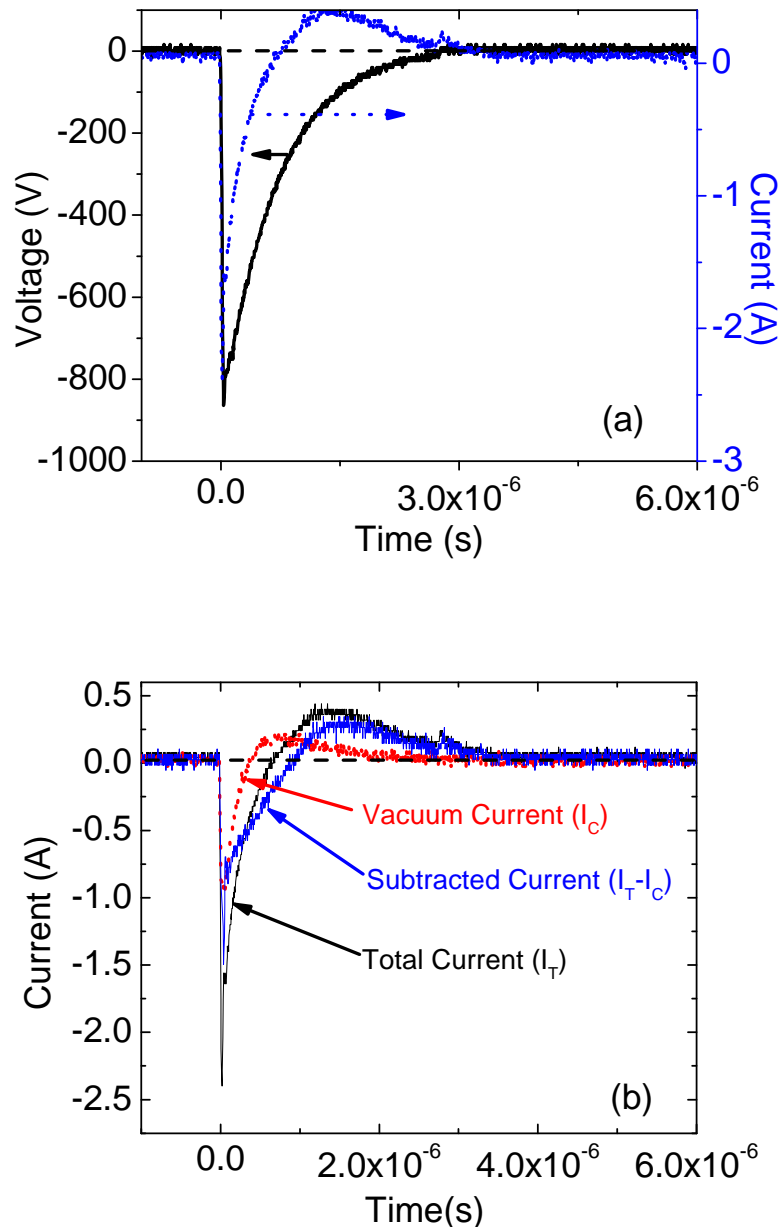


Figure 6.2 (a) The applied negative voltage (solid line) and total current (dotted line) pulse on the dielectric electrode in the presence of plasma. Here $d_d = 0.8$ mm and $n_0 = 9 \times 10^8$ cm⁻³. **(b)** The total current, vacuum current (capacitive current at vacuum) and the subtracted current (subtraction of vacuum current from the total current).

Table I Ion and electron charges for various plasma densities for both negative and positive pulse bias. The charges can be calculated from the integration of the current pulses, i.e., the area under the curve. Here $d_d = 0.8$ mm.

Bias Characteristics	$n_0 \times 10^9$ cm^{-3}	Ion charge ($\times 10^{-7}$) $(= \int_{\tau_1}^{\tau_2} I_i dt)$	Electron charge ($\times 10^{-7}$) $(= \int_{\tau_3}^{\tau_4} I_e dt)$	Net charge (Q) on the dielectric surface after pulse removal ($\times 10^{-7}$)	Potential drop on the dielectric surface (Q/C) (V)
-850 V, 2.5 μs	2.25	3.82	4.22	0.4	110
	3	5.3	6.35	1.05	291
	3.9	6.5	7.98	1.48	410
+850 V, 2.5 μs	2.25	6.2	8.2	2	555
	3	8.6	10.8	2.2	610
	3.9	10	12.5	2.5	690

Figure 6.3(a) shows the applied positive voltage pulse (solid line) and current pulse (dotted line) to the metal electrode, which is covered by the dielectric film in the presence of plasma. Here the applied pulse width is greater than the ion plasma period (1 μs). Figure 6.3(b) shows the total current in presence of plasma (which is also shown in Fig. 6.3(a)), vacuum current (the capacitive current in the absence of plasma) and the subtracted current from total current to vacuum current. The vacuum current is same for both negative and positive pulses, but with a sign change. Here first a positive current (electron current) and later a negative current (ion current) is shown and for increasing plasma density, applied voltage pulse magnitude and the pulse width, the ion and electron currents are increased. Table I shows electron and ion charges for one particular plasma condition.

Now we should discuss about the charging effect of dielectric material. We consider a planar electrode of dielectric thickness d_d , as shown in Fig. 6.1. The dielectric is kept on a metal electrode and immersed in a low pressure argon plasma. When a large negative or positive voltage pulse U_0 is applied to the metal electrode, instantly the full potential will be at the dielectric surface. Due to this potential the ions or electrons will be accelerated and accumulate on the dielectric surface and will start charging the dielectric surface. So a potential drop occurs due to this charge layer on the dielectric surface. Tian et al. [16] has

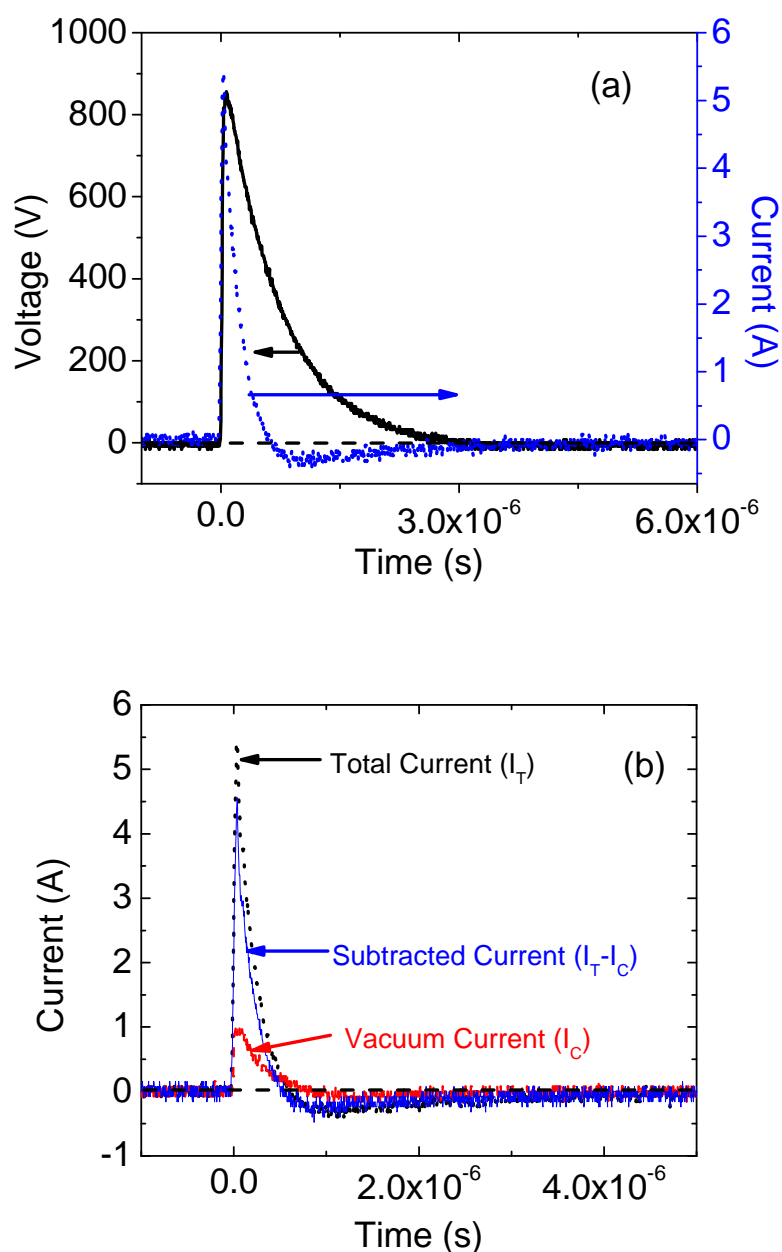


Figure 6.3 (a) The applied positive voltage (solid line) and current (dotted line) pulse on the dielectric electrode. Here $d_d = 0.8$ mm and $n_0 = 9 \times 10^8$ cm⁻³. **(b)** The total current, vacuum current (capacitive current at vacuum) and the subtracted current (subtraction of vacuum current from the total current).

also shown that the contribution from the plasma sheath capacitance to the potential drop is very small and the potential drop is mainly responsible for the charging. Emmert et al. [15] has shown that the dielectric surface charging is more severe for thicker targets. Considering the charging effects, the relation between the voltage induced by the free charge $Q(t)$ on the

Chapter 6: Excitation of Electrostatic Waves Using Pulsed Capacitive Process

surface of the dielectric electrode $U_s(t)$ and the external voltage applied on the metal electrode $U_0(t)$ is given as follows [17, 20-21]:

$$U_s(t) = U_0(t) - \frac{Q(t)}{C} \quad (6.1)$$

where, $C = \frac{\epsilon_0 \epsilon_r A}{d_d}$ is the effective capacitance of the dielectric electrode, ϵ_r is the relative permittivity (4 for Kapton), A is the area of the dielectric electrode surface. The second term is the potential drop on the dielectric surface after the pulse removal. Since the plasma potential is slightly positive with respect to reference ground potential (few kT_e), some researchers assume that $U_0 - V_p \approx U_0$. A smaller dielectric thickness gives rise to a larger capacitance and a smaller potential reduction. The Eq. (6.1) can be rewritten as

$$U_s(t) = U_0(t) - \frac{\sigma d_d}{\epsilon_0 \epsilon_r} \quad (6.2)$$

where $\sigma = Q/A$ is the total net charge density accumulated on the dielectric surface during the pulse. Since the implantation depth in the dielectric is small compared with the dielectric thickness, the charge layer can be treated as surface charge density σ . In Eq. (6.2), if d_d is very small, the capacitance will be large and the second term will be negligible. Thus the dielectric electrode for a smaller thickness, will behave like a metal plate. If the dielectric thickness increases, the capacitance will be small and the charging effect will be dominant. Table I shows the potential drop on the dielectric surface after the pulse removal for the dielectric thickness of 0.8 mm, which can be calculated from the net charge accumulating on the dielectric surface. It is seen that for dielectric thickness of 0.8 mm, there are more potential drops for positive pulse bias.

After the end of the dielectric surface charging, if the applied pulse is removed, the dielectric surface will be discharged by electrons or ions from the plasma and the dielectric surface potential gradually returns to zero. A longer time scale is needed for the discharge, because the charges may be implanted into the dielectric surface. The discharge time scale of charged dielectric surfaces is thus determining by the applied voltage pulse, pulse magnitude, plasma density and duration of the applied pulse.

6.4.2 Positive Bias

First the experiments have been done for the dielectric thickness of 0.1-0.5 mm. When the electrode is biased with a positive high voltage pulse, then potential perturbations are observed. Oscilloscope traces of the floating potential perturbations or the signals for different positions of the detector are shown in Fig. 6.4 for dielectric thickness of 0.5 mm. Similar trend of floating potential perturbations are obtained for the dielectric thickness of 0.1-0.5 mm. Fig. 6.4(a) shows the floating potential signals for lower applied pulse width ($\tau_p < 3f_i^{-1}$), as in Chapter 5 (Fig. 5.4). The first peak does not propagate with distance, but the second peak propagates with distance. The first peak detected by the detector is an electrostatically coupled signal [22] from the electrode, during the application of pulse to the electrode. However, the second peak propagates in two opposite directions (initially moves towards the electrode and after some distance it moves away from the electrode) from a location around 4 cm from the electrode, indicating the presence of a virtual source [8]. Taking 4 cm as the virtual source point, we can say two waves propagate in opposite directions with decrease in amplitude. Fig. 6.4(b) shows the floating potential signals for higher applied pulse width ($\tau_p \geq 3f_i^{-1}$), as in Chapter 5 (Fig. 5.5). Here the second peak propagates only in one direction with decrease in amplitude.

The time-of-flight phase velocity plots are shown in Fig. 6.5 for dielectric thickness of 0.5 mm. Fig. 6.5(a) shows the phase velocity for $\tau_p < 3f_i^{-1}$. The plot shows two phase velocities: with a phase velocity of $0.26-0.37v_e$ (left propagating signal) towards the electrode and with another phase velocity of $1.32v_e$ (right propagating signal) away from the electrode, as in Chapter 5 [8], where v_e is the electron thermal speed. Here the virtual source distance does not depend upon the plasma density. Fig. 6.5(b) shows the phase velocity for $\tau_p \geq 3f_i^{-1}$. For longer applied pulse width, the signals move only in one direction away from the electrode, but with one phase velocity ($1.32v_e$).

Figure 6.6 shows the phase velocity of the signals for various applied pulse magnitudes to the electrode of dielectric thickness 0.5 mm. The signals move with $1.32v_e$. Here it is seen that the speed of the propagation does not depend on increase the pulse magnitude. This is similar to observations as reported earlier in Chapter 5 for metal electrode only [8].

In Chapter 5, the exciter was a metal plate and the excited potential structures were solitary electron holes (SEHs) and propagated with the speed of $1.36v_e$. A SEH in plasma is

identified as a positive potential hump and propagates with the phase velocity of $1.31v_e$ [23]. In our case, the exciter is now a metallic electrode, covered by a dielectric material and the results (Figs. 6.4-6.6) obtained for the dielectric thickness of 0.1-0.5 mm are satisfied with the conditions of SEH. So for dielectric thickness between 0.1 and 0.5 mm, the propagation characteristics are similar to that obtained for without dielectric, as in Chapter 5 [8].

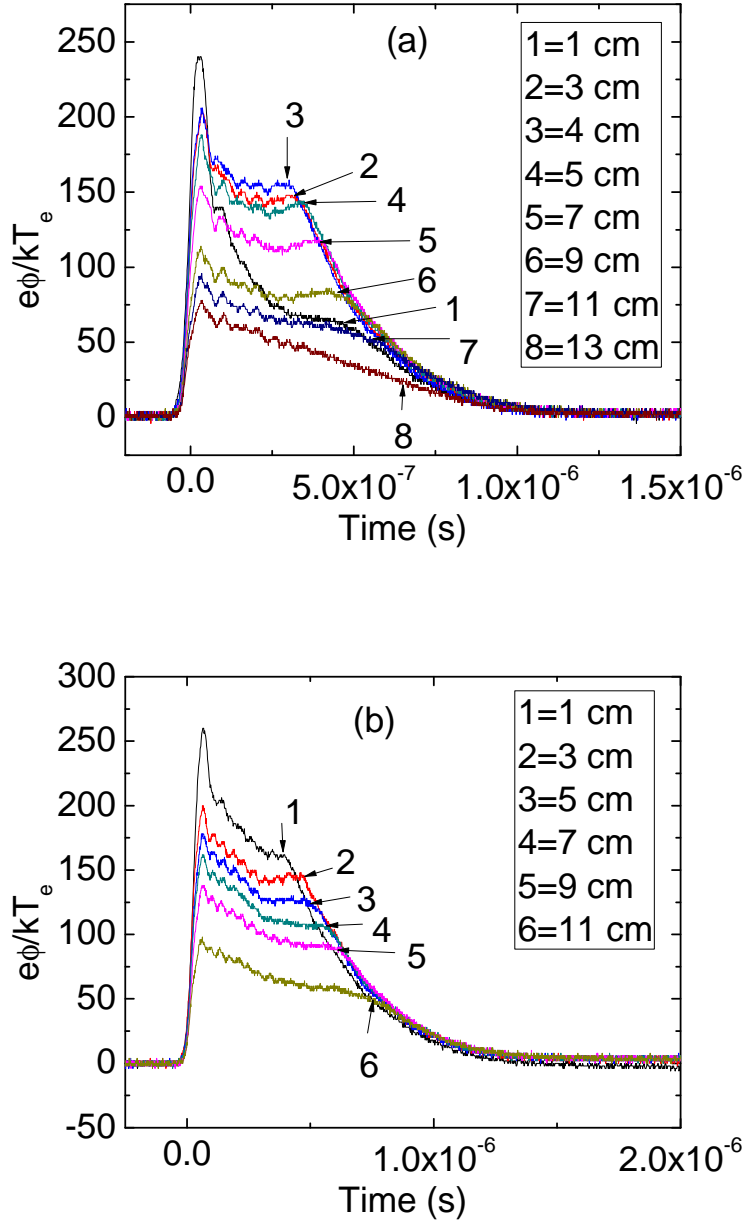


Figure 6.4 Oscilloscope traces of the floating potential disturbances measured by the detector from the positive biased dielectric exciter of 0.5 mm thickness. It shows only the second peak propagates with distance from the exciter. The numbers show the distances from the exciter. ϕ is the perturbation potential amplitude. **(a)** Here pulse width is 300 ns ($\tau_p < 3f_i^{-1}$), $U_0=1000$ V and $n_0 = 1.36 \times 10^9$ cm⁻³. **(b)** Here pulse width is 2 μ s ($\tau_p > 3f_i^{-1}$), $U_0=1000$ V and $n_0 = 1.36 \times 10^9$ cm⁻³.

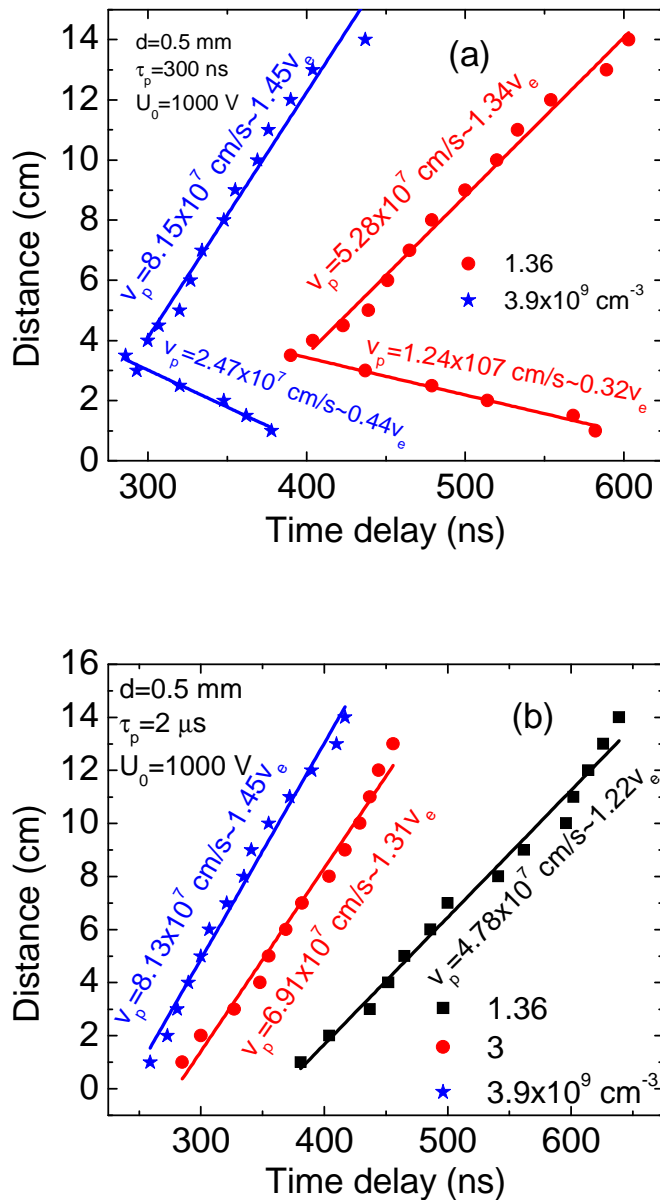


Figure 6.5 (a) Time delay vs the detector position for $\tau_p < 3f_i^{-1}$ for the dielectric thickness of 0.5 mm. This plot is for various plasma densities and shows two slopes. It indicates a virtual source around 3 cm from the exciter. **(b)** Time delay vs the detector position for $\tau_p > 3f_i^{-1}$. This is for various plasma densities and also shows two slopes in one direction. Here is no indication of virtual source.

Again the experiments are performed for the dielectric thickness of 0.6-0.9 mm. For these dielectric thicknesses, the propagating trend of the floating potential perturbations is same. Figure 6.7 shows the floating potential signals of the detector at various distances from the electrode for dielectric thickness of 0.8 mm. Strikingly these results are quite different from the results of below 0.6 mm dielectric thickness. Here initially the negative floating

Chapter 6: Excitation of Electrostatic Waves Using Pulsed Capacitive Process

potential signal propagates towards the electrode (left propagating signal) and after some distance it propagates away from the electrode (right propagating signal). Such type of nature indicates the presence of a virtual source. If we take 4 cm as the virtual source point, then we can say two waves propagate simultaneously in opposite directions with decrease in amplitude without significant change in shape. Interestingly, it is observed that these floating potential perturbations only excite for the applied pulse width in the range of $f_i^{-1} < \tau_p < 3f_i^{-1}$.

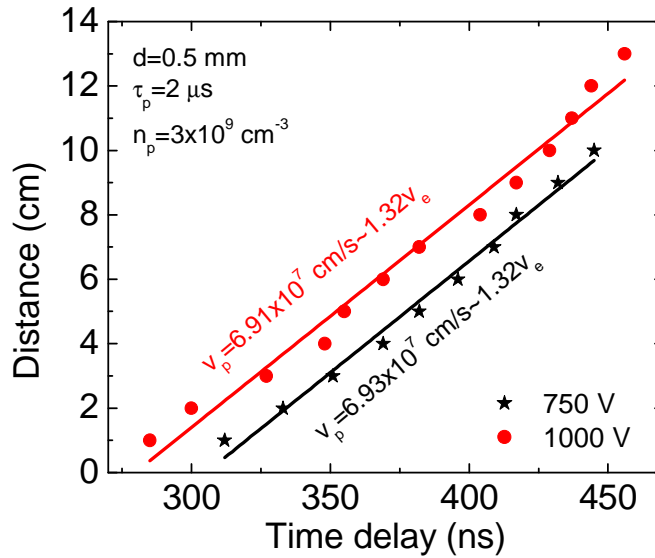


Figure 6.6 Time delay vs detector position for various applied pulse magnitude and the pulse width is greater than the thrice of ion plasma response time for the dielectric thickness of 0.5 mm. It shows the phase velocity is independent of applied pulse magnitude.

Figure 6.8 shows the phase velocity plot of the floating potential signals for the dielectric thickness of 0.8 mm for various plasma densities. This reveals two phase velocities: with a phase velocity comparable or less than the ion thermal velocity ($v_{t,i}$) towards the electrode (left propagating signal) and with another phase velocity comparable to C_s away from the electrode (right propagating signal). Here the virtual source distance increases with increase in plasma density.

Figure 6.9 shows the phase velocity plot of the floating potential perturbations for the dielectric thickness of 0.8 mm for various applied pulse magnitudes. Here also the left propagating signal propagates with the phase velocity comparable to ion thermal velocity and the right propagating signal propagates with C_s . Here the virtual source distance depends

Chapter 6: Excitation of Electrostatic Waves Using Pulsed Capacitive Process

upon the pulse magnitude, i.e., the virtual source distance increases with increase in pulse magnitude.

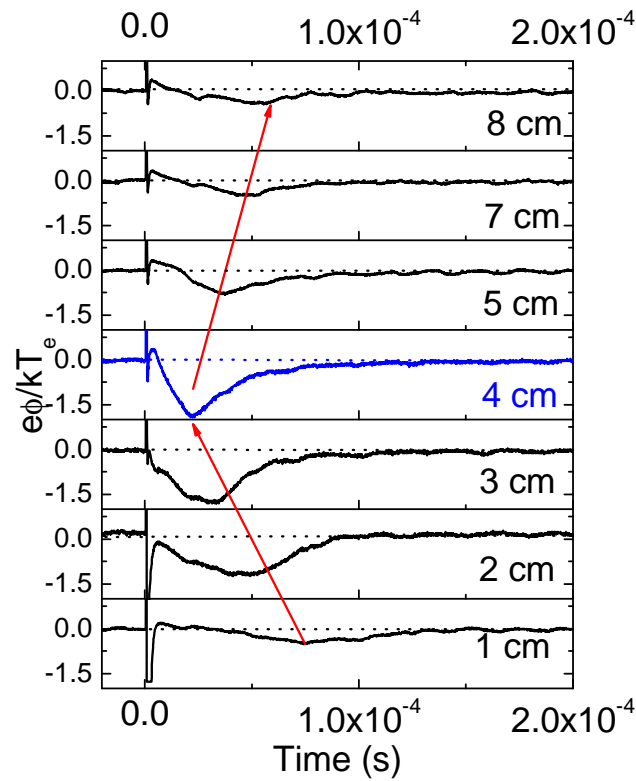


Figure 6.7 Oscilloscope traces of the floating potential signals measured by the detector from the positive biased dielectric exciter of 0.8 mm thickness. Here pulse width is 1 μs , $U_0 = 450 \text{ V}$ and $n_0 = 1.36 \times 10^9 \text{ cm}^{-3}$.

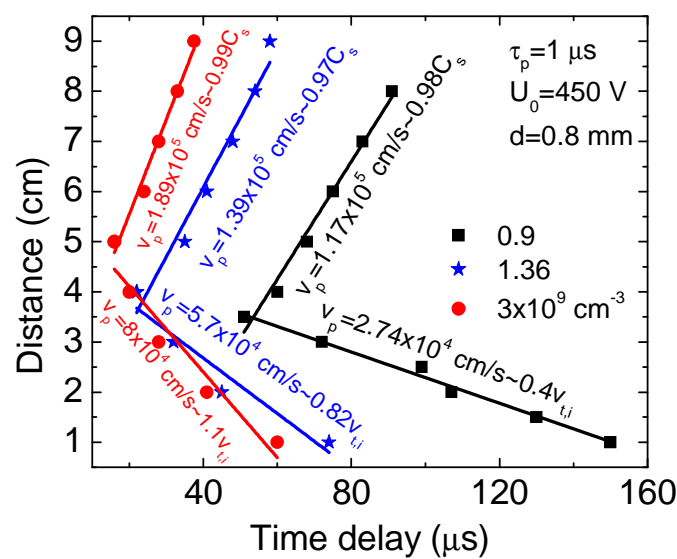


Figure 6.8 Time delay vs detector position for various plasma densities for the dielectric thickness of 0.8 mm.

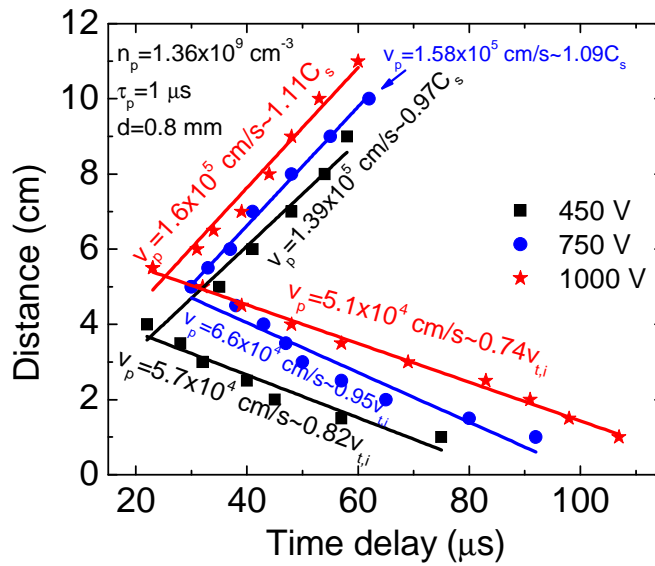


Figure 6.9 Time delay vs detector position for various applied pulse magnitude for the dielectric thickness of 0.8 mm.

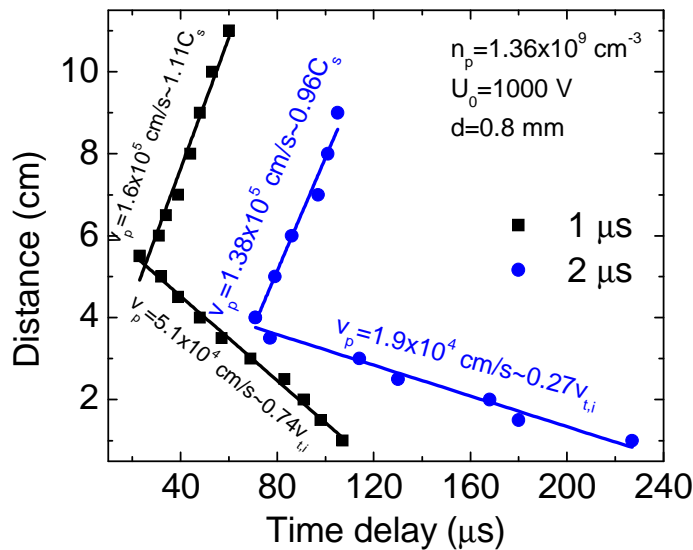


Figure 6.10 Time delay vs detector position for various applied pulse widths for the dielectric thickness of 0.8 mm.

Figure 6.10 shows the phase velocity plot of the floating potential perturbations for the dielectric thickness of 0.8 mm for various applied pulse widths. Here also the left propagating signal propagates with the phase velocity comparable or less than the ion thermal velocity and the right propagating signal propagates with C_s . Here the virtual source distance

Chapter 6: Excitation of Electrostatic Waves Using Pulsed Capacitive Process

depends upon the pulse width, i.e., the virtual source distance decreases with increase in pulse width.

According to previous literature [23-27], a solitary structure in plasma is identified as an ion hole (IH) by a negative potential dip, in which groups of ions are trapped. The overall density depression in this region leads to the IH. An IH propagates with a speed of comparable to or less than the ion thermal speed [23-28]. For an IH the electron density is assumed to be Boltzmann-type. The conditions of IHs to exist [23-26] are

$$(i) \frac{T_e}{T_i} > 3.5, \quad (6.3)$$

$$(ii) \left| \frac{e\phi}{kT_e} \right| \leq 1. \quad (6.4)$$

IH is a nonlinear version of the slow ion acoustic mode [29], which was first discovered and described by Schamel and Bujarbarua [24-25] theoretically. They showed that nonlinearly, IH can exist due to distortion of the ion distribution function in the resonant region. Recently theoretical and numerical studies of relativistic IHs [30] in a relativistically hot electron-ion plasma are reported.

The first experimental observation of the solitary IHs has been made by Pecseli et al. [27]. This experiment was performed in a double plasma device, excited by waves or pulses and found IHs behind the ion acoustic shocks. Later on Franck et al. [28] has observed the snoidal or periodic IHs in a double plasma device, excited by particle beam. They found that the IHs propagate comparable to $v_{t,i}$ and perform a sudden transition, by an apparent speed-up, to an ordinary ion acoustic mode.

Our experimental results shown in Figs. 6.7-6.10 satisfy the conditions of IH for a negative potential dip, speed is comparable to or less than the ion thermal speed and Eq. (6.3). We, therefore, speculate that the left propagating signals for the dielectric thickness of 0.6-0.9 mm are the nonlinear solitary ion holes. In our experimental case, in Fig. 6.7, it is observed that $\left| \frac{e\phi}{kT_e} \right|$ of the IHs from 1 cm to 4 cm is varied from 0.4 to 2 which shows large

amplitude solitary IHs for $\left| \frac{e\phi}{kT_e} \right| > 1$.

At and above 1 mm thickness of dielectric there is no excitation of perturbations.

For a positive pulse biased electrode, different electrostatic waves are excited for different dielectric thicknesses. Charging effect increases with dielectric thicknesses [15]. For the dielectric thickness of 0.1-0.5 mm, SEHs are excited, as the results observed for metal electrode in Chapter 5 [8]. So for the dielectric thickness of 0.1-0.5 mm, the charging effect is not significant. Figure 6.11 shows the electron current drawn for the metal and 0.5 mm dielectric thickness, which shows that the difference is not more.

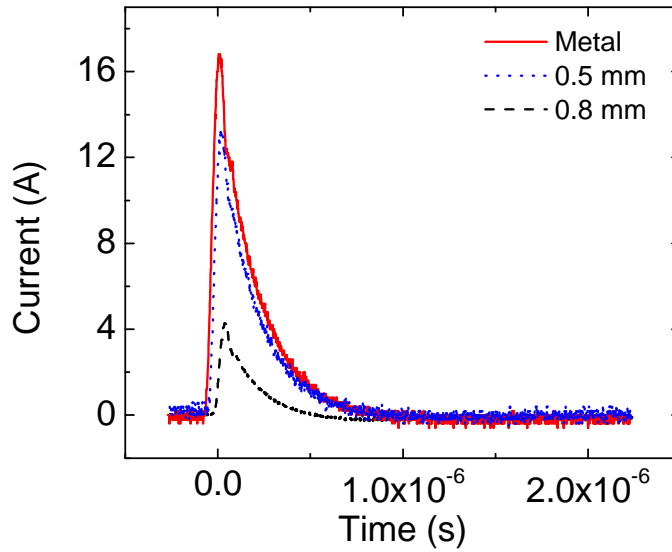


Figure 6.11 The electron current drawn for the metal and various dielectric thicknesses. Here $U_0 = 450 \text{ V}$, $n_0 = 1.36 \times 10^9 \text{ cm}^{-3}$ and $\tau_p = 1 \mu\text{s}$.

Solitary IHs are excited for the dielectric thickness of 0.6-0.9 mm. Here the charging effect is severe than the dielectric thickness of 0.1-0.5 mm (Fig. 6.11 and Table I). Here the floating potential perturbations only excite for the applied pulse width in the range of $f_i^{-1} < \tau_p < 3f_i^{-1}$. For increasing plasma density (Fig. 6.8) and applied pulse magnitude (Fig. 6.9), the virtual source distance increases. For larger plasma density and pulse magnitude, charging effect is more, i.e., a large opposing electric field exists. This opposing electric field attracts the ion holes from a longer distance towards the dielectric exciter. For longer applied pulse width (Fig. 6.10), charging effect is less, i.e., a small opposing electric field exists, which acts from a shorter distance.

Chapter 6: Excitation of Electrostatic Waves Using Pulsed Capacitive Process

In Fig. 6.7, if we take 4 cm as the virtual source, then the ion holes propagate towards the electrode with a speed of less than or comparable to ion thermal speed. Near to the electrode a less number of ions will be trapped in the ion hole structures and such kind of a new electrostatic wave propagates at a phase velocity significantly below the ion acoustic speed (comparable to or less than the $v_{t,i}$). This mode performs a sudden transition, by an apparent speed up, to an ordinary ion acoustic mode away from the electrode. Far from the electrode the number of trapped ions is more (an ion-neutral collision effect region) and the concomitant loss of the existence of the trapped ion hole structures lead a fastening ion acoustic mode.

In our experiments, the ion holes are excited after the applied pulse goes-off to zero. So the ion holes are excited during the discharge process and take a longer finite time to discharge. There is no charge dissipation during the pulse because the pulse time is short compared with the time scale for charge dissipation in dielectric materials [15]. In our case, the experimentally obtained discharge time scale is about 60-240 μs (Figs. 6.8-6.10) depending on various plasma parameters. For higher voltage, lower plasma density and longer pulse duration, may be the electrons impinge up to some depth (much less than the dielectric thickness) to the dielectric surface, results a longer time to discharge in plasma. This is valid for the assumption that the conductivity of the dielectric is sufficiently low that the charge being implanted can't dissipate during the pulse.

6.4.3 Negative Bias

Now the electrode is biased with a negative pulse for the dielectric thickness of 0.1-0.9 mm. For all the cases the trend of the floating potential signals are same. The signals propagate in one direction away from the electrode with decrease in amplitude. Figure 6.12 shows the oscilloscope traces of the floating potential signals detected by the detector from the electrode, for the applied pulse width less than the f_i^{-1} . Same floating potential signals are obtained for $\tau_p > f_i^{-1}$. At and above 1 mm thickness of dielectric there is no excitation of perturbations.

Figure 6.13 shows the time-of-flight plot to find speed of the excited signals for the dielectric thickness of 0.8 mm. The signals propagate linearly in one direction away from the electrode. The speed of the signals is comparable to ion acoustic speed.

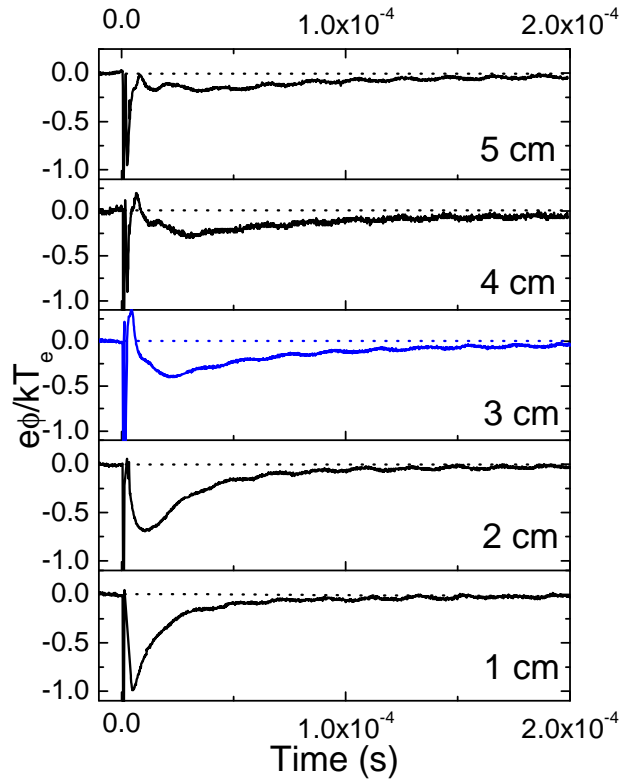


Figure 6.12 Oscilloscope traces (floating potential measurements) of the rarefaction disturbances observed at various distances from the dielectric exciter, when a single negative pulse is applied for the dielectric thickness of 0.5 mm. Here $U_0 = -1000$ V, $n_0 = 1.36 \times 10^9$ cm⁻³ and $\tau_p = 300$ ns.

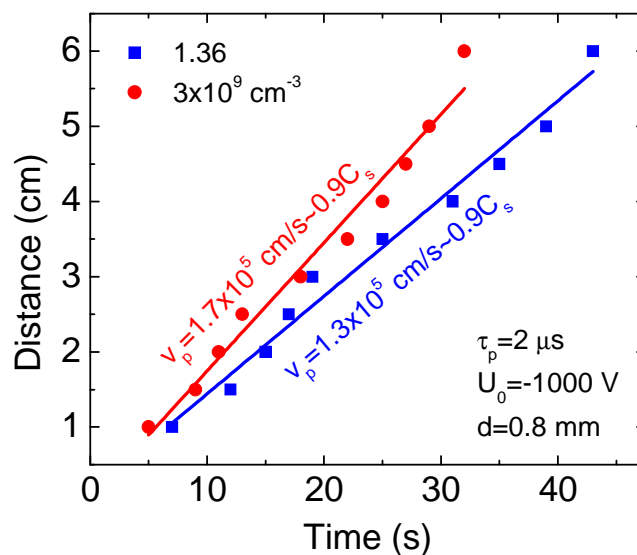


Figure 6.13 Time delay versus detector position showing the rarefaction wave speed for various plasma densities. Here $U_0 = -1000$ V and $\tau_p = 2 \mu\text{s}$.

Chapter 6: Excitation of Electrostatic Waves Using Pulsed Capacitive Process

Generally rarefaction waves are excited when the ions move towards a negative biased electrode, when the applied pulse width is greater than the ion plasma period (f_i^{-1}). If only a short pulse ($\tau_p < f_i^{-1}$) acts on the plasma, the density is depleted locally, i.e., when $U_0 \gg kT_e/e$ ($eU_0/kT_e \approx 100 - 1500$), the shielding effect is not perfect and the negative potential penetrates into the quasi-neutral plasma region (“pre-sheath”) where the ions are accelerated [31] and after the end of the pulse, the plasma is in a non-equilibrium state. Because diffusive process is slow due to charging effect, to reach the equilibrium state and a fast moving rarefactive wave forms. The rarefactive waves propagate with a velocity in the ion sound regime.

Table II Summary of the observed results for positive and negative pulse bias to the dielectric electrode for various parameters.

Pulse type	d_d (mm)	τ_p	Signal type	Virtual source	Velocity	Signals called
+ve	0.1 – 0.5	$\tau_p < 3f_i^{-1}$	Positive potential	Present	$0.3v_e/1.32v_e$	Solitary electron hole
		$\tau_p \geq 3f_i^{-1}$	Positive potential	No	$1.32v_e$	Solitary electron hole
	0.6 – 0.9	$f_i^{-1} < \tau_p < 3f_i^{-1}$	Negative potential	Present	$\leq v_{t,i}/C_s$	Solitary ion hole
-ve	0.1 – 0.9	$\tau_p < f_i^{-1}$, $\tau_p > f_i^{-1}$	Negative potential	No	C_s	Ion rarefaction wave

All the results explained above for both positive and negative pulse bias are summarized in Table II. It is seen that for dielectric thickness of 0.1 -0.5 mm, when the electrode is biased positive, solitary electron holes are observed which is similar to that obtained for without dielectric, as in Chapter 5 [8]. For these dielectric thicknesses, the capacitance is large and the charging on the dielectric surface is less. For $d_d = 0.5$ mm, the potential drop on the dielectric surface is around 100 V for applied pulse magnitude of

1000V. So the dielectric surface potential (U_s) is sufficient to excite the solitary electron holes. The solitary electron hole will be only excited when the excitation potential exceeds a critical value φ_c [8, 32]

$$\varphi_c = \frac{1}{2} \frac{m_e}{e} \left(\frac{\omega_{pe}}{2\pi} \frac{a}{2.4} \right)^2 \quad (6.5)$$

where m_e is the electron mass, ω_{pe} is the electron plasma frequency and a is the electrode radius. For $n_0 = 1.36 \times 10^9 \text{ cm}^{-3}$, φ_c is around 150 V, which is less than the dielectric surface potential and solitary electron holes are excited.

When the dielectric thickness increases, i.e., for 0.6 – 0.9 mm, solitary ion holes are excited for positive pulse bias. Here the capacitance is small and the charging of the dielectric is dominant, as shown in Table I. After the removal of pulse, as shown in Table I, U_s is smaller than the φ_c ($= 327 \text{ V}$ for $n_0 = 2.25 \times 10^9 \text{ cm}^{-3}$ and $d_d = 0.8 \text{ mm}$) for these dielectric thicknesses, which doesn't satisfy the condition of the excitation of electron holes. Due to this small dielectric potential, slow ion holes are excited. These IHs are only excited for the applied pulse width in the range of $f_i^{-1} < \tau_p < 3f_i^{-1}$. When the applied positive pulse width is less than the ion plasma period, ions will not respond. For longer pulse widths, i.e., when $\tau_p > 3f_i^{-1}$, after the pulse removal, may be all the accumulated charges on the dielectric surface are discharged and plasma doesn't show any potential for perturbation.

When the electrode is biased negative for dielectric thickness of 0.1 – 0.9 mm, ion rarefaction waves are excited. Chang et al. [33] have shown that minimum 50 V is required to excite the nonlinear ion acoustic waves. Here the dielectric surface potential, although the dielectric thickness increases (from 0.1 – 0.9 mm) with increase in surface charging, is sufficient to excite the ion rarefaction waves as in metal case, in Chapter 4 [31]. For negative bias, the charging effect is very less as shown in Table I.

6.5 Conclusions

The present investigation shows the excitation of electrostatic waves using a pulsed capacitive process in a homogeneous electron-ion plasma. The excitation of electrostatic waves depends upon the dielectric thickness and polarity of the applied pulse. When the electrode of dielectric thickness 0.1-0.5 mm is biased pulsed positive, solitary electron holes

Chapter 6: Excitation of Electrostatic Waves Using Pulsed Capacitive Process

are excited and up to this dielectric thickness, the electrode covered by the dielectric film behaves as a conducting electrode. The presence of a virtual source indicates for solitary electron holes, when the applied pulse width is less than the thrice of ion plasma period. Solitary ion holes are excited for the positive biased dielectric thickness of 0.6-0.9 mm. Here initially, the solitary ion holes propagate towards the electrode with a speed of comparable to or less than the ion thermal velocity and performs a sudden transition away from the electrode with ion acoustic speed, indicating the presence of a virtual source. For positive bias, the waves, solitary electron and ion holes, are dependent on the combined effect of applied pulse magnitude, pulse duration and dielectric film characteristics (thickness and dielectric constant).

When the dielectric electrode (0.1-0.9 mm thickness) is biased pulsed negative, ion rarefaction waves are excited and propagate with ion acoustic speed.

The dielectric surface charging is more for positive pulse bias than the negative pulse bias. Above 0.9 mm dielectric thickness, there is no excitation of any electrostatic waves for both positive and negative pulse bias, at least for the applied pulse magnitude and plasma conditions considered here. As our knowledge, excitation of such type of electrostatic waves explained above from a dielectric electrode is reported first time.

- The work presented in this Chapter is published as
S. Kar and S. Mukherjee, Phys. Plasmas 18, 112303 (2011).

6.6 References

- [1] H. Ikezi, P. J. Barrett, R. B. White and A. Y. Wong, *Phys. Fluids* **14**, 1997 (1971).
- [2] M. Widner, I. Alexeff, W. D. Jones and K. E. Lonngren, *Phys. Fluids* **13**, 2532 (1970).
- [3] C. Chan, M. Khazei and K. E. Lonngren, *Phys. Fluids* **24**, 1452 (1981).
- [4] E. Okutsu and Y. Nakamura, *Plasma Phys.* **21**, 1053 (1979).
- [5] S. Ikezawa and Y. Nakamura, *J. Phys. Soc. Japan* **50**, 962 (1981).
- [6] G. Karlstad, J. Trulsen and R. J. Armstrong, *Proceedings of Contributed Papers, 1984 International Conference on Plasma Physics, Lausanne*, edited by M. Q. Tran and M. L. Sawley (Centre de recherches en physique des plasmas, Ecole polytechnique federale, Lausanne, Switzerland, 1984), Vol. **2**, p. 12.
- [7] M. Berthomier, R. Pottelette, M. Malingre and Y. Khotyaintsev, *Phys Plasmas* **7**, 2987 (2000).
- [8] S. Kar, S. Mukherjee, G. Ravi and Y. C. Saxena, *Phys. Plasmas* **17**, 102113 (2010).
- [9] J. R. Conrad, J. L. Radtke, R. A. Dodd, F. J. Worzala and N. C. Tran, *J. Appl. Phys.* **62**, 4591 (1987).
- [10] M. A. Lieberman, *J. Appl. Phys.* **66**, 2926 (1989).
- [11] K. G. Kostov, J. J. Barroso, and M. Ueda, *Braz. J. Phys.* **34**, 1689 (2004).
- [12] S. Quin, and C. Chan, *J. Vac. Sci. Technol.* **B 12**, 962 (1994).
- [13] T. Ikehata, K. Shioya, N. Y. Sato and K. Yukimura, *Surf. Coat. Technol.* **186**, 209 (2004).
- [14] Xue-Chun Li and You-Nian Wang, *Surf. Coat. Technol.* **201**, 6569 (2007).
- [15] G. A. Emmert, *J. Vac. Sci. Technol.* **B 12**, 880 (1994).
- [16] X. Tian, R. K. Y. Fu, J. Chen, P. K. Chu and I. G. Brown, *Nuclear Inst. Methods in Phys.* **B 187**, 485 (2002).
- [17] A. Lacoste, F. L. Coeur, Y. Arnel, J. Pelletier and C. Grattapain, *Surf. Coat. Technol.* **135**, 268 (2001).
- [18] X. B. Tian, K. Y. Fu, P. K. Chu and S. Q. Yang, *Surf. Coat. Technol.* **196**, 162 (2005).
- [19] B. P. Linder and N. W. Cheung, *IEEE Trans. Plasma Sci.* **24**, 1383 (1996).
- [20] E. V. Barnat and T. M. Lu, *J. Appl. Phys.* **90**, 5898 (2001).
- [21] Z. Dai and Y. Wang, *J. Appl. Phys.* **92**, 6428 (2002).
- [22] I. Alexeff and W. D. Jones, *Phys. Rev. Lett.* **15**, 286 (1965).
- [23] H. Schamel, *Phys. Reports* **140**, 161 (1986).
- [24] H. Schamel and S. Bujarbarua, *Phys. Fluids* **23**, 2498 (1980).
- [25] S. Bujarbarua and H. Schamel, *J. Plasma Phys.* **25**, 515 (1981).

Chapter 6: Excitation of Electrostatic Waves Using Pulsed Capacitive Process

- [26] H. Schamel, Phys. Lett. **89A**, 280 (1982).
- [27] H. L. Pecseli, R. J. Armstrong and J. Trulsen, Phys. Lett. **81A**, 386 (1981).
- [28] C. Franck, T. Klinger, A. Piel and H. Schamel, Phys. Plasmas **8**, 4271 (2001).
- [29] T. H. Stix, The Theory of Plasma Waves (McGraw-Hill, New York, 1962), Chaps. 9-14.
- [30] B. Eliasson, P. K. Shukla and M. E. Dieckmann, New J. Phys. **8**, 55 (2006).
- [31] S. Kar, S. Mukherjee and Y. C. Saxena, Phys. Plasmas **18**, 053506 (2011).
- [32] K. Saeki, P. Michelsen, H. L. Pecseli and J. J. Rasmussen, Phys. Rev. Lett. **42**, 501 (1979).
- [33] H. Y. Chang, C. Lien, A. Seyhoonzadeh, P. Forsling and K. E. Lonngren, IEEE Trans. Plasma Sci. **16**, 50 (1988).

CHAPTER 7

7 Summary and Future Scope

7.1 Summary

The main focus of this thesis has been on experimental studies on plasma response to transient high voltage pulses in a uniform and unmagnetized low pressure argon plasma. In particular the investigations have centered on the excitation and propagation characteristics of nonlinear electrostatic waves, i.e., ion rarefaction waves, electron and ion holes. These waves are dependent on the pulse polarity, pulse width and the type of exciter, i.e., conducting or dielectric.

The experiments were carried out in a cylindrical stainless steel (SS 304) vacuum chamber which was used as anode and the tungsten filaments as cathode. The plasma was generated by impact ionization of gas neutrals by primary electrons coming out from dc biased hot tungsten filaments. Langmuir probes and emissive probes were used to measure the plasma parameters such as, the plasma density, the electron temperature, the floating potential and the plasma potential. In our experiments the plasma density was in the order of $1 \times 10^{15} \text{ m}^{-3}$, whereas the electron temperature was varied between 0.5 – 6 eV and the ion temperature was assumed cold as 0.2 eV.

In the first set of experiments, we have estimated the number of electrons lost to the chamber wall, during the negative pulse bias to a metallic electrode. The pulse width was in between the electron and ion plasma periods. It has seen that the percentage of electron loss to the chamber wall is very less, i.e. 0.1 – 1%. The origin of the lost electrons is the ion matrix sheath as well as the bulk plasma. These experimental results are compared with a PDP1 computer simulation which has shown a good agreement.

Chapter 7: Summary and Future Scope

In the second set of experiments, the ion rarefaction response to a high negative voltage pulse applied to a metal plate immersed in a low pressure argon plasma, for time duration lower than ion plasma period is investigated. Such a pulse duration is chosen so that ions are collectively undisturbed and, according to general understanding, no energy is given to ions. Hence no ion rarefaction wave should be excited. But, contrary to the general understanding, excitation and propagation of ion rarefaction waves are observed. When the applied pulse magnitude is much greater than the electron temperature (100-1500 times), the shielding effect is not perfect and the negative potential penetrates into the quasineutral plasma region (pre-sheath), where the ion are accelerated. So the rarefaction waves are excited in the pre-sheath region after the pulse goes to zero. The rarefaction waves are detected by the floating potential measurements, ion and electron saturation current measurements. These ion rarefaction waves are propagated comparable to ion acoustic speed. Overall, the excitation of ion rarefaction waves depends upon the product of pulse width and pulse magnitude. Another observation is, after a distance of $\frac{3}{4}$ th of exciter diameter from the exciter, the rarefaction waves turned to ion acoustic waves.

In the third set of experiments, plasma response to a fast rising high positive voltage pulse is experimentally studied in a uniform and unmagnetized plasma, where solitary electron holes are excited. The pulse is applied to a metallic disc electrode immersed in a low pressure argon plasma with the pulse magnitude much greater than the electron temperature. Experiments have been carried out for various applied pulse widths ranging from less than ion plasma period to greater than thrice of ion plasma period. The solitary electron holes are detected by floating potential measurements. For pulse width less than thrice of ion plasma period, solitary electron holes are observed to propagate in two opposite directions from a location different from the actual exciter, indicating the presence of a virtual source. For pulse widths equal or greater than the thrice of ion plasma period, electron holes are propagated away from the exciter in one direction and there is no indication of virtual source. These electron holes are propagated with two speeds, one is comparable to electron thermal speed and the other is less than to electron thermal speed.

In the fourth set of experiments, plasma response to high positive and negative voltage pulses is studied using a dielectric material (Kapton) in a uniform and unmagnetized plasma. The positive or negative voltage pulse is applied to a metallic electrode covered by a dielectric film, immersed in a low pressure argon plasma and the pulse magnitude is much greater than the electron temperature. Experiments are carried out for, how the plasma

Chapter 7: Summary and Future Scope

perturbations behave at various applied pulse widths in comparison to ion plasma period and at different plasma parameters. Plasma perturbations are studied with respect to the thickness of the dielectric film. Due to poor conductivity of dielectric, dielectric charging plays an important role. The dielectric thickness up to 0.5 mm shows the same results as in metal for both positive and negative pulses, i.e., solitary electron holes and ion rarefaction waves are excited respectively. Above 0.5 mm to 0.9 mm dielectric thickness, plasma perturbations show strikingly different results for positive pulse, i.e., solitary ion holes are excited, but for negative pulse it is same as in metal case, i.e., ion rarefaction waves. And there is no excitation of plasma perturbations on and above 1 mm dielectric thickness for both positive and negative pulses. The solitary electron and ion holes are detected by floating potential measurements. Here the solitary electron holes are propagated with comparable to electron thermal speed, while the solitary ion holes are propagated with comparable to or less than the ion thermal speed.

7.2 Future Scope

The experimental studies of the present thesis can form the basis for further in-depth investigations of plasma response to transient high voltage pulses and can motivate new theoretical, experimental and computer simulation studies. The possible future extensions can be divided into two parts: one is for metallic case and other is for the dielectric case.

A few possible future directions of research related with fundamental studies are discussed below:

- All the experiments described above are for the un-magnetized plasma. These experiments can be repeated for the magnetized plasma to show the magnetic field effects on the un-magnetized results, like for positive plate bias electron or ion acoustic shocks may be excited instead of solitary electron holes.
- Computer simulation can be done for the effect of applied negative pulse width and magnitude on the excitation of ion rarefaction waves.
- In Chapters 3 and 4, the applied negative pulse duration is less than the ion plasma period. When the applied negative pulse duration will much greater than the ion plasma period, ion response begins and a significant amount of ions will be accelerated towards the electrode. The ions reaching the electrode

Chapter 7: Summary and Future Scope

will have a distribution of energy, corresponding to the instantaneous acceleration voltage and ion transit time through the dynamic evolving ion sheath. So the ion energy distribution behind the electrode can be measured.

- When the negative pulse bias duration is approximately equal to the electron-neutral ionization time scales, the secondary electrons emitted from the electrode because of ion bombardment cause significant ionization. While this is not taken into account in many applications and it is not unavoidable. Understanding of additional ionization in the presence of background plasma can be an area of investigation.
- To understand more about the presence of a virtual source related to the solitary electron and ion holes, computer simulations of chapters 5 and 6 can be done.
- In the present thesis, all the experiments are performed for single pulse excitation. Experiments can be performed for repetitive pulses. When longer pulse durations are applied on an electrode of large area, a significant amount of ions are lost to the substrate, leading to ion density depletion in plasma. During the time in between the pulses, plasma will try to recover the initial density. Understanding the overall balance of charges can be an area of investigation.
- Another experiment can be done that is; scattered dust charging with positive biased plate.

In the present thesis, solitary electron and ion holes are excited for the dielectric case, i.e., using pulsed capacitive process. Here also single pulse excitation was used. The future directions in this area can be studied for charging effect and surface modification for

- High pulse magnitude and low repetition rate
- Low pulse magnitude and high repetition rate.

For the above conditions, surface modification of dielectric can be studied. In addition to this a thin metallic film (around 10 nm thickness) can be coated on the dielectric, which may prevent surface charging, and the corresponding surface modification can be studied under the above 2 conditions.